Nutrient Dynamics in a Coupled Terrestrial Biosphere and Land Model (ELM-FATES)

Ryan G. Knox[1], Charles D. Koven[1], William J. Riley[1], Anthony P. Walker[2], S. Joseph Wright[3], Jennifer A. Holm[1], Xinyuan Wei[2], Rosie A. Fisher[4], Qing Zhu[1], Jinyun Tang[1], Daniel M. Ricciuto[2], Jacquelyn K. Shuman[5], Xiaojuan Yang[2], Lara M. Kueppers[1]and Jeffrey Q. Chambers[1]

[1]Lawrence Berkeley National Laboratory, Berkeley, USA
[2]Oak Ridge National Laboratory, Oak Ridge, USA
[3]Smithsonian Tropical Research Institute, Ancon, Panama
[4]CICERO Center for International Climate Research, Oslo, Norway
[5]National Center for Atmospheric Research, Boulder, USA

Corresponding author: Ryan Knox, `rgknox@lbl.gov`

Abstract

We present a representation of nitrogen and phosphorus cycling in the vegetation demography model the Functionally Assembled Terrestrial Ecosystem Simulator (FATES), within the Energy Exascale Earth System (E3SM) land model. This representation is modular, and designed to allow testing of multiple hypothetical approaches for carbon-nutrient coupling in plants. The model tracks nutrient uptake, losses via turnover from both live plants and mortality into soil decomposition, and allocation during tissue growth for a large number of size- and functional-type-resolved plant cohorts within a time-since-disturbance-resolved ecosystem. Root uptake is governed by fine root biomass, and plants vary in their fine root carbon allocation in order to balance carbon and nutrient limitations to growth. We test the sensitivity of the model to a wide range of parameter variations and structural representations, and in the context of observations at Barro Colorado Island, Panama. A key model prediction is that plants in the high-light-availability canopy positions allocate more carbon to fine roots than plants in low-light understory environments, given the widely different carbon versus nutrient constraints of these two niches within a given ecosystem. This model provides a basis for exploring carbon-nutrient coupling with vegetation demography within Earth System Models (ESMs).

Plain Language Summary

This work introduces a new set of nutrient cycling hypotheses integrated with a coupled terrestrial biosphere model. This includes the cycling of carbon, nitrogen and phosphorus, and focuses mainly on plant acquisition, allocation, and turnover. An analysis shows the model offers reasonable response to perturbations in parameter constants and boundary conditions, considering its design balance between process complexity and parameterization burden.

Key Points:

- The nutrient enabled ELM-FATES model represents reasonable pattern responses to nutrient availability and parameter perturbations.
- The model has been designed to introduce a reasonably small parameterization burden, considering the total number of newly introduced parameters and the relative ease of finding values (i.e. directly from observations, or through calibration).
- The model formulation described here does not make any assertions that it offers a complete representation of nutrient and carbon dynamics, rather that these are a set hypothesis that can capture certain element of carbon-nutrient dynamics and can be further intercompared with other hypotheses.

1 Introduction

Projections of the global climate system response to anthropogenic CO_2 emissions require coupled models of the climate system and carbon cycle. Much of the uncertainty in current climate projections arises from the global terrestrial carbon cycle, and in particular the responses of plants to elevated CO_2 (Arora et al., 2020). Many current Earth System Models (ESMs) do not take into account plant size structure, disturbance history, and other aspects known to govern ecosystem function and thereby current and future responses to anthropogenic pressures (D. Purves & Pacala, 2008). Additionally, limitation by nutrients of plant productivity under elevated CO_2 has been shown to strongly affect both the historical and future uptake of carbon (Hungate et al., 2003; P. Thornton et al., 2007; Zaehle & Friend, 2010; Wang et al., 2015). The importance of includ-

ing nutrient dynamics in projecting the global terrestrial carbon budget is evidenced by its expanded role in Earth System land models, such as CASACNP (Wang et al., 2010), GFDL LM4.1-BNF (Kou-Giesbrecht et al., 2021a; Sulman et al., 2019), ED2-MEND-NCOM (Medvigy et al., 2019), and Quincy v1.0 (Thum et al., 2019) to name a few. The processes that govern nutrient cycling rates in ecosystems are highly uncertain, since many of them occur belowground where observation is more difficult than in plant canopies. To allow exploration of this epistemic uncertainty, we propose here a modular approach to representing nutrient cycling that facilitates exploration of alternative process hypotheses and parameter and structural uncertainty quantification.

This manuscript describes a modeling methodology for plant acquisition, storage, and allocation of nutrients and carbon within the terrestrial biosphere of an ESM. This manuscript also describes how the plant nutrient dynamics interface with existing soil nutrient hypotheses, but does not introduce new soil modeling hypotheses. This system is an extension of the coupled modeling framework of the Energy Exascale Earth System Model (E3SM) (Caldwell et al., 2019) and the Functionally Assembled Terrestrial Ecosystem Simulator (FATES). E3SM includes a land model (ELM) among other components such as atmosphere, ocean, ice, and human. The terrestrial vegetation simulated in FATES is based on the plant size and time-since-disturbance structured approach derived from the Ecosystem Demography model (Moorcroft et al., 2001; R. A. Fisher et al., 2015).

The nutrient modeling framework we describe here can be summarized in three model components: 1) a new module that handles on-plant nutrient and carbon allocations to different organs, designated the Plant Allocation, Reactions, and Transport Extensible Hypotheses (PARTEH), 2) a restructuring of the rest of the FATES model to track variable chemical elements in seed, unfragmented litter, and coarse woody debris pools, and 3) a means of acquisition and competition for nutrients by FATES plants amongst microbes and mineral surfaces. An evaluation of the model at a tropical test-bed site follows.

2 Model Description - Plant-Soil Nutrient Dynamics

The Energy Exascale Earth System Model Land Model component (Burrows et al., 2020), resolves numerous processes related to the cycling of water, energy, carbon, nitrogen and phosphorus in natural and anthropogenic ecosystems. Soil decomposition is handled via a derivative of the CENTURY approach (C. Koven et al., 2013; Parton et al., 1988). Total ecosystem nitrogen fixation has been represented in ELM by assuming proportionality with either evapotranspiration or net primary productivity (Cleveland et al., 1999; P. Thornton et al., 2007). Symbiotic fixation at the plant level is introduced in the Methods section and will be described in more detail. When symbiotic fixation is represented by FATES, the total ecosystem fixation module in ELM is scaled down to represent on free-living fixation in the soil. Soil biogeochemical dynamics lead nitrogen to cascade from organic pools with different turnover times to ammonium (NH_4) and nitrate (NO_3) pools. ELM contains two alternative representations of competition for these these nutrient species amongst plants, microbes (decomposers for organic pools, as well as nitrifiers and denitrifiers for mineral nitrogen pools), and mineral surfaces (for phosphorus). These are the Relative Demand (RD) approach (P. Thornton et al., 2007; X. Yang et al., 2014, 2019) and a Capacity-Based approach that applies the Equilibrium Chemistry Approximation (CB) (Tang & Riley, 2013; Zhu et al., 2016, 2019).

FATES is a vegetation demography model(R. A. Fisher et al., 2015; C. D. Koven et al., 2020) that represents the demographics of vegetation using plant size and time-since-disturbance structured scaling algorithms defined in the Ecosystem Demography (ED) Model (Moorcroft et al., 2001). FATES represents vegetation by grouping plants of similar size and functional type into cohorts, which inhabit patches of the landscape

that are defined by their time since last disturbance. Unlike unstructured vegetation models, which treat growth and mortality processes as changes to the size of whole ecosystem-level carbon and nutrient pools, cohort-based vegetation models like FATES explicitly track the growth of plants, the size (volume, height, etc) growth of various components, and the resulting carbon and nutrient pools of their tissues using allometrically-defined scaling relationships with stem diameter. FATES also allows for competition for light between plant types in the same vertical profile, which leads to self-thinning dynamics and other spatio-temporal changes in vegetation composition to emerge as a function of variation in plant functional traits. FATES estimates mortality at the plant cohort scale, based on several factors including carbon starvation, understory impact survival, hydraulic stress (R. A. Fisher et al., 2015), background mortality (i.e. unspecified or unknown effects)(Moorcroft et al., 2001), fire (Thonicke et al., 2010), and relationships with plant age or size (Needham et al., 2020). In the current version of FATES, the time-since-disturbance patch discretization only resolves heterogeneity in the above-ground environment, with all cohorts on all patches drawing water and nutrients from the same soil pools.

FATES represents a variety of processes, including but not limited to: photosynthesis and its coupling with water limitations on stomatal conductance (Farquhar et al., 1980; Collatz et al., 1991; Oleson et al., 2013; G. Bonan et al., 2014), respiration (Ryan, 1991) of live tissues, vertical distribution of canopy functional trait parameters (G. B. Bonan et al., 2012), radiation scattering (Norman, 1979), phenology (Botta et al., 2000), and turnover into coarse woody debris and fine litter (R. A. Fisher et al., 2015; Oleson et al., 2013). FATES' radiation scattering module accounts for both the vertical structure of vegetation and the variable scattering characteristics of different plant functional groups in parallel (R. A. Fisher et al., 2015). The spatial configuration of the canopy scattering elements is driven by a modified perfect plasticity approximation (D. W. Purves et al., 2008; R. A. Fisher et al., 2015; C. D. Koven et al., 2020). While FATES can optionally utilize sophisticated representations of plant hydraulics (Christoffersen et al., 2014; Fyllas et al., 2014; Fang et al., 2022) and fire (Thonicke et al., 2010; Buotte et al., 2021; Ma et al., 2021), in order to maintain a focus on nutrient dynamics, these options were not active in the modeling exercises described herein. Details on all of these process representations can be found in the FATES technical documentation (FATES-Development-Team, 2019).

The introduction of nutrients to FATES, via the PARTEH approach to (Plant Resource Allocations, Reactions, and Transport Extensible Hypotheses) described here, follows a sequence of operations that are shown in Figure 1. The descriptions of these processes follow the flow-chart order and can be found in the following subsections: symbiotic fixation in 2.1, plant acquisition of aqueous soil nutrients in 2.2, re-absorption during senescent turnover in 2.3, updating the target fine-root biomass (the optimal fine-root biomass associated with the plant's nutrient requirements) in 2.6, and allocation to the various plant organs in 2.5. Soil hydrology in ELM is the same as that described in the CLM technical manual (Oleson et al., 2013).

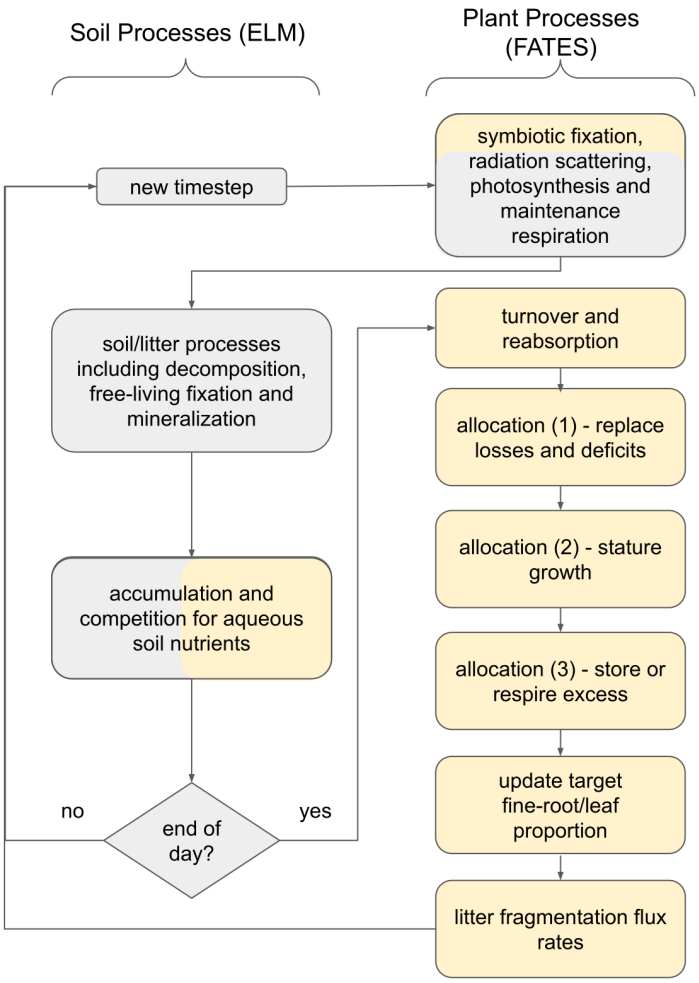

Figure 1. Flow-chart of key processes and order of operations for nutrient cycling in ELM-FATES. This chart places more emphasis on plant-side processes. New processes described in this manuscript are shown in yellow boxes. Grey boxes indicate a pre-existing but relevant processes in the model. For the process of soil nutrient competition, nothing has changed from the original schemes, except how plants present themselves as competitors (shown as with a split grey/yellow color). In the box highlighting symbiotic fixation, scattering, etc., symbiotic fixation is a new process and the others are un-modified.

An overview of the nutrient mass fluxes through the key nutrient pools in the soil-plant system are shown in Figure 2. Also, a list of all variables and parameters described in this manuscript are provided in Appendix A Table A1.

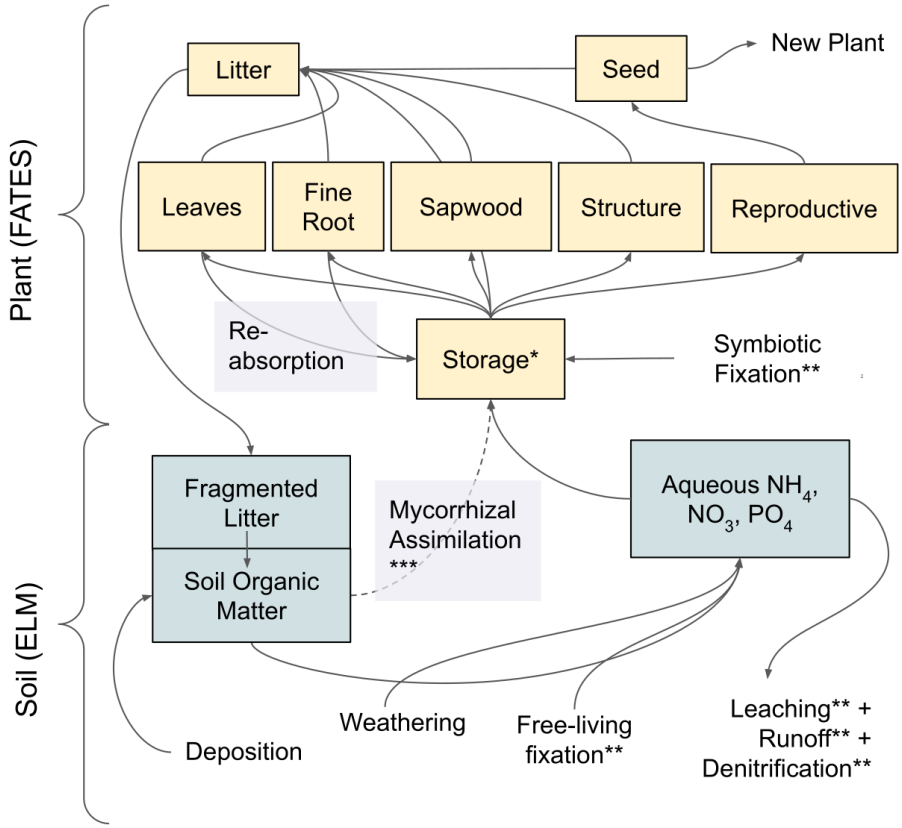

Figure 2. Diagram showing the key pools and fluxes for nitrogen and phosphorus cycling in ELM-FATES. Plant pools are shown with yellow boxes, soil pools are shown with slate colored boxes. Similar to the convention in Figure 1, this conveys new model content, in this case the introduction of nitrogen and phosphorus mass accounting in FATES. *Denotes the special status of nutrient storage, in that storage nutrient pools are distinct from the carbon storage pool. The leaf, fine-root, sapwood, structure and reproductive tissues assume that carbon, nitrogen and phosphorus are bound together in the tissues. **Fixation fluxes only refer to nitrogen. Leaching refers to phosphate and nitrate (not ammonium) and denitrification losses are only from nitrate. ***Myccorhizal uptake is not currently represented in the model, but may be in the future.

Three chemical elements are tracked and conserved by mass within the plant, litter and soil system: carbon (non isotope specific), nitrogen, and phosphorus. The masses of these elements at any given instance in time are designated $C_{(o)}$ for carbon and $M_{(o,s)}$ for the two nutrients elements, where o is the generic subscript for the organs and s is the generic subscript for the two nutrient elements nitrogen and phosphorus.

In the following model description, parameter constants are indicated by lowercase Greek letters. Some variables not associated with a mass use lower-case letters. Unless specified otherwise, fluxes and rates of change use an over-dot (i.e. $\dot{X}$). All plant states have units of [kg plant^{-1}]. Turnover and allocation within the plant occur at a daily frequency. Thus, they have units of [kg plant^{-1} day^{-1}]. Nutrient competition between plants and soil competitors (e.g., microbes, mineral surfaces) is resolved at sub-diurnal timescales

(typically 30 minutes), and is integrated over the day and presented as a daily uptake [kg plant^{-1} day^{-1}].

Each plant cohort is represented by an average individual that maintains discrete mass pools for the following organs (and associated sub-scripts): leaf (lf), sap-wood (sa), dead-wood (de), fine-root (fr), reproductive (re) and storage (so) (see Table 1).

Organ Name	Subscript Symbol
leaf	lf
fine-root	fr
live (sap) wood	sa
dead (structural) wood	de
reproductive	re
storage*	so

Table 1. The plant organs and their subscripts represented in a FATES cohort. *Storage is not technically an organ, but its sum throughout the plant is tracked.

Sapwood refers to all living woody tissues, including organs such as the cambium, phloem, and xylem. Dead-wood refers to all non-living tissues such as heartwood and bark. Both cases (dead and live) include below and above-ground components. The dead pool should not be confused with the coarse woody debris associated with dead trees. Fine-roots are functionally classified as tissues with high turnover and respiration rates, as compared to below-ground sapwood (coarse roots). Reproductive organs encompass all ephemeral tissues associated with reproduction, including seeds, cones, flowers, fruits, etc. For storage, the term "organ" is used loosely because reserves are spatially distributed throughout the plant, often in vacuoles, referring to all forms of C, N, and P that can be re-mobilized for growth or maintenance of other tissues. Carbon storage refers to non-structural carbohydrates of starches and sugars. Storage of N is often comprised of proteins and amino compounds (Millard & Grelet, 2010), whereas phosphate compounds are typical for phosphorus storage (S.-Y. Yang et al., 2017).

Plants represented in FATES can acquire nutrients through several means: 1) uptake of mineral nutrients from soil solution, 2) symbiotic nitrogen fixation, and 3) re-absorption preceding litterfall. In PARTEH, each function is designed to be modular and interchangeable with alternative hypotheses. Here we describe the default options for these uptake processes.

2.1 Acquisition through Symbiotic Fixation

The carbon cost of symbiotic nitrogen fixation is modeled as an obligate (temperature dependent) increase in maintenance respiration (Houlton et al., 2008). Plants that are designated as nitrogen fixers generate a fixation rate $\dot{M}_f$ [kgN plant^{-1} day^{-1}] by respiring carbon r_f [kgC plant^{-1} second^{-1}] at a rate that is a constant fraction $\rho_{f(pft)}$ of all non-fixation fine-root maintenance respiration (Ryan, 1991) (non-growth) costs r_m [kgC plant^{-1} second^{-1}]. This simplification assumes that all resources driving nitrogen fixation are mediated through respiration, and those costs act as a surrogate for other costs such as building and maintaining nodules and feeding specialized bacteria. This represents an obligate strategy because all plants of a Plant Functional Type (PFT) with a nonzero value of $\rho_{f(pft)}$ constantly fix N and incur the respiratory cost of doing so. The representation of facultative nitrogen fixation strategies in FATES is left for future work.

The nitrogen fixation flux is accumulated on each sub-daily time-step (of duration $\Delta t =$ 1800 seconds) over the total steps for the day t_d.

$$\begin{aligned} r_f = &\quad r_m \cdot \rho_{f(pft)} \\ \dot{M}_f = &\quad \sum_{t}^{t_d} r_f n_f \Delta t \end{aligned} \tag{1}$$

The rate of nitrogen fixed per unit carbon respired, n_f [gN gC^{-1}], follows the functional form by (Houlton et al., 2008). Calibrated constants are taken from (J. Fisher et al., 2010) ($a_{f1} = -6.25$) and (Houlton et al., 2008) ($a_{f2} = -3.62$, $a_{f3} = 0.27$, $a_{f4} = 25.15$) and the soil temperature T_{soil} is prognostic variable of ELM.

$$n_f = a_{f1} \left(e^{a_{f2} + a_{f3} \cdot T_{soil} \left(1 - 0.5 \cdot \frac{T_{soil}}{a_{f4}}\right)} - 2 \right) \tag{2}$$

2.2 Plant Acquisition of Aqueous Soil Nutrients

In both supported nutrient competition schemes (CB and RD, see below for details), FATES cohorts compete with other cohorts, as well as microbes and mineral surfaces (for phosphorus) for aqueous nutrients in each discrete soil layer j. (Note that the CB scheme does allow for occlusion of ammonium and nitrate in clay soils) Plants compete for 1) ammonium (NH_4) with decomposer and nitrifier microbes, 2) nitrate (NO_3) with decomposer and denitrifer microbes, and 3) phosphate (PO_4) with decomposer microbes and mineral surfaces.

In the native "big-leaf" vegetation representation in ELM, each functional type competes for nutrients as a group. In contrast, FATES enables many cohorts of different sizes and functional types, all to compete independently for resources with soil competitors (typical cohort counts on a site can number anywhere from tens to more than a thousand, depending on local biodiversity and modeler decisions on how to delineate functional groups and size-similarity). Both CB and RD schemes require each cohort to provide a potential uptake rate, or uptake capacity, for each mineral nutrient species ($\hat{M}_{u,NH_4(j)}$, $\hat{M}_{u,NO_3(j)}$, or $\hat{M}_{u,PO_4(j)}$ units [kg m^{-2} s^{-1}]). The actual net daily uptake flux $\dot{M}_{u(s,j)}$ [kg m^{-2} day^{-1}] results from the competition schemes, which we denote with a generic "competition function" $\Gamma_{c(j,t)}$. The Relative Demand (RD) (P. Thornton et al., 2007) method distributes nutrient uptake to competitors in proportion to their demands. It also provides controls to scale up or down the relative competitiveness of each entity when total mineralized nutrients are less than total demand. If the total demand exceeds availability, all uptake rates are down-scaled to ensure that the scheme does not generate negative soil N and P concentrations. The Capacity Based (CB) (Zhu et al., 2019) method utilizes a Michaelis-Menten approach to estimate the simultaneous uptake of competing entities with half-saturation parameters, and is therefore influenced by the soil aqueous nutrient concentrations. The CB model also accommodates phosphatase dynamics following (Wang et al., 2010). The ELM-FATES modeling coupling does enable these phosphatase dynamics, as well as resulting preferential phosphorus availability to the plants. The exact form of the competition functions and details about the schemes are described in Zhu et al. (2019).

FATES calculates plant growth and allocation on a daily basis, hence, the total daily uptake for each cohort includes the sum of the uptake over each of the total number of

j_s soil layers and sub-daily time-steps (of duration Δt seconds) over the total for the day t_d.

$$\begin{aligned}\dot{M}_{u(N)} &= \sum_{j}^{j_s}\sum_{t}^{t_d}\left(\hat{M}_{u,NH_4(j)}\cdot\Gamma_{c,NH_4(j,t)} + \hat{M}_{u,NO_3(j)}\cdot\Gamma_{c,NO_3(j,t)}\right)\Delta t \\ \dot{M}_{u(P)} &= \sum_{j}^{j_s}\sum_{t}^{t_d}\left(\hat{M}_{u,PO_4(j)}\cdot\Gamma_{c,PO_4(j,t)}\right)\Delta t\end{aligned} \tag{3}$$

The nutrient uptake capacity of a FATES cohort is defined by the per-plant fine-root biomass $C_{(fr)}$ [kg plant^{-1}], the plant density n_p [plants m^{-2}], the fraction of fine-root biomass in each soil layer $f_{fr(j)}$ (see Section Appendix C), and the maximum uptake rate per unit fine-root biomass $\nu_{max(pft)}$. This parameter is unique to each mineral nutrient chemical species (NH_4, NO_3, PO_4) for each PFT represented by FATES [kg kg^{-1} s^{-1}]. Cohort density and fine-root biomass are prognostic variables in FATES.

$$\begin{aligned}\hat{M}_{u,NH_4(j)} &= \nu_{max,NH_4}\cdot C_{(fr)}\cdot n_p\cdot f_{fr(j)} \\ \hat{M}_{u,NO_3(j)} &= \nu_{max,NO_3}\cdot C_{(fr)}\cdot n_p\cdot f_{fr(j)} \\ \hat{M}_{u,PO_4(j)} &= \nu_{max,PO_4}\cdot C_{(fr)}\cdot n_p\cdot f_{fr(j)}\end{aligned} \tag{4}$$

Note that for the RD approach, the nitrate uptake capacity $\hat{M}_{u,NO_3(j)}$ is handled slightly different than equation 4. With RD, uptake for nitrogen happens sequentially. The uptake capacity for ammonium and nitrate are combined, and used to drive uptake first from the ammonium pool. This will fulfill some of the plant's needs, and reduce the joint uptake capacity. The remaining joint uptake capacity is then applied to draw down the nitrate pool.

2.3 Losses and Re-acquisition During Turnover

FATES tracks the daily turnover from senescent tissues on live plants with a carbon loss rate $\dot{C}_{t(o)}$ and nutrient loss rates $\dot{M}_{t(o,s)}$ [kg plant^{-1} day^{-1}] for all non-reproductive plant tissue pools: leaf, fine-root, sapwood, storage, and structural wood, for each cohort. These turnover fluxes are non-episodic, and the rates are controlled by the turnover period parameter $\tau_{(o,pft)}$ [years] associated with the plant's phenological dynamics, which are PFT dependent. The storage, sapwood, and structural wood all share the same turnover rate which is associated with branch-fall. A module that explicitly tracks damage legacies and represents degraded crowns exists (Needham et al., 2022), but is not used here to reduce confounding model factors during analysis.

$$\begin{aligned}\dot{C}_{t(o)} &= C_{(o)}/(365\cdot\tau_{(o,pft)}) \\ \dot{M}_{t(o,s)} &= M_{(o,s)}/(365\cdot\tau_{(o,pft)})\end{aligned} \tag{5}$$

Plants re-absorb a portion of nutrients before leaf and fine-root tissues are shed during senescent turnover. This rate $\dot{M}_{ra(o,s)}$ [kg plant^{-1} day^{-1}] is drawn from the turnover rate, is directed towards plant storage $M_{(so,s)}$, and is removed from the litter mass flux.

There is no re-absorption during fire, and no re-absorption from wood tissues. This re-absorption happens at a constant proportion for leaves $\omega_{lf(s,pft)}$ and fine-roots $\omega_{fr(s,pft)}$ [kg kg^{-1}] specific to each nutrient (N or P) and PFT. Plants with high re-absorption rates will require less nutrient acquired from other sources, and will generate litter with lower nutrient density per unit carbon. A description of how re-absorption rates are estimated is described in Section 3.1.

$$\begin{aligned} \dot{M}_{ra(lf,s)} = &\quad \dot{M}_{t(lf,s)} \cdot \omega_{lf(s,pft)} \\ \dot{M}_{ra(fr,s)} = &\quad \dot{M}_{t(fr,s)} \cdot \omega_{fr(s,pft)} \end{aligned} \tag{6}$$

Litter mass nutrient fluxes from senescent turnover of live plants follow the same proportion rules and constants as carbon for how they are proportioned into the labile, lignin and cellulose litter pools. For more details, see the FATES technical manual (FATES-Development-Team, 2019).

2.4 Definition of Plant Organ Targets

In FATES-PARTEH, plants grow (to the extent possible, as described below) their organs to preserve observationally-constrained allometric relationships. As the plant grows and increases in stature (defined by stem diameter at reference height d), these allometric functions define a target carbon mass for each organ, $\grave{C}_{(o)}$. The plant will always attempt to allocate resources such that mass in an organ matches the target (i.e. replace what has been lost), before it attempts to further grow in stature. The method of defining carbon targets in FATES remains unchanged from (R. A. Fisher et al., 2015; C. D. Koven et al., 2020) for all organs except fine-root. Fine-root mass targets now vary as a function of carbon and nutrient storage. This is a key new model mechanism introduced in this work and is explained in Section 2.6. Details on carbon targets and allometry functions for the other organs can be found in the FATES technical manual (FATES-Development-Team, 2019).

Nutrient targets $\grave{M}_{(o,s)}$ for leaf, fine-root, sapwood, and structural wood seek to maintain a constant stoichiometry (i.e., constant P:C and N:C ratios), defined as parameter constants $\alpha_{(o,s,pft)}$ specific to each plant functional type, element (N or P) and organ.

$$\grave{M}_{(o,s)} = \alpha_{(o,s,pft)} \cdot C_{(o)} \qquad (o = lf, fr, sa, de) \tag{7}$$

Unlike the other organs, the nutrient to carbon ratio of the reproductive tissues and storage ($o = re, so$) are not defined directly by parameter constants. FATES, like many vegetation demography models, does not mechanistically resolve germination or other processes of plants below a minimum recruitment size (Hanbury-Brown et al., 2022); instead it assumes that a fraction of carbon flux allocated to reproduction emerges as new recruits at some time later. We extend this approach to nutrients as well. The stoichiometry of reproductive tissues is set to match the nutrient to carbon ratios of a newly recruited plant (i.e. a plant with the smallest trackable stem diameter $d = d_{min}$). This approach means that only the nutrients that are needed to produce recruits with a known stoichiometry are allocated to reproduction, and represents the optimal reproductive allocation stoichiometry that also satisfies mass conservation. FATES initializes newly recruited plants with no reproductive tissues, and they start "on-allometry" (i.e. when their actual mass matches the allometrically defined target).

$$\alpha_{(re,s,pft)} = \frac{\sum \dot{M}_{(o,s)}}{\sum \dot{C}_{(o)}} \qquad (d = d_{min}, \quad o = lf, fr, sa, de, so) \tag{8}$$

The target nutrient storage $M_{(so,s)}$ is a special case, because it is not associated with a specific tissue. Therefore the target is scaled ($\mu_{(s,pft)}$) based on the target nutrient content of the leaves when "on-allometry". Alternative hypotheses are available for users to test, allowing for storage capacity to scale off of any combination of other organs (e.g., sapwood, fine roots).

$$\dot{M}_{(so,s)} = \mu_{(s,pft)} \cdot \dot{M}_{(lf,s)} \tag{9}$$

2.5 Plant Allocation and Mass Balance Accounting

Both the carbon and nutrient fluxes in the plant and soil systems are mass conservative (i.e. all mass fluxes are accounted for and nothing is created or destroyed). Supplemental nitrogen and phosphorus are often added to the soil in the early years of a spin-up simulation. These effective 'accelerate' the accumulation of nutrient pools in the soil, and the unresolved processes pf primary succession. These fluxes are tracked in the overall balance as well. The FATES code performs mass-balance checks at both plant and landscape (i.e. contains all disturbance history patches in each FATES site) scale every day. The following rules are stated explicitly for nutrients M, but are also valid for carbon C. The sum of daily allocated nutrient $\dot{M}_{a(o,s)}$ over all organs, should equal the difference between the plant's total gains for the day $\dot{M}_{g(s)}$ and losses due to exudation $\dot{M}_{e(s)}$. The total change in mass over the course of the day $\dot{M}_{(o,s)}$ is therefore the difference between what is allocated $\dot{M}_{a(o,s)}$ and lost in turnover $\dot{M}_{t(o,s)}$.

$$\begin{aligned} \sum_o \dot{M}_{a(o,s)} =& \dot{M}_{g(s)} - \dot{M}_{e(s)} \\ \dot{M}_{(o,s)} =& \dot{M}_{a(o,s)} - \dot{M}_{t(o,s)} \end{aligned} \tag{10}$$

For nitrogen, the daily gain $\dot{M}_{g(s=N)}$ includes aqueous uptake $\dot{M}_{u(s=N)}$ and symbiotic fixation $\dot{M}_f$. As per the ELM soil biogeochemistry model, any nitrogen made available by free-living fixers in the soil are assumed to be added directly to the aqueous NH_4 pool, and does not need to be explicitly included in this calculation.

$$\begin{aligned} \dot{M}_{g(s=N)} =& \quad \dot{M}_{u(N)} + \dot{M}_f \\ \dot{M}_{g(s=P)} =& \quad \dot{M}_{u(P)} \end{aligned} \tag{11}$$

The model considers three phases for allocation. In each phase, the mass pool for the daily gain $\dot{M}_g$ is reduced as portions of this mass are transferred into plant organs $M_{(o,s)}$. This phase proceeds sequentially in this order, as described next:

- Phase 1: Replacement of Turnover
- Phase 2: Stature Growth
- Phase 3: Remainder and Overflow

2.5.1 Allocation Phase 1: Replacement of Turnover

In the first phase, replacement of tissues lost to turnover is controlled by a prioritization scheme, whereby a user controlled parameter indexed by plant organ $\delta_{(o)}$ is used to assign priority. Organs with the highest priority have a $\delta_{(o)}$ of 1, organs with the lowest priorities will have larger values of $\delta_{(o)}$. A priority of 1 indicates the organ of interest has the first opportunity, along with other organs with that priority, to replace losses and thus increase the mass of the organ toward the allometric target (turnover losses shift organ masses "off-allometry"). Other organs with incrementally increasing $\delta_{(o)}$ are then allowed to replace losses while there is still mass in the daily gain pool $\dot{M}_g$. The highest priority organs ($\delta_{(o)} = 1$) have some special considerations to how they are applied (see Appendix Appendix B). This flexible scheme reflects persistent uncertainty over the prioritization of allocation by plants and in principle allows rapid hypothesis testing.

The amount of nutrient $\dot{M}_{a(o,s)}$ (or carbon) sent to each organ is driven by the deficit between the actual element mass of the organ and its target mass $\grave{M}_{(s,o)}$. We define a set of organs $\Theta_{1(p)}$ (subscript 1 is for "phase-1" allocation") at priority level p, and the fraction of the total allocation demand that can be filled $f_{a(s)}$ for all organs in this priority level (bounded between 0 and 1). The allocation for each organ is simply its portion of the total replacement demand, scaled by the total replaceable fraction $f_{a(s,p)}$.

$$
\begin{aligned}
f_{a(s,p)} &= \min\left(1, \dot{M}_{g(s)} / \sum_{\Theta_{1(p)}} \max\left(0, \grave{M}_{(s,o)} - M_{(s,o)}\right)\right) \\
\dot{M}_{a(o,s)} &= f_{a(s,p)} \cdot \max\left(0, \grave{M}_{(s,o)} - M_{(s,o)}\right) / \sum_{\Theta_{1(p)}} \max\left(0, \grave{M}_{(s,o)} - M_{(s,o)}\right)
\end{aligned}
\tag{12}
$$

With each successive allocation, mass is removed from the daily gain $\dot{M}_{g(s)}$.

2.5.2 Allocation Phase 2: Stature Growth

If mass remains in all of the daily gain pools ($\dot{M}_{g(s=N)}$, $\dot{M}_{g(s=P)}$, and $\dot{C}_g$) following the replacement phase, the plant will grow in stature. The stem diameter will increase, the target masses of the plant organs (which are tied allometrically to diameter) will increase, and the mass of each organ will increase. All organs grow together as a group, but exceptions can occur for numerical reasons (this is discussed in Section Appendix D). This set of organs that are "on-allometry" are defined as set Θ_2.

The first task is to determine which of the three elements (C, N or P) is in shortest supply and will limit growth. We do this by estimating the mean stoichiometric ratios of the potential new plant growth. Note that to get the relative proportions of new mass allocated to the organs, we evaluate the derivative of the target carbon with respect to change in diameter d, $\frac{d\grave{C}_{(s,o)}}{dd}$, for the organs in set Θ_2, which can be retrieved the from allometric functions at the current stem diameter. The estimated mean stoichiometries (represented by the two summation terms in the brackets to the right of the $M_{g(s)}$ term in Equation 13) are then used to transform the daily nutrient gain into an equivalent carbon $\dot{C}_{g,eq(s)}$ gain.

$$
\dot{C}_{g,eq(s)} = \dot{M}_{g(s)} \left[\sum_{\Theta_2} \frac{d\grave{C}_{(o)}}{dd} / \left(\sum_{\Theta_2} \alpha_{(ft,s,o)} \frac{d\grave{C}_{(o)}}{dd}\right)\right]
\tag{13}
$$

The minimum of the actual carbon gain $\dot{C}_g$ and the two equivalent carbon gain pools $\dot{C}_{g,eq(s)}$ then defines the carbon that is available for stature growth $\dot{C}_{sg}$.

$$\dot{C}_{sg} = \min(\dot{C}_g, \dot{C}_{g,eq(s=N)}, \dot{C}_{g,eq(s=P)}) \tag{14}$$

The carbon fluxes into each plant organ are solved via a set of coupled differential equations, conducted via numerical integration from bounds zero to $\dot{C}_{sg}$ for each organ in set Θ_2. The proportion of carbon gain directed to each organ is defined by the derivative of the diameter-to-mass allometry functions, as a fraction of the sum of all derivatives in set Θ_2. The derivatives of the target masses with respect to diameter $\left(\frac{d\dot{C}_{(o)}}{dd}\right)$ are readily available by differentiating the allometry functions. These are coupled equations because they are all simultaneously drawing down $\dot{C}_{sg}$ together, and the derivatives are continuously changing as they grow.

$$\dot{C}_{a(o)} = \dot{C}_{a(o)} + \int_0^{\dot{C}_{sg}} \left[\frac{d\dot{C}_{(o)}}{dd} / \left(\sum_{\Theta_2} \frac{d\dot{C}_{(o)}}{dd} \right) \right] d\dot{C}_{sg} \tag{15}$$

To handle the allocation of nutrient gains, the same allocation rules from Phase 1 are applied here in Phase 2, using the updated carbon biomass of each organ just explained. Refer to Equations 7 and 12. It should be noted that this modelling hypothesis holds the stoichiometries of plant organs (aside from storage) to the values provided by the parameter constants $\alpha_{(ft,s,o)}$. Small deviations may periodically occur, but they will be corrected automatically by the nature of the algorithm.

2.5.3 Allocation Phase 3: Remainder and Overflow

Daily gain pools ($\dot{M}_{g(s=N)}$, $\dot{M}_{g(s=P)}$, and $\dot{C}_g$) that were not limiting stature growth or replacement may still be available and must be allocated to storage or removed from the plant. Unlike other pools, we allow storage to exceed the target, up to a maximum "overflow" capacity that is based on the target and a user-defined PFT-level parameter constant $\mu_{ov(pft)}$. An overflow flux $\dot{M}_{ov(s)}$ captures this transfer from gains to storage; carbon fluxes follow the same rules as nutrients and are omitted for simplicity.

$$\begin{aligned} \dot{M}_{ov(s)} &= \max(0, \min(\dot{M}_{(so,s)}(1 + \mu_{ov(ft)}) - M_{(so,s)}, \dot{M}_{g(s)})) \\ \dot{M}_{g(s)} &= \dot{M}_{g(s)} - \dot{M}_{ov(s)} \\ \dot{M}_{a(so,s)} &= \dot{M}_{a(so,s)} + \dot{M}_{ov(s)} \end{aligned} \tag{16}$$

If the storage overflow capacity is full and there are still gains (i.e. $\dot{M}_{g(s=N)} > 0$) that have not been allocated, the plant will exude residual nutrient $\dot{M}_{e(s)}$ into the metabolic (i.e. from labile sources, contains no lignin or cellulose) litter pool with vertical profile fluxes proportional to the fine-root density of each soil layer. If excess carbon remains, there are two options to get rid of the excess $\dot{C}_e$. The default method is to burn it off as autotrophic respiration. Alternatively, users can also opt to exude the carbon with the same partitioning rules along with the nutrients. As will be described in the next section, this model features optimization process that seeks to balance uptake of carbon and nutrients, which will also serve to minimize these excesses. This is evaluated in the analysis.

2.6 Dynamic Fine-root Biomass Response

Along with symbiotic relationships with nitrogen-fixing bacteria, plants also modify their network of fine-roots to regulate uptake of mineralized nutrient (Forde & Lorenzo, 2001). Some plant and ecosystem models have utilized this behavior for some time (Thornley, 1995; de Kauwe et al., 2014), and a dynamic fine-root optimization scheme is detailed here as well. This scheme seeks to adjust resource allocation above- and below-ground in order for plant growth to be equally limited by carbon, nitrogen and phosphorus (Bloom et al., 1985). If the resource limitations on growth are balanced, the relative amount of carbon in storage (i.e. mass of carbon currently in storage $C_{(so)}$ divided by the target amount of carbon storage $\grave{C}_{(so)}$) will match the relative amount of nutrient in storage (i.e. mass of nutrient currently in storage $M_{(so,s)}$ divided by target amount of nutrient storage $\grave{M}_{(so,s)}$). Given the high complexity of within-plant signalling mechanisms that govern allocation and growth of leaf and root tissues, we do not try to mechanistically represent these processes, and instead aim to tractably represent with as few parameters as possible the net effects of these mechanisms via the optimality-based approach developed here.

We quantify a plant's carbon to nutrient balance with the term f_{cn}, see Equation 17. The term is calculated for the two nutrient elements and takes the maximum, which represents the nutrient with lowest relative storage. A natural log transform is applied for several reasons: 1) the metric becomes centered on zero, where carbon limited plant is less than and a nutrient limited plant is greater than zero, 2) by not being a ratio, it can be averaged and/or smoothed, and 3) enables additive properties in the algorithm that optimizes fine-root (explained below).

$$f_{cn} = \ln\left(\max_{s}^{N,P}\left[\frac{C_{(so)}/\grave{C}_{(so)}}{M_{(so,s)}/\grave{M}_{(so,s)}}\right]\right) \tag{17}$$

Fine-root biomass is living tissue that both respires (where maintenance respiration r_m is a function of mass, nitrogen concentration in the tissue, and temperature, following (Ryan, 1991)) and requires continual replacement of losses. An increase in fine-root mass will therefore result in more respiration and lower carbon use efficiency per unit leaf area, but it will also increase capacity for acquiring mineralized nutrients in the soil (recall Equation 4). This is visualized in Figure 3. Thus, positive values of f_{cn} will drive fine-root growth, and negative values of f_{cn} will drive fine-root reductions.

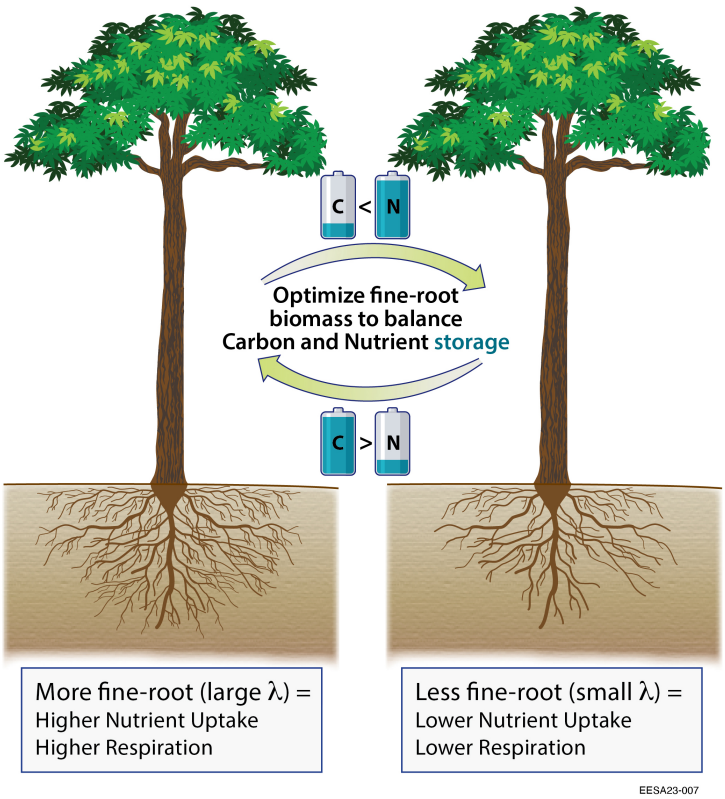

Figure 3. Visualization of the dynamic interaction between differential carbon-nutrient storage and fine-root growth. A plant (left) with proportionally more fine-root will tend to have decreased carbon allocation and increased nutrient allocation, than a plant (right) with proportionally less fine-root. The algorithm presented here seeks to balance these allocations through modifying fine-root growth. Illustration by Diana Swantek, Lawrence Berkeley National Laboratory.

In the FATES allometric model, the fine root target is defined by its proportionality λ with target leaf biomass $\grave{C}_{(lf)}$. The target leaf biomass is defined by the plant's allometry (function of diameter), for details see the FATES technical manual (FATES-Development-Team, 2019).

$$\grave{C}_{(fr)} = \lambda \cdot \grave{C}_{(l)} \tag{18}$$

In previous versions of FATES, the proportionality λ between leaf and fine-root was a constant user specified parameter. Here, we create an algorithm where it is allowed to be dynamic, and it's value is optimized to result in a differential carbon to nutrient storage f_{cn} that tends towards zero. This system of carbon and nutrient regulation is summarized in Table 2.

condition		root response		plant response
high/positive f_{cn}	$\rightarrow$	$\lambda\uparrow$, $C_{(fr)}\uparrow$	$\rightarrow$	$r_m\uparrow$, $\dot{M}_u\uparrow$, CUE $\downarrow$
low/negative f_{cn}	$\rightarrow$	$\lambda\downarrow$, $C_{(fr)}\downarrow$	$\rightarrow$	$r_m\downarrow$, $\dot{M}_u\downarrow$, CUE $\uparrow$

Table 2. Table describing the plant's response to the f_{cn} storage metric. Relatively high and positive f_{cn} drives increases in the fine-root bimoass target, which drives increases in fine root biomass, which results in higher respiration (lower carbon use efficiency CUE) yet increased uptake. The reverse is true for low and negative f_{cn} status (ie proportionally high nutrient).

In early iterations of developing this hypothesis, we found that a linear model between λ and f_{CN} was prone to over and undershooting an optimal solution, leading to oscillations of λ in steady state climate conditions. To suppress the oscillatory behavior, we included the temporal derivative of f_{CN}. With this, the methodology became a reduced form of a Proportional Integral Derivative (PID) "control-loop" system. In this particular example, f_{cn} is the "process variable" which is driven by a "set-point" (λ). PID controllers also contain an integral term along with the proportion and derivative term. Each of the three terms is given a scaling coefficient, see Equation 19. The calibration of the controller is discussed further in Section 3.3.

$$\lambda_t = \lambda_{t-1} + K_{p(pft)} f_{cn} + K_{i(pft)} \int f_{cn} dt + K_{d(pft)} \overline{\frac{df_{cn}}{dt}} \tag{19}$$

2.7 Software Features

The processes described here are encoded in a modular and extensible software structure. It is modular because the software for the plant algorithms do not reference data structures from the FATES (or other) model and uses a lightweight coupler to communicate with FATES. This approach allows the plant model to be ported to any terrestrial biosphere model that uses a cohort or individual plant type of scaling approach. It is extensible because the software is written so that other configurations of plant organs (e.g. leaf spatial layering, storage pools with different functions, mycorrhizae, etc) and chemical elements (e.g. Potassium, Magnesium, etc) can be readily adapted, if the user can provide relevant parameter constants and the surrounding terrestrial biosphere model can accommodate the boundary fluxes. Further, the FATES model code that processes litter fluxes has been written to loop over the self-describing data structures for the chemical elements present (instead of explicitly defining new variable primitives for each mass pool or flux associated with a chemical species).

3 Model Calibration and Evaluation

An evaluation of the new model mechanics is performed via simulations at the Smithsonian Tropical Research Institute's Barro Colorado Island (BCI) site in Panama. The BCI site is conducive to evaluating a nutrient enabled terrestrial biosphere model because it has an extensive 100 year history of ecological monitoring and analysis in areas including forest demography and census (Condit et al., 2017), growth and mortality (Wright et al., 2010), plant allometry (Martínez Cano et al., 2019; Cushman et al., 2021), nitrogen fixation (Wieder & Wright, 1995; Batterman et al., 2013), litter and soil biogeochemistry (Mirabello et al., 2013; Yavitt et al., 2011; Yavitt & Wright, 2001; Powers et al., 2005) and many more. It also stands out among tropical monitoring sites for

the long (> 30 year) and quality controlled meteorological data that is used to drive the FATES model (Patton, 2019a, 2019b, 2019c, 2019d; Faybishenko et al., 2018).

Over the course of our analysis, we found that evaluating both nitrogen and phosphorus dynamics simultaneously expanded our scope beyond what can be covered in one manuscript. We therefore decided to focus solely on evaluating nitrogen limitations, given the following considerations: 1) the model mechanics for phosphorus within the plant are almost exactly the same as with nitrogen with the exception of different parameter constants; 2) nitrogen has a more complicated representation in the model because it has two soil mineral pools and can be fixed by the plant; and 3) there is a companion paper evaluating phosphorus dynamics at a different site (Wei et al. in prep). While previous research at Barro Colorado Island has found phosphorus and potassium limitations to vegetation growth (Wright et al., 2011), we still find this an excellent site to evaluate the model mechanics in a carbon-nitrogen framework. This is because of wealth of previously mentioned observations at the site, and also that previous experiments with FATES are available to provide a solid calibration basis (C. D. Koven et al., 2020). Further, the objective here is not to make predictions, but rather determine if the model can capture pattern responses in a test-bed that has realistic parameter constraints and boundary conditions.

Turning off phosphorus limitations is straightforward and achieved by 1) providing a supplementation term that feeds phosphorus directly to soil decomposers, plants, and mineral surfaces so that their nutrient demands are completely met and 2) using a plant uptake affinity parameter $\nu_{max(s=P)}$ that is excessively efficient (large). This results in the plants ignoring phosphorus effects on the fine-root biomass optimization, acquiring more than enough phosphorus for growth requirements and therefore releasing the excess back to the soil and litter.

3.1 Initial Parameter Calibration

A set of model parameter constants derived from previous research were used as a basis for investigating the sensitivity and function of newly introduced parameters. C. D. Koven et al. (2020) performed a parameter sensitivity analysis of the pre-existing carbon-only ELM-FATES at BCI, where they generated an ensemble of 576 parameter combinations to explore model response to twelve plant traits. Their model output was retrieved and compared at different size classes to measurements of growth increment (centered at 7.5, 12.5 and 40cm), mortality rate (centered at 5.5 and 30 cm), and integrated total basal area (< 30 cm, < 70 cm and all) (Condit et al., 2017). Only two size classes were used for mortality (compared with 3 for basal area and growth increment), to compensate for fewer data points (observations) associated with mortality. Scalar values of leaf area and gross primary productivity (GPP) were also compared (Ely et al., 2019). This totals 10 values that can be compared: 10 = 2 size classes of mortality + 3 size classes of basal area + 3 size classes of growth increment + 1 for leaf area and + 1 for GPP.

For each ensemble member i and each of these 10 comparison points (subscript j), a difference between the observed and modeled $x_{(i,j)}$ were aggregated to a single fitness metric ϵ_i for each ensemble member, by summing the difference squared between the modeled and observed variables, divided by the variance of the difference across across ensembles. The parameter set associated with the simulation that minimized the fitness metric was used as a basis for simulations described here, a comparison of that parameter set with data is provided in Figure 4.

$$\Delta x_{(i,j)} = x_{obs(j)} - x_{(i,j)}$$
$$\epsilon_{(i)} = \sum_{j} \left(\Delta x_{(i,j)}\right)^2 / \sigma_{\Delta x_{(j)}} \tag{20}$$

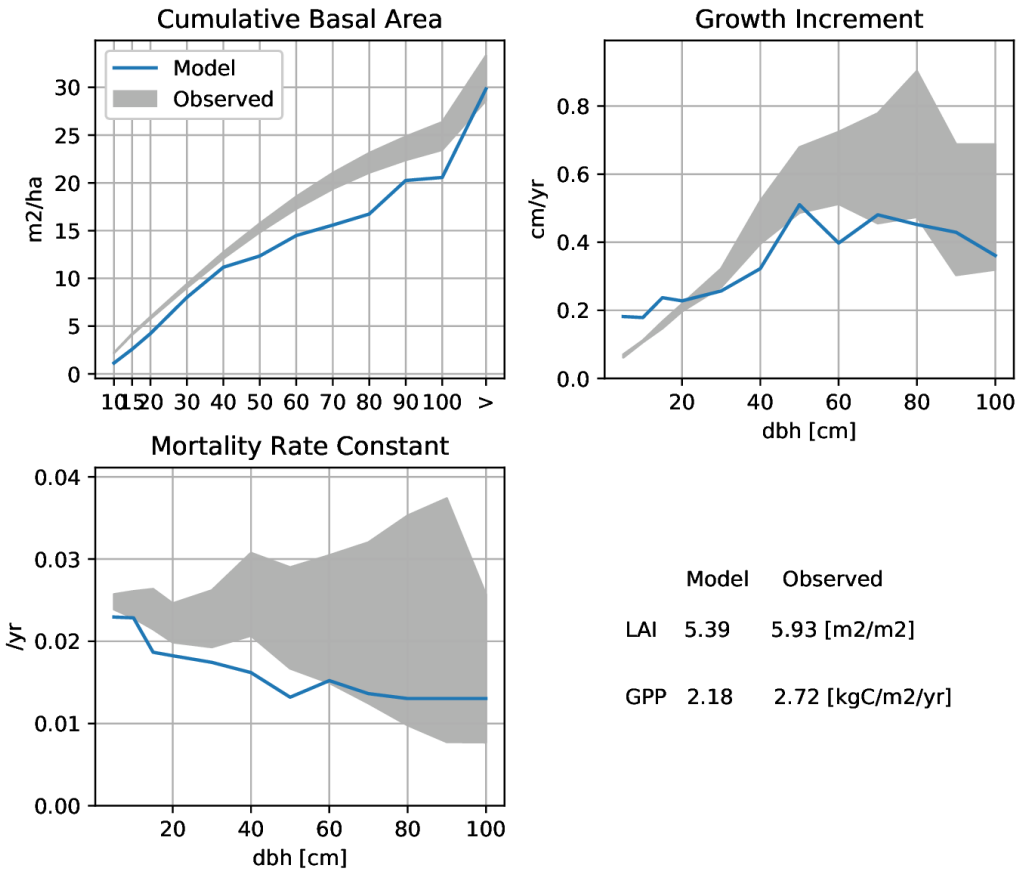

Figure 4. Comparison of observations with the most optimal ELM-FATES parameter set from the ensemble of simulations generated in (C. D. Koven et al., 2020).

Some of the parameters described in Table A1, organ stoichiometries $\alpha_{o,s,pft}$ and organ turnover rates $\tau_{o,pft}$, are also derived from the optimization of output (C. D. Koven et al., 2020). For nutrient enabled simulations, there are several new parameter constants that must be estimated. The methods for estimating the parameter constants for this study are explained here:

$\omega_{lf(N,pft)}$ Leaf re-absorption fractions are set at 0.45, and are derived from measurements of leaf litter and live on-tree leaf stoichiometries at BCNM (unpublished dataset provided by S Joseph Wright).

$\omega_{fr(N,pft)}$ Evidence of root re-absorption of N and P is sparse, but has been observed in extratropical sites(Nambiar, 1987; Freschet et al., 2010). It is also believed that

if roots do not actively retranslocate nutrients before senescent turnover, some portion of nutrient in the newly made root litter will be made available for plant uptake by mycorrhizae. We assume a 0.25 fine-root re-absorption fraction of nitrogen on senescence. Given this uncertainty, this modeling framework could be used in further studies to better understand the sensitivity of different re-absorption assumptions on ecosystem response.

$\delta_{(o)}$ We assign leaves and fine-roots the highest replacement priority, followed by storage and then sapwood and structural wood. We view other prioritization groupings as alternative modeling hypotheses that can be explored in further study.

$\mu_{(N,pft)}$,μ_{ov} The parameter that controls the size of the nitrogen storage target $\mu_{(N,pft)}$, and how much storage overflow is allowed μ_{ov} is explored in experiment IV (see Table 3 and Section F2). Understanding plant nutrient storage is a difficult, but there is some thought that plants store enough nutrient for seasonal use (Millard & Grelet, 2010). As a base assumption, for all other experiments, we assume the overflow is 100% of the target, and target nitrogen storage is 1-times the size of total nitrogen bound in leaf tissues.

$\rho_{f(pft)}$ The maintenance respiration surcharge fraction for obligate symbiotic dinitrogen fixation is explored in experiment VII (See Table 3 and Section 3.5. Symbiotic fixation is turned off in all other experiments, and total ecosystem fixation is used as a surrogate in those cases.

$\nu_{max(N)}$ Nitrogen uptake efficiency was viewed as a model calibration parameter, and not something directly determined via field measurements. Although calculations based on field inventory data provided a rough starting point. A spectrum of uptake efficiencies were tested and model output was evaluated for basal area comparable to field observations (30 m2 ha^{-1}). For relative demand soil competition mechanics, this resulted in a base value of $\nu_{max(N)} = 5e^{-9}$ [gN gC^{-1} s^{-1}]. Sensitivity is evaluated in experiment VIII. The capacitance based competition nutrient scheme has a much smaller actual/potential uptake ratio due to a different algorithm, and thus we arrived at higher values of $\nu_{max(NH4,NO3)} = 1.75e^{-7}$. Further details are provided in Experiment IX.

$K_{p(pft)}, K_{i(pft)}, K_{d(pft)}$ The calibration and sensitivity of the PID scaling parameters are covered in Experiment I and II (see Table 3 and Section 3.3).

3.2 Description of Experiments and Simulations

We conduct a series of experiments to elucidate the model's behavior and parameter spaces that focus on nutrient dynamics. A list of the experiments and the simulations used in each is provided in Table 3.

Some simulations are "spin-ups". In these simulations, FATES vegetation is initialized with saplings (if more than 1 plant-functional type is present, the abundances are equal). For the first 30 years of the simulation, nitrogen is added to the soils to accommodate the potential uptake capacity of the plants and microbes that is not met by the existing aqueous nitrogen in the soil (i.e. nitrogen limitations are removed from all competitors). After this 30 year phase, nitrogen then accumulates in the system through the natural mechanisms of deposition and fixation (fixation is the dominant input in the system and evaluated further). The modeled decomposition process in this phase uses increased rate constants (often referred to as Accelerated Decomposition (P. E. Thornton & Rosenbloom, 2005)). The atmospheric CO_2 concentration in spin-ups is fixed at pre-industrial levels (290 PPM). Eventually, the nitrogen and carbon content of the soils reaches an equilibrium, as the vegetation evolves towards a mature demographic (quantified by a steady basal area distribution across size and functional types) and the litter fluxes from the vegetation reaches a steady state.

The objective of several spin-up simulations were to provide an initial-condition for industrial-era simulations with transient CO_2 concentrations. In those, we determined

that the spin-ups had reached steady-state because the log of the absolute value of Net Biome Productivity had reached very small values (approx 10^{-4} [kgC m^{-2} $year^{-1}$]) (C. Koven et al., 2013).

Industrial-era simulations used normal (un-accelerated) decomposition rate constants, initialized size and age structure of vegetation from preceding spin-up simulations, and likewise initialized organic soil C and N pools using a multiplier of the values passed in from the preceding spin-up simulations. In some experiments where simulations were evaluated into the future, CO_2 concentrations follow from scenario SSP2-4.5.

All simulations utilized the 13-year (2003-2016) meteorological record from Faybishenko et al. (2018) to provide ELM-FATES with rainfall, down-welling solar radiation, down-welling thermal radiation, atmospheric pressure, humidity, wind-speed and surface temperature. The simulations were all much longer than the meteorological record, so the forcing was looped. Most experiments made use of the relative demand competition scheme, solely because this approach is mathematically and conceptually simpler, which is helpful in probing the complexities of the plant dynamics it is coupled with. The final experiment uses the capacitance based scheme because it was effective at maintaining aqueous soil nutrient pools under high demand from competitors, as well as to see if its dynamics were sensible and coupled correctly.

Experiment	Description	Competition Scheme	Period Period	Section Section
I	Single cohort simulations for controller sensitivity	RD	150 year spin-up	3.3
II	Competition based controller calibration	RD RD	1000 year spin-up	3.3
III	Evaluation of base parameterization	RD RD	500 year spin-up + 300 year industrial-era	3.4
IV	Sensitivity to storage capacity	RD	500 year spin-up	F2
V V	Sensitivity to sub-module hypotheses	RD	500 year spin-up	F3
VI	Sensitivity to free-living fixation hypotheses	RD	500 year spin-up + 300 year industrial-era	F4
VII	Evaluation of competition between symbiotic fixers and non-fixers	RD	500 year spin-up	3.5
VIII	Evaluation of interplay between uptake efficiency ($\nu_{max(N)}$) and soil N availability	RD	500 year spin-up + 300 year industrial-era year industrial-era	3.6
IX	Evaluation of fine-root biomass estimates against field data	CB	500 year spin-up + 300 year industrial-era	3.7

Table 3. List experiments, a brief description, the ELM nutrient competition scheme used (Relative Demand RD or Capacitance Based CB), the simulations periods used for each, and the section.

3.3 Experiments I and II: Controller Calibration

The three terms in the PID control system serve distinctly different functions. The proportion term serves to push the process variable back towards its target value ($f_{cn} = 0$) when there is a large difference between the current and target value. The derivative term serves to promote stability by suppressing rapid change in the process variable. The

integral term is most useful in reducing small and/or persistent biases between the process variable and its target; as the bias grows over time it will exert greater influence to change the set variable. In testing the PID controller and exploring all three terms, we were able to achieve stable results without the integral term, so we decided to set it's scaling constant K_i to zero for this study.

This system of nutrient cycling is fairly complex, with many plant and soil actors competing for and cycling resources, all amongst changing meteorological conditions. The plants are not experiencing a steady availability of nutrients for acquisition, and thus the relationship between controller set point (root proportion λ) and the process variable (storage ratio f_{CN}) are continually experiencing perturbations. To reduce the impact of these perturbations in destabilizing the control system, we apply a multi-day smoother to the derivative term. We use simple exponential smoothing where the future smoothed value X_{t+1} is updated by the instantaneous value Y, the previous smoothed value X_t and a weighting factor D synonymous with the number of time-points (days) over which to weight the instantaneous variable: $X_{t+1} = X_t \cdot (1 - 1/D) + Y \cdot (1/D)$. In the experiments described here, we apply an $D = 10$ day smoother. We also tested 5 and 20 day smoothing windows. Ultimately, reasonable controller response was found with all windows depending on the strength of the scaling constants.

In Experiment I, special reduced complexity simulations were conducted over a two dimensional log-scale grid search of the K_p and K_d terms from Equation 19. These reduced complexity simulations turned off recruitment and disturbance, which resulted in a simulation of a single plant cohort over a 100 year life-cycle trajectory. Each simulation was assessed for the variance and mean of the process variable $f_{CN(N)}$ (Figure 5), leaf to fine-root biomass multiplier λ (set point, Figure F1) and growth increment (an indicator of optimization of resource use, Figure F2).

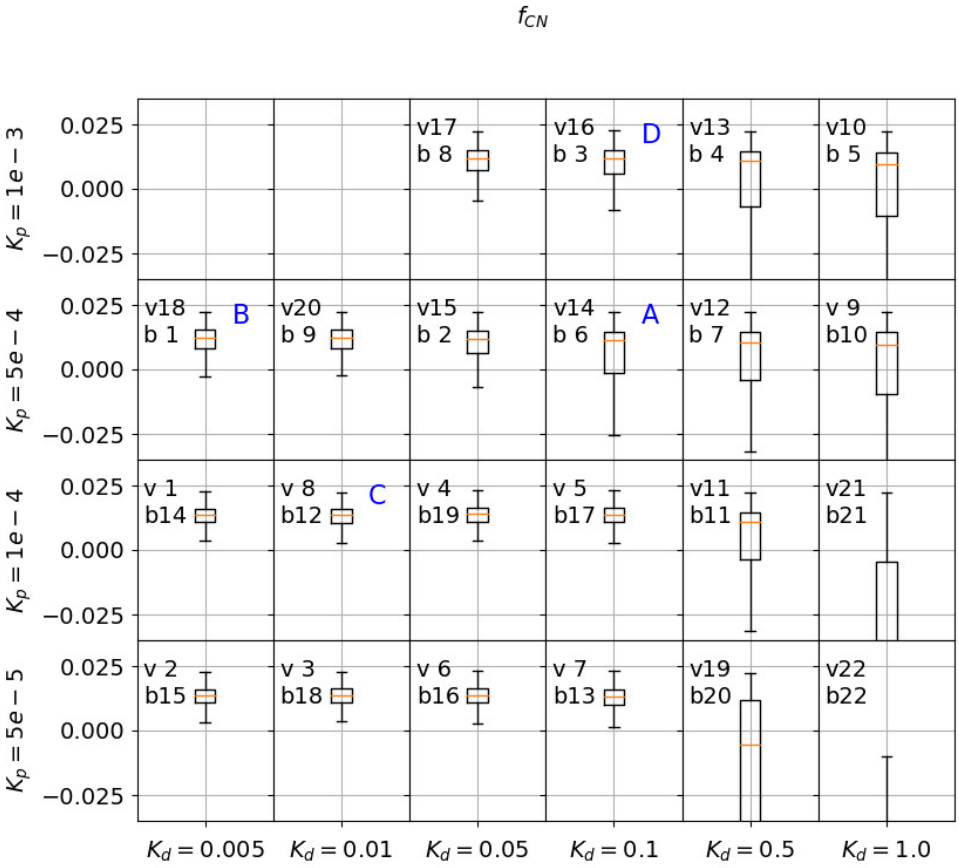

Figure 5. Mean and variance of the relative storage of carbon to nitrogen variable (and Proportion Integral Derivative controller process variable) $f_{CN(N)}$, over a range of proportion and derivative controller settings. The values next to "v" and "b" indicate the ascending rank of each parameter couplet for bias and variance. Test v1 and b1 had the lowest variance and biases. Couplets designated A,B,C and D are used in the follow-up simulation.

The grid search shows that the model simulations are stable and viable (i.e. the plants survive and can adequately adapt their root sizes to become productive) over a large range of parameters (> 2 orders of magnitude each). However in Experiment II, to determine which parameters offer a solution that is most in line with the optimality-based idea that underlies this approach, we create a simulation with four different functional types of plants that compete against each other for resources. A comparison of their basal area trajectories, and the root proportion λ of newly recruited plants in open and exposed sunlight are shown in Figure 6. The plant functional types have the same parameters (i.e., traits) and initial seedling density (this is a spin-up style simulation) with the exception of different PID controller constants. These parameter couplets are labeled A, B, C, and D in Figure 5.

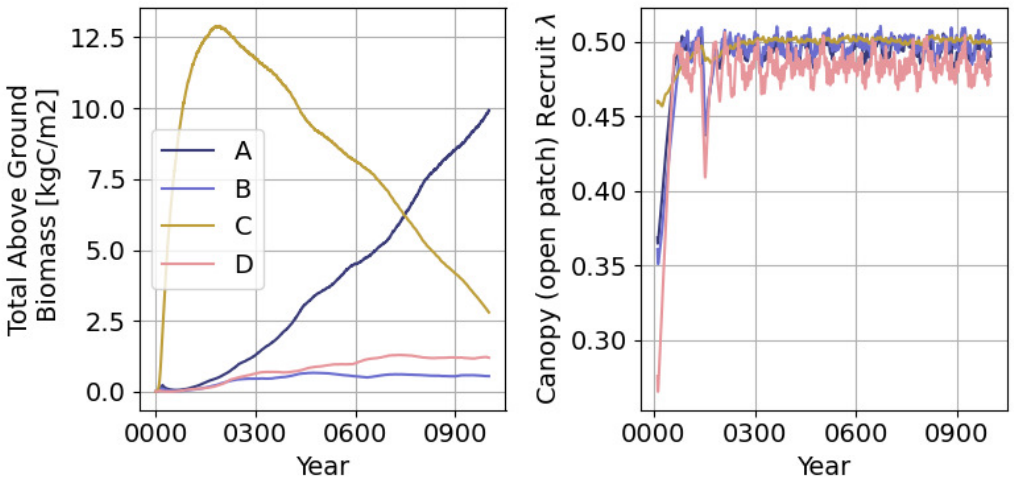

Figure 6. ELM-FATES spin-up simulation output containing four competing plant functional types, labeled A-D. These four PFTs have identical traits and parameters, with the exception of their propotion and derivative PID parameters. The values of their PID parameters are provided in 5. The right hand panel shows the mean root proportionality λ term for the different PFTs for open patch recruits. Patches that are open, do not have closed canopies and thus light availability to recruits. Recruit λ values are shown to avoid any differences associated with differences in size structure.

The result of Experiment II shows that the "C" PID parameter couplet was most effective at rapidly adjusting to the competitive resource environment and homing in on a reasonable λ value fairly quickly (see right panel of F1), thus initially occupying the canopy. The "B" and "D" parameter couplets, while not dominating during any phase, persisted through the simulation. The "A" PID parameter couplet eventually out-competes "C" to dominate the canopy, and was ultimately chosen as a default set of PID constants moving forward. The complex competition and coexistence dynamics of the four different parameter couplets prompts the question as to whether the responsiveness of a plant to adjust to nutrient and carbon needs is a part of how plants navigate and find niches in the multidimensional coexistence space, and this responsiveness might align with other traits that determine successional dynamics.

3.4 Experiment III: Towards an Optimality-Based Root Allocation Model

In experiment III, a single spin-up style simulation is conducted, using a single plant functional type, and the base set of parameters. The purpose of this experiment is to view the emergent stand structure of the simulated vegetation under the new nitrogen constraints and fine-root biomass optimization algorithm.

In Figure 7, size-structured estimates of Basal Area, Above Ground Biomass, and the leaf to fine-root proportion term λ partitioned into canopy and under-story plants, are projected across time. All plots show the signature of the spin-up simulation, where over the course of 400 years the trees grow into the larger size classes from saplings.

By the completion of the simulation, there is a fairly uniform distribution of basal area across size classes. There is also a signature of inter-annual variability at any given size. This feature emerges due to the internal dynamics of the cohorts, as similar cohorts fuse together, and grow from one size-classification to a larger one. Other simulations

(not shown) were conducted that removed the inter-annual meteorological signal by looping a single year of data, and similar patterns emerged there as well. AGB dynamics are similar but with more strongly weighted towards larger trees, as they contain a greater proportion of the ecosystem-level biomass than basal diameter.

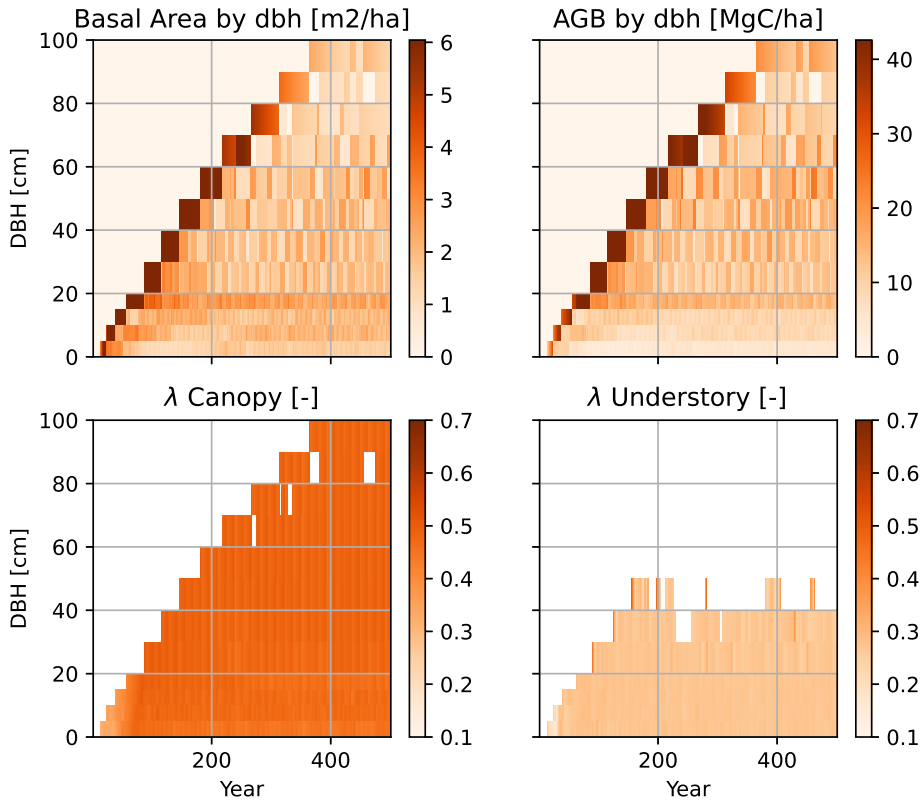

Figure 7. Evaluation of the size structure of vegetated biomass accumulation, and the size and canopy position structure of the fine-root proportion term λ [gC fine-root gC$-$1 leaf]. Canopy plants display distinctly larger λ values than understory plants at similar size classes.

Notably, the λ values in the canopy plants are distinctly and consistently larger than those in the understory. Canopy plants have greater access to light and have increased primary productivity compared to their understory neighbors. This increased productivity places a greater demand on nitrogen acquisition to keep pace with more rapid construction of plant tissues. Moreover, the increased productivity of the canopy plants provides adequate carbon reserves to pay for the increased respiration associated with more fine-root biomass. Plants that are in the understory have limited access to light and subsequently lower productivity. Without the carbon to build new tissues there is a correspondingly lower demand on nutrients to match the construction costs of the carbon. This potentially triggers a response in the plant to decrease investments (respiration costs of fine-roots) in the acquisition of nutrients it doesn't need.

The massive biological diversity of tropical forests is often associated with a multidimensional competition space. Different species allocate their resources into different

organs and traits, features that maximize their success in different niches. A classic example is the growth versus mortality trade-off (Wright et al., 2010). There are examples of species at BCI that bide their time in the understory for many years without growth, and then accelerate growth when light conditions change. This difference in strategy between understory and canopy plants is captured in ELM-FATES, and demonstrated by decreased proportions of fine-root biomass λ in understory plants.

3.5 Experiment VII: Incorporating Cohort-Scale Symbiotic Fixers

In Experiment VII, we test if the symbiotic nitrogen fixation module can generate an expected ecosystem response. One way to test this is to see if a nitrogen-fixing plant functional type can coexist with a non-fixing functional type in simulation. In this experiment, the two plant functional types have the same traits with the exception of the symbiotic fixing parameters themselves. This test is a simple proof of concept, and ignores the multifaceted trait space that fixers and non-fixers may occupy.

By introducing symbiotic fixation to the simulation, the pre-existing total ecosystem fixation scheme (Cleveland et al., 1999) must be modified to only represent free-living fixation. This approach is similar to the approach used by CLM5 (Lawrence et al., 2020), which identifies that the original total ecosystem fixation rates estimated in Cleveland et al. (1999) projected low and high ranges of fixation. Here, we downscale the NPP-derived total ecosystem nitrogen fixation rate by a multiplicative scaling factor of 0.2.

For plants to achieve co-existence in this model configuration, the unit cost of symbiotic fixation must be higher than the uptake of aqueous nitrogen at its potential rate (i.e. uptake when aqueous nitrogen is abundant and no source side limitation exists), yet must be lower than aqueous uptake under some amount of limitation. Otherwise, symbiotic fixers would always be more efficient and out-compete non-fixers, not only when nitrogen from the mineralized soil pool is limited. Menge et al. (n.d.) has made this type of argument, pointing out that the energetic costs of breaking the triple bonds in N_2 and supporting the nodules in symbiotic fixers are thought to be costly. The expectation is that the two functional types will reach an equilibrium in their relative proportion, where the symbiotic fixers will support a mineralized nitrogen pool to an amount where the carbon costs of actual plant nitrogen uptake balance with that of fixation.

In ELM-FATES, we assess the unit carbon efficiency [gN gC^{-1}] (inverse of cost) for potential mineralized nutrient acquisition, as the sum of the potential uptake rate of the plant $\nu_{max(NH4,pft)}+\nu_{max(NO3,pft)}$ [gN gC^{-1} s^{-1}] (for RD based competition), divided by the maintenance respiration and replacement costs of the roots [gC gC^{-1} s^{-1}]. Note this is the steady state rate, and ignores the initial cost to grow the root. The unit cost of fixation is directly quantified by Equation 2, (Houlton et al., 2008; J. Fisher et al., 2010). In the base parameterization, the carbon efficiency for potential mineralized uptake was lower than the fixation efficiency. We found that by increasing the total potential uptake rate $\nu_{max(NO3)} + \nu_{max(NH4)}$ and increasing the fine-root lifespan $\tau_{(fr)}$ from 1 to 4 years, the potential mineralized uptake efficiency exceeded that of fixation, see Figure 8.

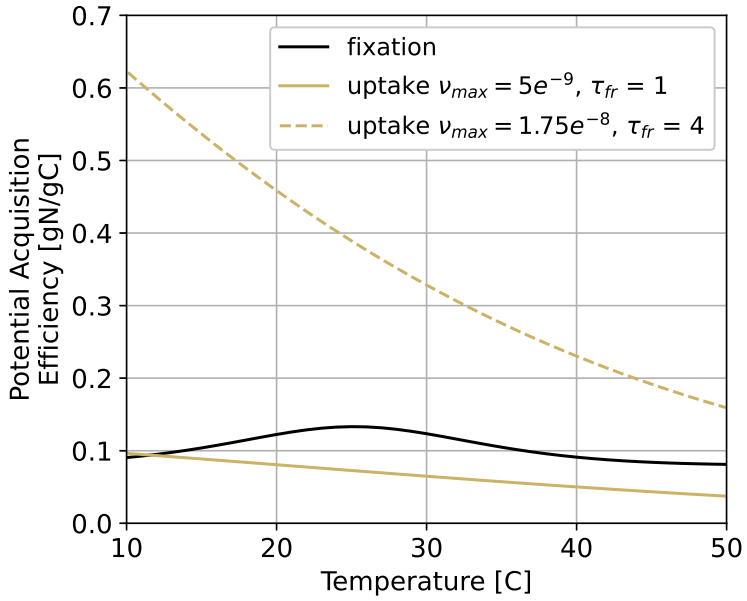

Figure 8. Comparison of the unit carbon efficiency for obligate symbiotic fixation (Houlton et al., 2008; J. Fisher et al., 2010) versus potential aqueous nitrogen uptake under the base parameterization and one with increased efficiency. Carbon costs for uptake efficiency consider maintenance respiration and replacement carbon costs, but not the initial investment.

The result of the test simulation is shown in Figure 9. The symbiotic-fixing PFTs were set to apply a 10% surcharge on fine-root maintenance respiration to fuel symbiotic fixation. This experiment also reduced the external N supplementation period from 30 to 5 years, to ensure that the symbiotic fixers had more control over the system N supply.

Fixers and non-fixers do show coexistence as demonstrated by their total aboveground biomass. The fixers have lower fine-root biomass fractions λ, which indicates their decreased need for mineralized nitrate and ammonium. Very early in the simulation, the non-fixers are more efficient due to the plentiful mineralized soil nitrogen. But after the supplementation period, plant mineralized nitrogen uptake becomes more limited (see bottom right panel), which then creates a competitive opportunity for the fixer PFT to emerge.

As a whole (considering both PFTs), symbiotic fixation accounted for about 5-10% of total plant acquisition, and slightly more than 50% of the total nitrogen fixed by the ecosystem (including free-living). The latter is roughly close to what is expected, Batterman et al. (2013) suggested that symbiotic fixation was the dominant mode of introducing nitrogen to the site at BCNM, but within the same order of magnitude. The proportion in the simulation could be increased by further regulating uptake efficiency parameters or scaling down the free-living fixation rate. There are also different symbiotic fixation temperature response functions available (Bytnerowicz et al., 2022), and future ELM-FATES testing may use these.

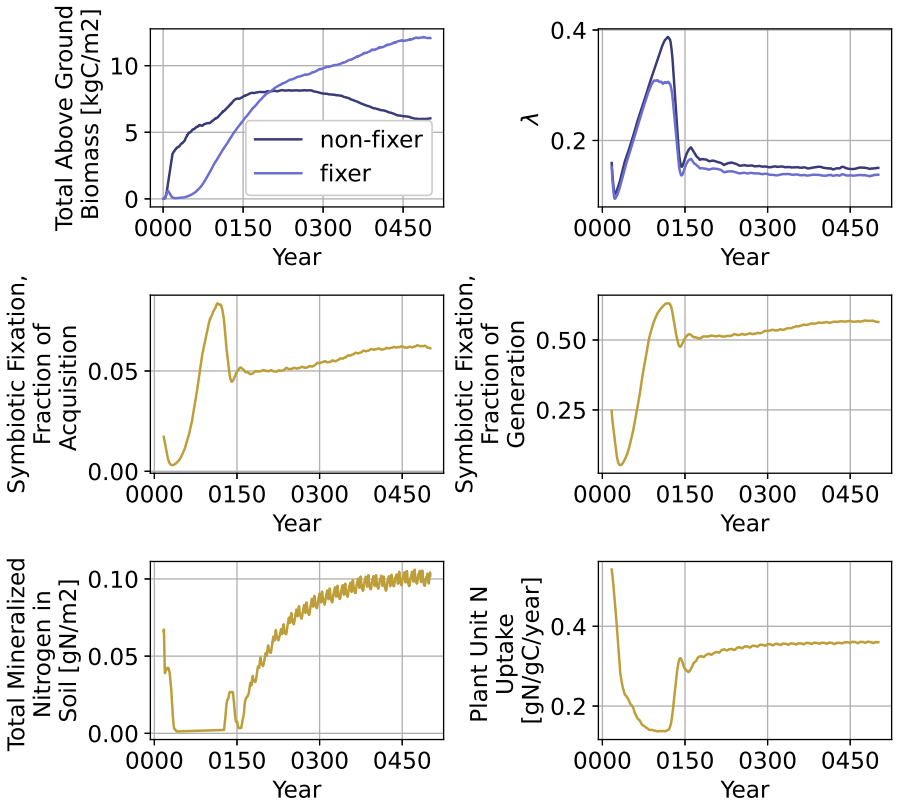

Figure 9. ELM-FATES simulation with coexistence between a fixer and non-fixer plant functional type. The symbiotic fraction of acquisition, refers to the fraction of plant acquisition that is from symbiotic-fixation, along with mineralized nutrient uptake. The fraction of generation looks at the relative contribution of symbiotic fixation to total nitrogen fixed by the system, also considering free-living fixation.

It takes about 500 years in this simulation for the fixer and non-fixer types to reach an equilibrium. Yet, the results are an average of the whole landscape, and not a representation of how a single plot of land recovers from a disturbance. Batterman et al. (2013) estimated that symbiotic fixation peaked near the first decade following a disturbance, but after several decades total fixation flux dwindled considerably. This suggested that symbiotic fixers play an important role in developing the nutrient environment in newly disturbed lands, but perhaps they became less competitive as the nitrogen built up in the soil and vegetation over time. The ELM-FATES model does have the ability to simulate disturbance and discretely track land of different ages (called "patches") and the plants that inhabit them. However in the current version of the model, the soil column and its biogeochemistry (i.e. nitrogen and phosphorus concentrations in all forms) are the same across patches of all ages, as the patch structure only represents heterogeneity in the aboveground environment. In future versions of the model it would be interesting to see if the competitive dynamic of symbiotic fixers and non-fixers can be achieved over the time-scales of decades where each patch has a dedicated nutrient environment in the soil.

3.6 Experiment VIII: Sensitivity to Parameter Constants that Control Nutrient Availability and Affinity

Experiment VIII tests model response to the intersection of three forces: nitrogen availability, plant nitrogen use efficiency and increasing atmospheric CO_2 concentration. Nitrogen use efficiency is modified by perturbing the plant functional parameter constant: unit potential nitrogen uptake rate per mass of fine root (efficiency) $\nu_{max(pft,N)}$ [gN gC^{-1}]. High values of $\nu_{max(pft,N)}$ (highly efficient) will acquire more nitrogen for less fine-root carbon. Nitrogen availability is controlled by applying a constant multiplicative scaling coefficient β to the NPP-based total ecosystem fixation function. The β parameter is not listed in Table A1, and is not considered a component of this model because existing total ecosystem fixation schemes were used in this manuscript and the scaling coefficient is only used here to test sensitivity. Four parameter combinations are provided in Table 4.

	low plant uptake affinity	high plant uptake affinity
low fixation	$\nu_{max(N)} = 5e^{-9}, \beta = 0.5$	$\nu_{max(N)} = 2.5e^{-8}, \beta = 0.5$
high fixation	$\nu_{max(N)} = 5e^{-9}, \beta = 2.0$	$\nu_{max(N)} = 2.5e^{-8}, \beta = 2.0$

Table 4. Parameter combinations for the four simulations in Experiment VIII. Each simulations used perturbations to only nitrogen acquisition efficiency $\nu_{max(pft,N)}$ and a scaling coefficient on total ecosystem fixation β. The red (compared to blue) indicates a higher nitrogen availability in the system. The darker shade (compared to lighter) indicates a higher plant uptake efficiency.

In all four simulations, there are several patterns that offer straightforward explanations. Increased productivity associated with higher CO_2 concentrations drive higher basal area (biomass) and leaf area, as well as increased demand on nitrogen acquisition to meet greater organ construction costs. Mineralized (aqueous) nitrogen depletes over time, as the new additions to the system (fixation) can not keep pace with the increased uptake. Faced with a greater need for (higher production) and a reduced supply of aqueous nitrogen, the plants respond by increasing uptake capacity by building more fine-roots (λ). With decreased aqueous nitrogen and higher root mass, the unit uptake of nitrogen per unit biomass decreases. The increase in CUE experienced by the plants is diminished (and mostly reversed) when the mineralized nitrogen pools fully deplete, and the plants are forced to respire newly assimilated carbon that cannot be used to build tissues.

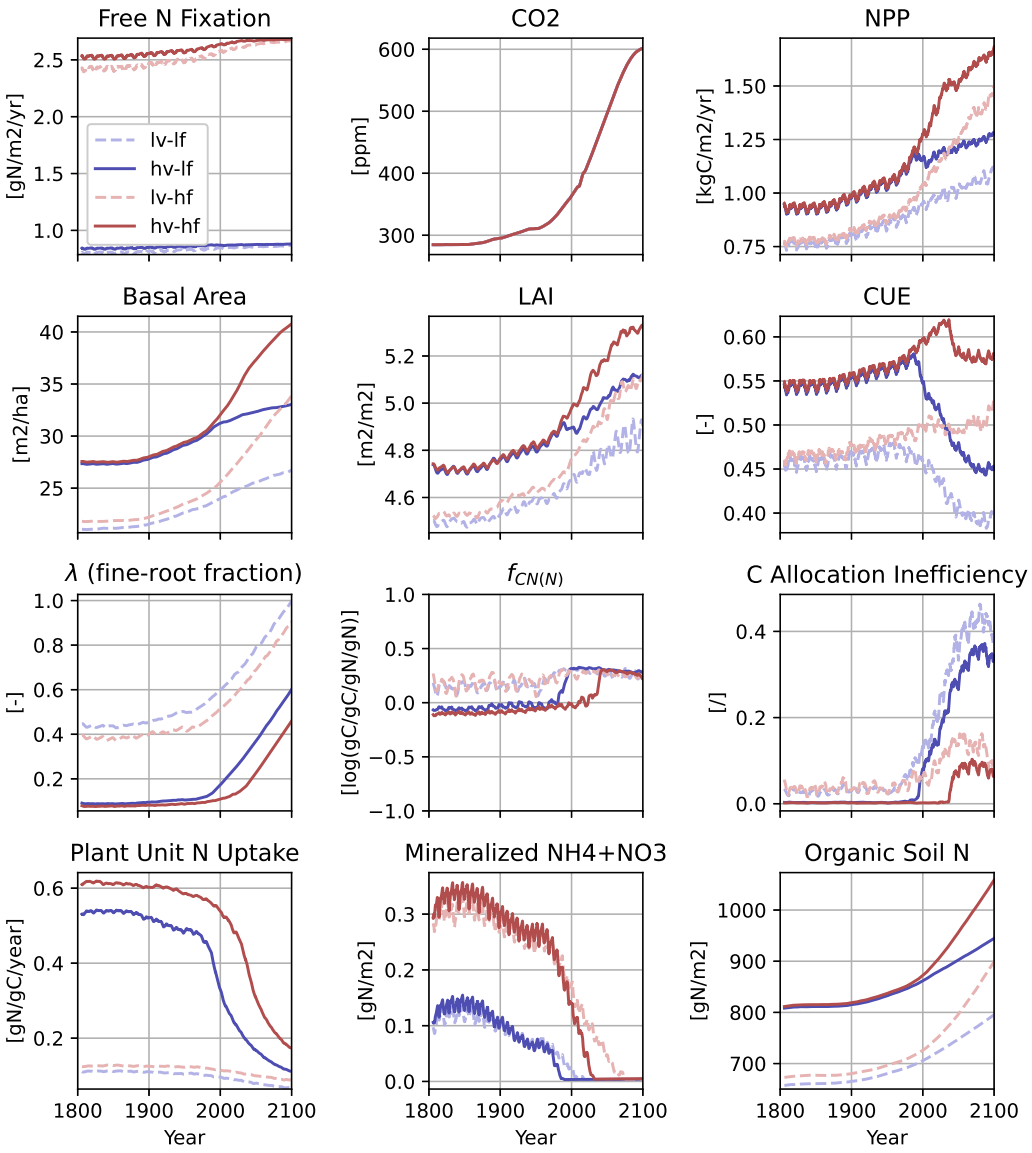

Figure 10. Time series model output for the four simulations described in Experiment VIII. Line colors match simulations described in Table 4, where: "lv-lf" is low-affinity low-fixation, "hv-lf" is high-affinity low-fixation, "lv-hf" is low-affinity high-fixation and "hv-hf" is high-affinity high-fixation". The CO_2 forcing signal uses observed industrial-era concentrations and follows the SSP2-4.5 scenario prediction to 2100. With no symbiotic fixation, Free N Fixation is synonymous with total fixation and is the primary source of nitrogen input. Carbon use efficiency (CUE) is the ratio of net primary production over gross primary production, where NPP accounts (i.e. subtracts) for any extra respiration of "excess carbon", that which couldn't be allocated due to nitrogen limitations. This extra respiration is also captured by "C Allocation Inefficiency", the fraction of grams of excess carbon burned per grams NPP. Plant Unit N Uptake refers to the grams of nitrogen uptake per gram of fine-root carbon.

Some patterns in the response are explainable, but less straightforward. Mineralized nitrogen depleted first in the low availability simulations, and also slightly earlier

in the high versus low affinity simulations. This suggested that plants can be overly competitive for nitrogen, ultimately to their detriment. In simulations with higher uptake affinity, the plants out-competed decomposers, which prevented the decomposers from mineralizing nitrogen into the system, which leads to a slightly earlier collapse.

Another interesting pattern was the shift in the process variable $f_{CN(N)}$, from unbiased (i.e. closer to 0) to a bias indicative of a perpetually nutrient limited state. In the high affinity case, the algorithm attempts to rectify the bias by increasing the λ value, however the slowly dwindling supply of aqueous nitrogen continually counteracts the affect that increased fine-root fraction (set variable) should have on the process variable. This raises the question: what is the appropriate time-scale of response for investing in plant nutrient uptake? In these simulations, the PID constants that control λ were chosen for competitiveness in a constant CO_2 environment, but perhaps a parameterization that favors more rapid adaptability would be more competitive in a changing CO_2 environment.

3.7 Experiment IX: Comparison of Fine-root Biomass Estimates with Field Observations

The objective of this experiment is to see if the new model formulation generates quantities of fine-root biomass comparable with observations in the field. In preliminary model simulations, estimated fine-root biomass was relatively low compared to observations. Decreasing nutrient uptake efficiency ν_{max} did generate larger fine-root proportions, however we learned from Experiment VIII that the increased respiration costs that come with higher root proportions also suppress net productivity and generated forests with less biomass.

There are various plant physiological model parameters that can be perturbed to increase carbon availability, in coordination with the decrease in nitrogen uptake efficiency. We chose to increase a parameter that directly impacts carbon assimilation, $V_{c,max}$ (catalytic capacity of Rubisco), from 30.9 to 55. And in increased a parameter that directly impacts carbon use efficiency, $\tau_{(fr)}$ (fine-root turnover timescale) from 1 to 3 years. We chose these because they were simple, powerful and directly related to net carbon acquisition.

Model output is compared to observed profiles by Yavitt et al. (2011), Yavitt and Wright (2001) and Powers et al. (2005) at BCNM (fig. 11). While the model captures the relative shape of fine-root biomass as a function of soil depth, the comparison shows us that the tendency of the model in this parameterization is to underestimate fine-root biomass. We discuss potential causes of the observed differences, and the interplay between carbon productivity, nutrient uptake efficiency and total nutrient availability in the following discussion.

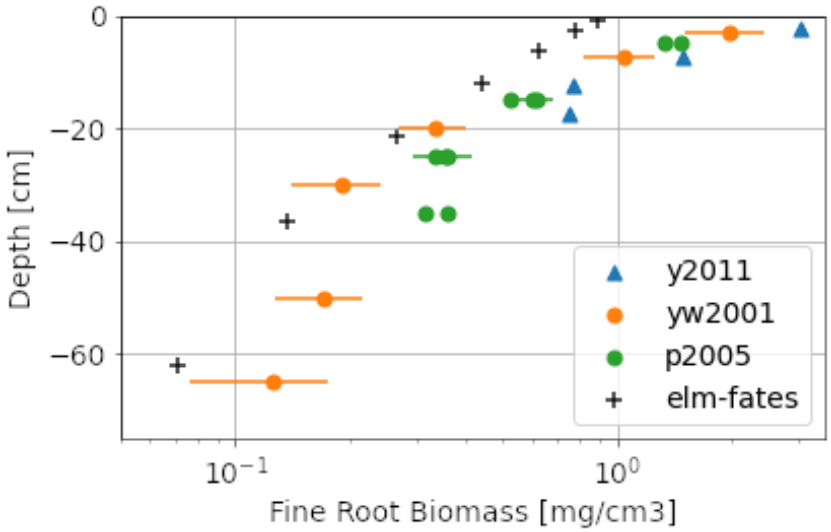

Figure 11. Comparison of ELM-FATES predicted fine-root biomass against observations at BCNM by Yavitt et al. (2011) (y2011), Yavitt and Wright (2001) (yw2001) and Powers et al. (2005) (p2005). All data was filtered to report only estimates of live roots from 0-2 mm diameter. Studies that did not differentiate between live and dead roots were corrected using the necromass to livemass ratio of 0.0806 (Yavitt & Wright, 2001). Data points with circles represent measurements on Barro Colorado Island, data points with triangles are on the other side of the river on the Gigante Peninsula.

4 Discussion

4.1 Regulation of Nutrient Uptake

There are multiple avenues plants employ to regulate nutrient acquisition, which include the fine-root growth response and obligate symbiotic fixation described in this manuscript. Yet the uptake of nutrient by plants harbours complexity, including modification of not just fine-root biomass, but morphology and structure (e.g., Taylor et al. (2014)), considerations of advection and diffusion (e.g., McMurtrie and Näsholm (2018)), symplastic and apoplastic transport (Steudle & Peterson, 1998), enzyme kinetics, symbiotic relationships with facultative nitrogen fixers, algal nitrogen fixation on leaves, mycorrhizal associations and moreover acquisition of other nutrients not considered here (K, Ca Mg, etc).

Employing dynamic fine-root response to nutrient gradients has both an established history in observation (Forde & Lorenzo, 2001) as well as model development (Thornley, 1995; Farrior et al., 2013; de Kauwe et al., 2014). This method differs from the Thornley models in how fine-root growth is controlled, where they tracked the substrate (C and N) concentrations in the roots and shoots dynamically. So while it is clear that certain plants do modify fine-root growth in response to nutrient availability, the signaling and what underlies these controls is less understood.

Several models also down-regulate mineral nutrient uptake in a more facultative form, outside of signaling increases or decreases in fine-root biomass (Thornley, 1995; Kou-Giesbrecht et al., 2021b; Thum et al., 2019; Zhu et al., 2019). Thornley (1995) called this downregulation product inhibition, and based it on N concentrations in the roots. Kou-Giesbrecht et al. (2021b) identified it as nitrogen stress, and tied it to the deficit of actual to target non-structural nitrogen content in the plant. Thum et al. (2019) also

downregulates uptake based on "internal-demand" which also assesses the labile (non-structural) nutrient content in the plant against the nutrient content of roots and leaves. The ELM-FATES nutrient cycling model does not include this facultative downregulation, for two reasons. The first is that it was not clear how to represent this economically by associating a cost to this regulation. Secondly, an imperative was placed on minimizing the accumulation of parameters with the interest of using nutrient limitations in global simulations and their calibrations.

Looking towards future model development and hypothesis testing of active acquisition, uptake capacity could be associated with dynamic activity levels of the fine roots, as well as the amount of fine-root biomass or their surface area. While many of these processes about to be mentioned are implicitly captured in the work presented here, through maximum uptake capacity of roots and the Michaeles Menten half-saturation constants, their explicit representation could be illuminating. For instance, dynamic activity could be described as enzymatic activity rates, which are tied to nutrient content, the production of exudates to prime decomposition (via mycorrhizae for instance) or to chelate nutrients, and/or the construction of specific infrastructure necessary for transferring nutrient across the root surface. This activity could be controlled explicitly by resource investments from the plant (e.g. respiration, carbon and nutrient allocations) and constrained (albeit not explicitly governed or proportional to) by fine-root surface area. Root nutrient uptake could be made more realistic by considering the diffusion and mass transport of nutrients in the soil, root surface area and root architecture using the model of McMurtrie and Näsholm (2018).

A plant-hydraulics model would likely make water transport of nutrients to the root surface more accurate. Further, the fine root allocation approach presented here does not consider the dual need for roots to provide both nutrients and water to plants, and thus future work will develop this allocation model to optimize both water and nutrient delivery. For instance, the FATES-HYDRO model evaluates fine-root surface area, hydraulic gradients between root surfaces and the soil and the conductivity across those gradients to drive water fluxes to and across the fine-root surfaces. FATES-HYDRO also has a basic representation of root structure that could support developments of the McMurtrie model.

This model formulation has not explicitly incorporated mycorrhizal activity or its affects on nutrient availability. In a sense, the effects of mycorrhizae are implicit or subsumed in the soil decomposition and nutrient competition schemes. However, without explicitly representing mycorrhizae, it is impossible to capture the symbiotic benefits of the association with the plants alone, and not just the broader affects of releasing mineralized nutrient to the soil system. It would be interesting to incorporate and test hypotheses of explicit mycorrhizal interactions, and their effects on nutrient cycling. In summary, ELM-FATES-CNP uses the processes of fine-root biomass growth and maintenance as a surrogate for representing a broader and more complex set of functions related to nutrient acquisition and regulation. Simulating a more complex plant response to nutrient uptake needs may also be more consistent with phenomena observed at BCNM, as fine-root biomass response to nitrogen fertilization is insignificant compared to that of potassium (Yavitt et al., 2011).

However calibration and uncertainty in earth system simulators has become an ever increasing challenge as all facets of the models steadily become more complex, with more tune-able parameter constants and greater process uncertainty. It was imperative that this formulation struck a balance between the desire to represent numerous complex processes and the desire to have a stable model that uses a reasonably small number of parameter constants (particularly those that cannot be directly retrieved from measurements). Without these concessions, terrestrial biosphere models cannot be extended beyond a handful of measurement-rich testbed sites.

In light of this, field experiments that uncover the when and why's associated with different modes of nutrient uptake regulation, their relative impacts on plant nutrient budgets, as well as the signaling from the plants that govern would be valuable.

4.2 Fine-roots at the Nexus of Productivity, Resource Availability and Acquisition Efficiency

Potential nutrient uptake in ELM-FATES is dictated by the amount of fine-root biomass and the maximum uptake rate parameter family ν_{max}, recall Equation 4. As demonstrated in Experiment VIII, small (inefficient) values of ν_{max} drive larger fine-root proportions (λ), and large (efficient) values of ν_{max} drive smaller fine-root proportions λ. The response of λ was also impacted by total system nutrient availability (tested in Experiment VIII by scaling total N addition to the system via community N fixation), and how carbon productive the plants are (See pertubation to catalytic capacity of Rubisco $v_{c,max}$ in Experiment IX). This model has shown an interplay between the processes of how carbon productive and efficient plants are and how nutrient productive and efficient plants are. The fine-root biomass is a manifestation of these processes, and ideally this would make a great point of model calibration.

In theory we could continue to decrease the uptake efficiency parameter ν_{max} until we achieve comparable estimates of fine-root biomass. This can not be done in isolation, as to support more fine-root biomass with a similar stand-structure, the plants would need greater productivity and would require a holistic calibration exercise that also looks at net carbon productivity parameters, such as those controlling organ turnover rates, respiration rates and gross primary productivity. However, we take the comparison of fine-root biomass with field data (see Figure 11) with a grain of salt, and see it more as a rough guide than a validation point. There are several reasons for this. Firstly, we have made the point that the representation of fine-root biomass in this model, and it's response, is a surrogate for other processes (and their associated carbon costs) that are not represented and would harbour increased complexity and uncertainty.

The second point, is that there is a difference between how the FATES model differentiates a fine-root from other tissues, and how fine-roots are differentiated in the field. FATES has a functional definition, and differentiates fine-roots as tissues that respire at a higher rate than coarse root or below-ground sapwood. Also FATES makes no differentiation of absorbing versus transporting fine-root tissues, or how how those tissues respire, turnover or impact nutrient cycling (McCormack et al., 2015). All fine roots are treated as absorbing tissues for the purposes of nutrient uptake. At the same time, the model applies a single fine-root lifetime for the purposes of calculating the costs and benefits of fine root allocation. Alternatively, fine-roots are typically differentiated in the field by size (diameter) and order (Iversen et al., 2017), and efforts to reconcile fine root biomass and ^{14}C isotopic ratios have demonstrated two distinct populations of fine roots with widely-varying turnover times (Gaudinski et al., 2010; Ahrens et al., 2014). In this respect, there is somewhat of a disconnect between the meaning of fine-root represented in the model and how fine-roots are currently conceptualized to influence plant and ecosystem function. However making a stronger better aligned comparison between what the model defines as fine-root, or what sub-classifications it has, and what is measured in the field, would be useful for verification and calibration. In future work, we intend to represent different fine root functional populations and associated turnover times to better represent the joint constraints of nutrient uptake rates, root biomass profiles, and root ^{14}C isotopic ratios.

5 Conclusions

The series of experiments presented here has demonstrated that this model framework can generate sensible patterns of ecosystem response, using a modest parameter

constant calibration effort. To summarize: 1) a small grid search of PID constants K_d and K_p rendered values that enable the model to adapt stable fine-root biomasses with reasonable levels of nutrient and/or carbon efficiency losses, 2) perturbations to parameters that control nutrient storage μ,μ_{ov} did not exert undue model instability or variability, and 3) subtle differences in how the model culls unnecesary roots and removes unused carbon showed modest differences in model output. The number of newly introduced and salient (to nutrient cycling) model parameters that aren't readily derived from field meausurements (i.e. stoichiometry α, and leaf reabsorption ω_{lf}) that exerted strong control on model response is small (namely, ν_{max}). Balancing model complexity with model robustness and preventing over-calibration is of critical importance and has been identified as a key need in land-surface modeling endeavors (Prentice et al., 2015).

The new model hypothesis captures a few simple yet important concepts. Nutrient acquisition requires resources and that the construction of plant biomass is limited by the acquisition of nutrients. In this case, the payment is the maintenance respiration, construction and turnover replacement cost of the fine-roots. The current model hypotheses can also work with existing hypotheses in free-living and symbiotic nutrient fixation. Finally, the dynamicism of fine-root proportion allows for a new competitive niche, where understory plants have a new method to conserve resources when there is low access to light and productivity.

Appendix A Table of Variables and Parameters

Symbol	Description	Units
State Variables		
$C_{(o)}$	carbon mass	[kg]
$\grave{C}_{(o)}$	target carbon mass	[kg]
$M_{(o,s)}$	nutrient mass	[kg]
$\grave{M}_{(o,s)}$	target nutrient mass	[kg]
d	reference stem diameter	[cm]
λ	leaf to fine-root target biomass multiplier	[-]
f_{cn}	the relative storage of carbon over the relative storage of nutrient, for the maximum (more limited) of nitrogen and phosphorus	[-]
External and Diagnostic Variables		
f_{trim}	canopy trim fraction	[-]
n_p	the number of plants in a cohort per square meter	[plants m^{-2}]
$f_{fr(j)}$	the fraction of fine-root biomass in each soil layer	[kg kg^{-1}]
Fluxes		
$\hat{M}_{u,NH4(j)}$	plant ammonium uptake capacity in each soil layer	[kg m^{-2} s^{-1}]
$\hat{M}_{u,NO3(j)}$	plant nitrate uptake capacity in each soil layer	[kg m^{-2} s^{-1}]
$\hat{M}_{u,POx(j)}$	plant phosphate uptake capacity in each soil layer	[kg m^{-2} s^{-1}]
$\dot{M}_{u(s)}$	daily uptake of mineralized soil nutrients in solution	[kg day^{-1}]
$\dot{C}_g$	daily carbon gain	[kg day^{-1}]
$\dot{M}_{g(s)}$	daily nutrient gain	[kg day^{-1}]
$\dot{M}_f$	daily nitrogen gained through symbiotic fixation	[kg day^{-1}]
$\dot{M}_{e(s)}$	excess nutrient exuded back to soil	[kg day^{-1}]
$\dot{C}_{t(o)}$	daily carbon lost to turnover	[kg day^{-1}]
$\dot{M}_{t(o,s)}$	daily nutrient lost via turnover	[kg day^{-1}]
$\dot{M}_{a(o,s)}$	daily nutrient net allocated	[kg day^{-1}]
$\dot{r}_e$	excess respiration of unusable carbon	[kg day^{-1}]
$\dot{r}_f$	respiration cost to fix Nitrogen	[kg day^{-1}]
Parameter Constants		
$\alpha_{(o,s)}$	nutrient stoichiometric target for non-labile tissue, nutrient mass per carbon mass	[kg kg^{-1}]
$\tau_{(o,pft)}$	non-mortal turnover timescale of plant organs	[years]
$\omega_{lf(s,pft)}$	* leaf re-absorption fraction of nutrient on turnover	[kg kg^{-1}]
$\omega_{fr(s,pft)}$	* fine-root re-absorption fraction of nutrient on turnover	[kg kg^{-1}]
$\mu_{(s,pft)}$	* proportion of target nutrient stored per target nutrient in tissues	[kg kg^{-1}]
μ_{ov}	* fractional overflow of storage (all chemical species) the plant will hold before exuding or respiring	[-]
$\rho_{f(pft)}$	* maintenance respiration surcharge fraction for obligate symbiotic dinitrogen fixation	[-]
$\nu_{max(s)}$	* maximum nutrient uptake demand per fine-root biomass	[kg kg^{-1} s^{-1}]
$\delta_{(o)}$	* allocation priority	[index]
$K_{p(pft)}$	* proportion term scaling parameter in PID controller	[-]
$K_{i(pft)}$	* integral term scaling parameter in PID controller	[-]
$K_{d(pft)}$	* derivative term scaling parameter in PID controller	[-]

Table A1. Non exhaustive list of variables and parameter constants in the FATES nutrient cycling model. All mass and mass fluxes are assumed to be "per plant" [$plant^{-1}$]. External variables refers to those variables that are resolved by FATES processes outside the scope of this manuscript and are described in the FATES technical manual. Parameter constants denoted with * are newly introduced in this study. PID stands for proportion integral derivative, and is the controller used to search for optimal fine-root biomass.

Appendix B Special Plant Organ Allocation Priority Levels

During the first phase of plant nutrient and carbon allocation, where allocation seeks to replace losses due to continuous turnover (i.e. maintenance replacement), different organs can have higher replacement priority $\delta_{(o)}$ than others.

Priority level $\delta_{(o)} = 1$ has special status. Similar to previous carbon-only versions of FATES (C. D. Koven et al., 2020; R. A. Fisher et al., 2015). Organs at this level are allowed to draw from storage to replace a fraction of their replacement needs. The model will first attempt to use the daily gains and will resort to using storage if daily gains are not available. This allows for different species of plants to have more or less aggressive strategies.

Priority level $\delta_{(o)} = 2$ also has special status, and is reserved solely for replacement of storage. Please refer to the FATES technical manual.

In this study, we follow an organ prioritization similar to previous FATES model studies, where leaves and fine-roots are given the highest priority level (level 1), storage is given second priority, sapwood is the third, and structural wood is the fourth priority

Appendix C Vertical Fine-root Profile

The vertical attenuation of the fine-root fraction follows a two parameter exponential scaling model based on the depth of the upper (z^+) and lower (z^-) edge of the layer (Oleson et al., 2013). This fraction sums to unity and has no bearing on how much fine-root is present. The mass of fine-root is defined by allometric equations and the growth model (both described later).

$$f_{fr(j)} = 1/2 \left(e^{-7 z^+_{(j)}} + e^{-z^+_{(j)}} - e^{-7 z^-_{(j)}} - e^{-z^-_{(j)}} \right) \tag{C1}$$

Appendix D A Note About Growth Allocation and Numerical Integration

As mentioned earlier, it is typical that during the second phase of growth and allocation "stature growth", all organs will be "on-allometry" as indicated by their masses being equivalent to the allometrically derived target mass for the plant's diameter. It is possible that some organs, due either to the process of cohort fusion (see FATES technical manual) or numerical integration truncation, will not have masses that exactly match the target. In other words, the scheme will slightly overshoot or undershoot the target mass. These differences are both very small, and immediately corrected in this scheme, preventing the mass of the organs from drifting away from the allometric targets (in situations where the plant is not in carbon deficit). This self correcting methodology is part of the existing carbon-only FATES model as well. Organs that have less mass than their target will be corrected on the next day's Phase 1 allocation, see the "max" functions in Equation 12. Organs that have masses larger than their target are exempt from Phase 2 allocation, and will be re-added to the list of organs in later iterations when the other organ masses have caught-up. That is why the set of organs $Theta_2$ does not always match the total set of non-reproductive organs.

The numerical integration can be handled by either an adaptive Euler or an adaptive Runge-Kutta-Fehlerg 4/5 integration scheme. Because the numerical integration errors (either overshooting or undershooting the target mass of an organ) have relatively small consequence due to the self correcting nature of the scheme, we therefore default

to the Euler integration scheme in all FATES allocation integrations, and retain the RKF4/5 for experimental purposes.

Appendix E Complementary analysis of the carbon-only model calibration phase

Measurements published by Ely et al. (2019) on leaf N:C ratio and SLA were used to filter the set of model simulations in C. D. Koven et al. (2020), by imposing that only simulations with parameter sets that fell within the 15-85 percentile bounds, see Figure E1. The histograms of other key carbon-only model parameters in C. D. Koven et al. (2020) ensembles are also shown, see Figure E2.

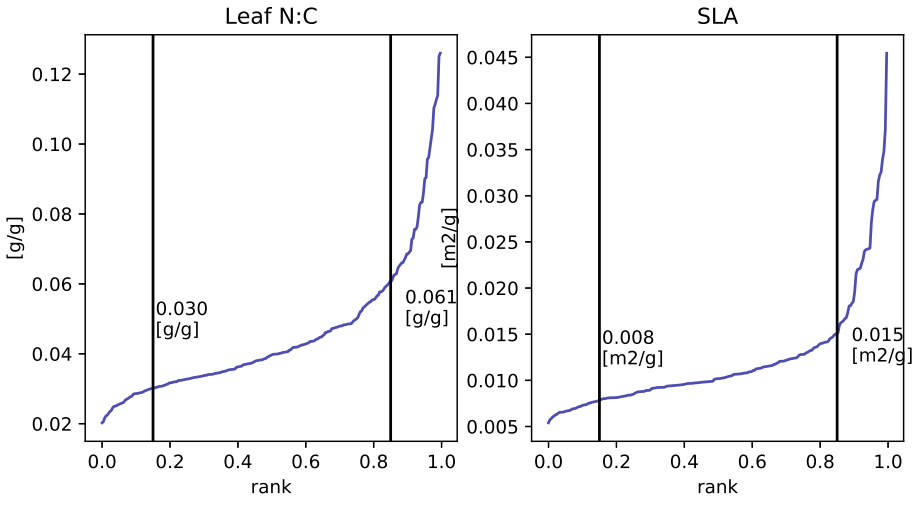

Figure E1. Rank plots of leaf nitrogen:carbon ratios and specific leaf area measured in Panama. Measurements by Ely et al. (2019). Vertical lines indicate the bounds of the 15-85 percentile.

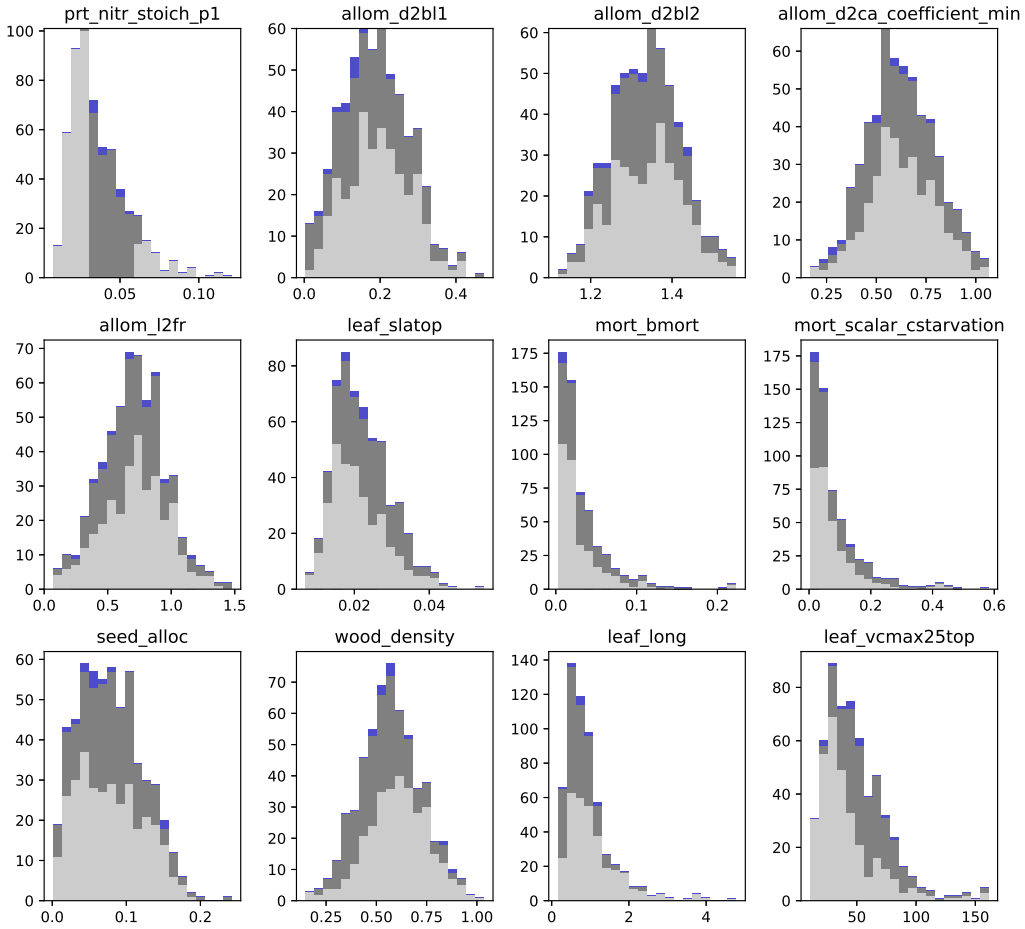

Figure E2. Histograms of model parameters from the parameter perturbation study of (C. D. Koven et al., 2020). Dark grey points represent parameters drawn from ensembles with leaf C:N ratios that fall within central $15-85\%$ ranks in Figure E1. Blue points represent a small selection of ensemble members with best agreement with the census data.

Appendix F Experiment Analysis Expanded

F1 Supplemental Proportion Integral Derivative Controller Analysis

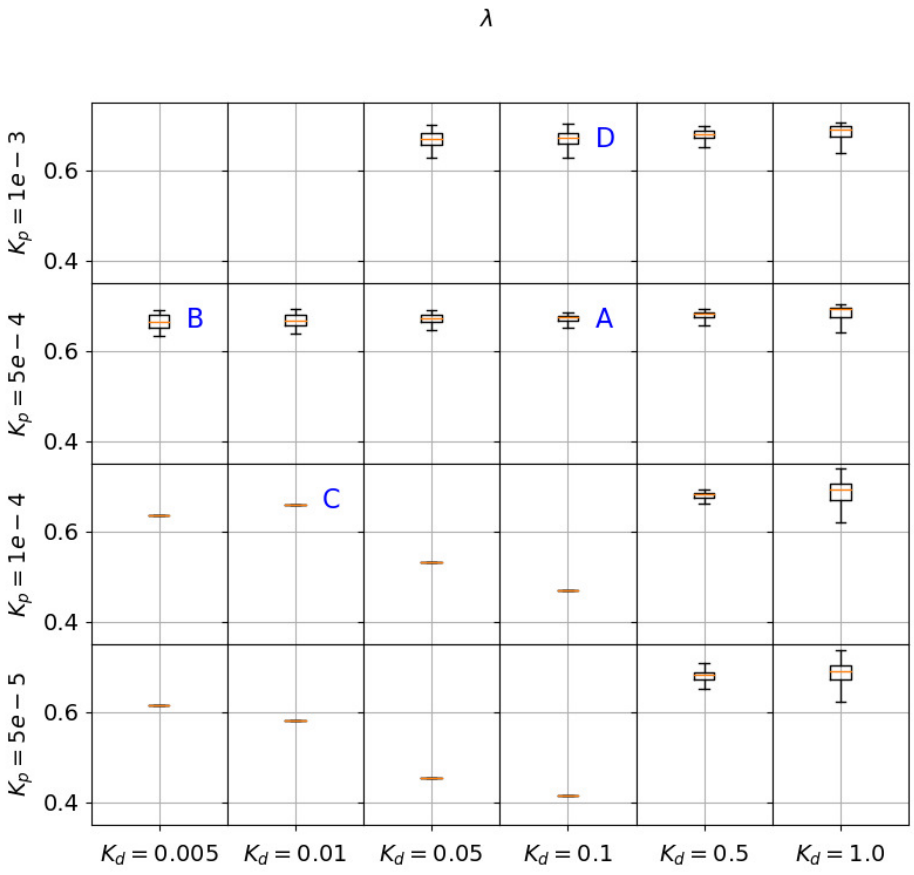

Figure F1. Mean and variance of the leaf to fine-root biomass multiplier variable (and PID set point) λ, over a range of PID proportion and derivative controller settings. Settings with letter designations are used in a follow-up simulation designed to identify a more optimal parameter couplet. PID stands for proportion integral derivative and is the fineroot biomass optimization controller.

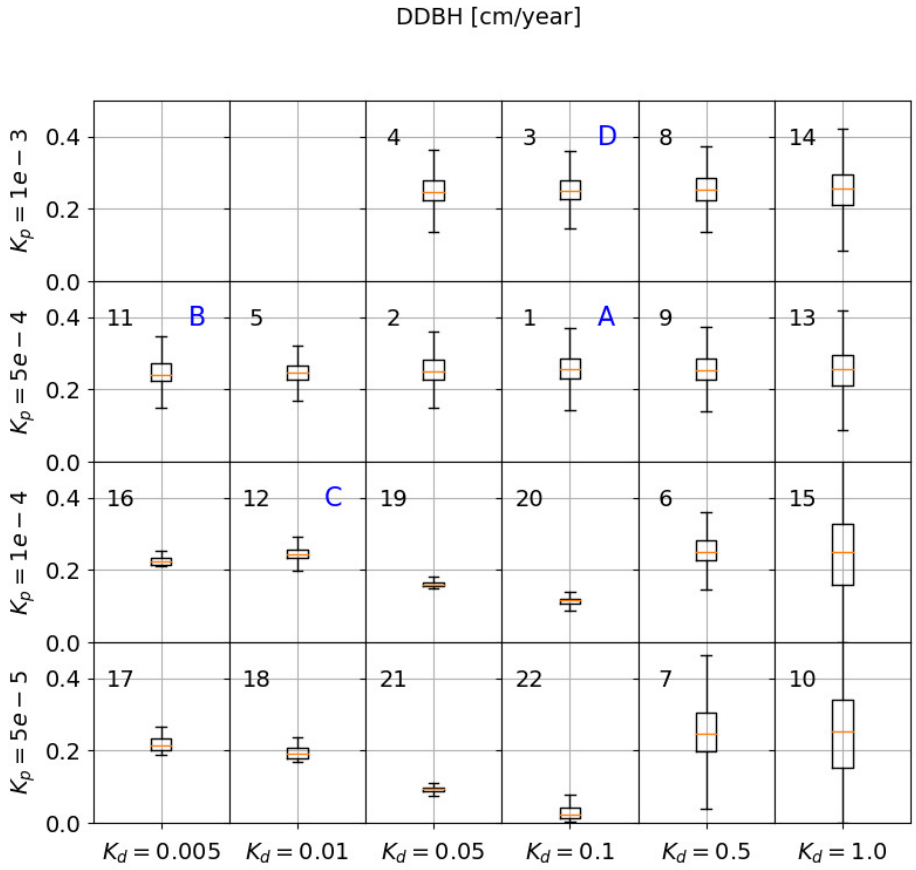

Figure F2. Mean and variance of the mean growth increment, over a range of PID proportion and derivative controller settings. Settings with letter designations are used in a follow-up simulation designed to identify a more optimal parameter couplet. PID stands for proportion integral derivative and is the fineroot biomass optimization controller.

F2 Experiment IV: Sensitivity to non-PID parameter constants that indirectly control fine-root growth

Since λ is driven directly by the differential nutrient storage ratios $f_{NC(s)}$, we focus on newly-introduced parameters that directly govern this differential, which includes the relative capacity the nutrient storage pools $\mu_{(s,pft)}$ and the allowable overflow of storage for all species μ_{ov}. While it would be interesting to investigate all correlations that exist between parameters, as well as how exiting parameters such as leaf photosynthetic traits govern this allocation, we leave that to future study.

In Experiment IV, we compare three simulations: the base simulation, one where the target N storage $\mu_{(N,pft)}$ is halved, and one where storage overflow μ_{ov} is halved. Time-series of model indicators are compared, see Figure F3. In summary, major perturbations to nutrient storage and overflow do not qualitatively change model results, and moreover, the changes are explainable. Changes in NPP, Basal Area, Carbon Use Efficiency, total nutrient uptake, organic nitrogen in the soil and aqueous nitrogen were also relatively unaffected. The largest changes were seen in those variables immediately connected to the parameters, such as differential storage.

With a smaller overflow capacity μ_{ov}, plants that acquire more nitrogen or carbon than required to fulfill construction costs, will be forced get rid of both at smaller tolerances. This was true for both species (see carbon use and nitrogen use inefficiency). However, halving overflow still generated a fairly high N allocation efficiency (i.e. plants were dumping less than 0.2% of what they acquired due to over-asking) and had small impacts on CUE.

A smaller nitrogen holding capacity $\mu_{(N,pft)}$ made plants slightly more net productive with higher carbon use efficiency, driven mostly by smaller allocations (and therefore respiration costs) to fine roots. With smaller holding capacity, a plant is more likely to fill up stores with excess nitrogen, which would signal to decrease root growth.

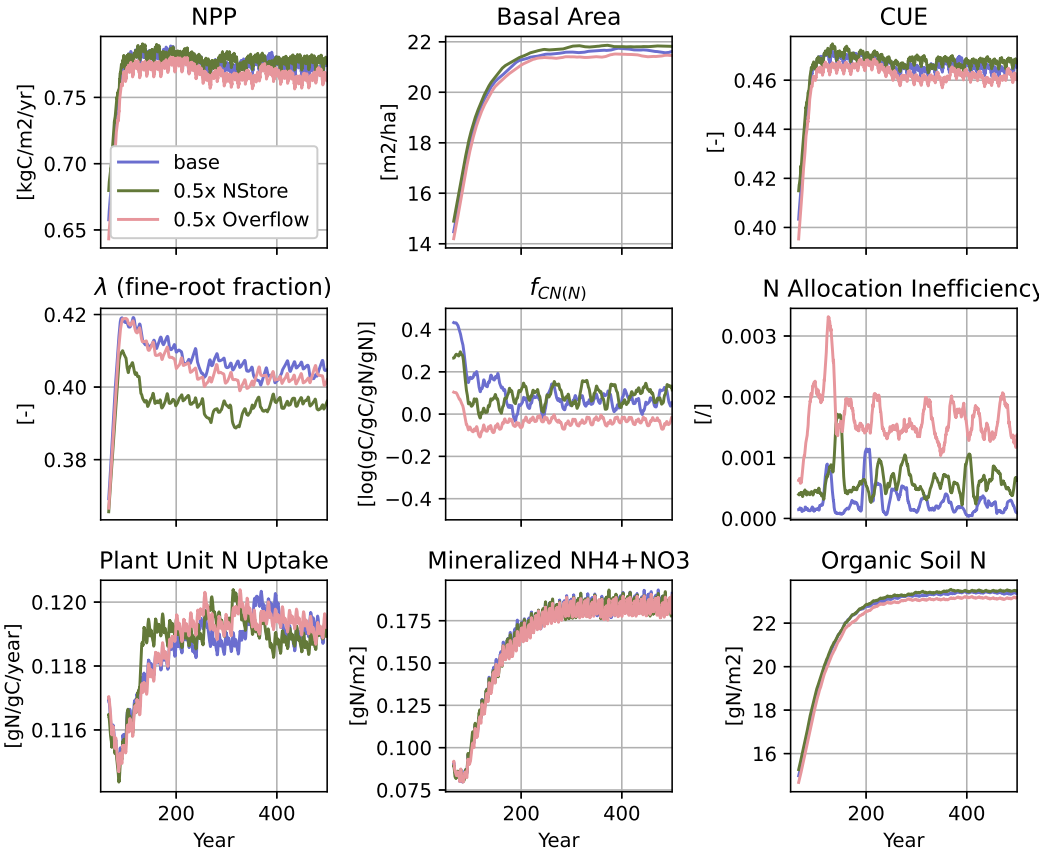

Figure F3. Sensitivity of model output to 0.5x reductions in plant Nitrogen Storage $\mu_{(N)}$ (0.5x Nstore) and overflow storage μ_{ov} (0.5x Overflow) parameters, as compared to a base simulation (1x for each).

F3 Experiment V: Sensitivity to alternative hypotheses for handling excess fine root and excess carbon gain

In experiment V, we evaluate how two subtle modifications to the core model hypotheses affect differences in the simulation compared to the base hypothesis. In the base hypothesis, when the fine-root biomass optimization algorithm signals a decrease in fine-root, the model will remove carbon and nutrients from the fine-root pool such that it matches the new (decreased) target. This removed mass is exported directly to the soil litter pool.

In an alternative configuration, called "efficient trim" (eff-trim), the carbon and nutrient removed from the fine-root is sent to the plant's storage. The storage accepts this mass until full (defined by the target and overflow parameters), beyond which the mass is either burned as respiration (for carbon) or exuded to the labile soil pool (for nitrogen and phosphorus). The other alternative hypothesis, "c-exude" assumes that excess carbon acquired by the plant that can not fit in storage (defined by the target and overflow parameters) will be released into the labile litter pool, in a manner similar to the nutrients (instead of released as respiration).

In summary, there is very little difference in the model predictions between the three model hypotheses. Part of this may be due to evaluating these differences through a parameter set that has reasonable parameters and some modest optimization (in the case of the PID parameters). The plants in the base parameterization do not waste that much carbon and nutrients (see the efficiency metrics in Figure F3), and these alternative hypotheses are oriented around how these waste terms are treated. If future experiments wish to activate these alternative hypotheses, they are maintained in the FATES code behind software switches that other modelers can activate if there is interest.

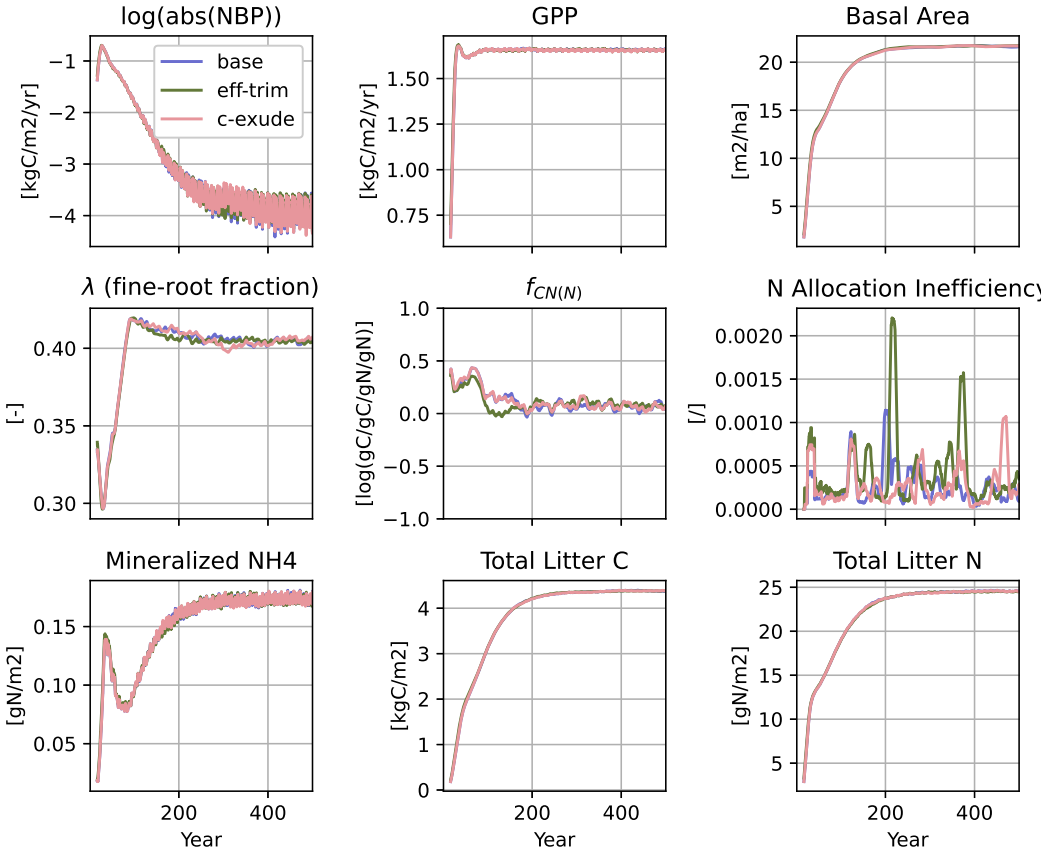

Figure F4. Comparison of model spin-ups for three different functional hypotheses. The "eff-trim" simulation re-captures the carbon and nutrients from fine-roots when the PID controller decreases λ and moves it into storage (instead of releasing it to the litter pool, like turnover). The "c-exude" simulation exports carbon that is in excess of overflow storage to the labile pool in the soil, instead of burning it as respiration. The "base" simulation (the default used for all other simulations) assumes that fine-root tissues are lost as turnover when the PID controller decreases λ, and that carbon gained in excess of overflow storage is burned as respiration.

F4 Experiment VI: Sensitivity to total ecosystem fixation hypothesis: evapotranspiration versus net primary production based

The ELM-FATES model can represent two sources of nitrogen fixation: 1) fixation that generates nitrogen in the soil and 2) obligate symbiotic nitrogen fixation that is available only to the plant individuals that spend the resources to fix. The nitrogen produced in the first method becomes available for competition between the nitrogen consumers in the soil (plants, nitrifiers and decomposers). In experiment IV, symbiotic nitrogen is turned off, and thus the fixation via method 1 is representative of total ecosystem fixation, acting as a catch all for free-living microbial fixers in the soil, symbiotic fixers in root nodules as well and potentially other sources.

Model response to the different total ecosystem nitrogen fixation (TEF) methods, proportionality with evapotranspiration (et-fix) and proportionality with net primary productivity (npp-fix) (Cleveland et al., 1999; P. Thornton et al., 2007), is evaluated over industrial-era atmospheric CO2 concentrations, see Figure F5. Both simulations were initialized with a pre-industrial 500 year spin-up.

Batterman et al. (2013) estimates that fixation at the BCI site is dominated by symbiotic fixation and almost negligible free-living fixation (with an exception for some old forest stands). Study at the nearby San Lorenzo (Stanton et al., 2019) site suggested that canopy microbial fixation can contribute significant sources of nitrogen.

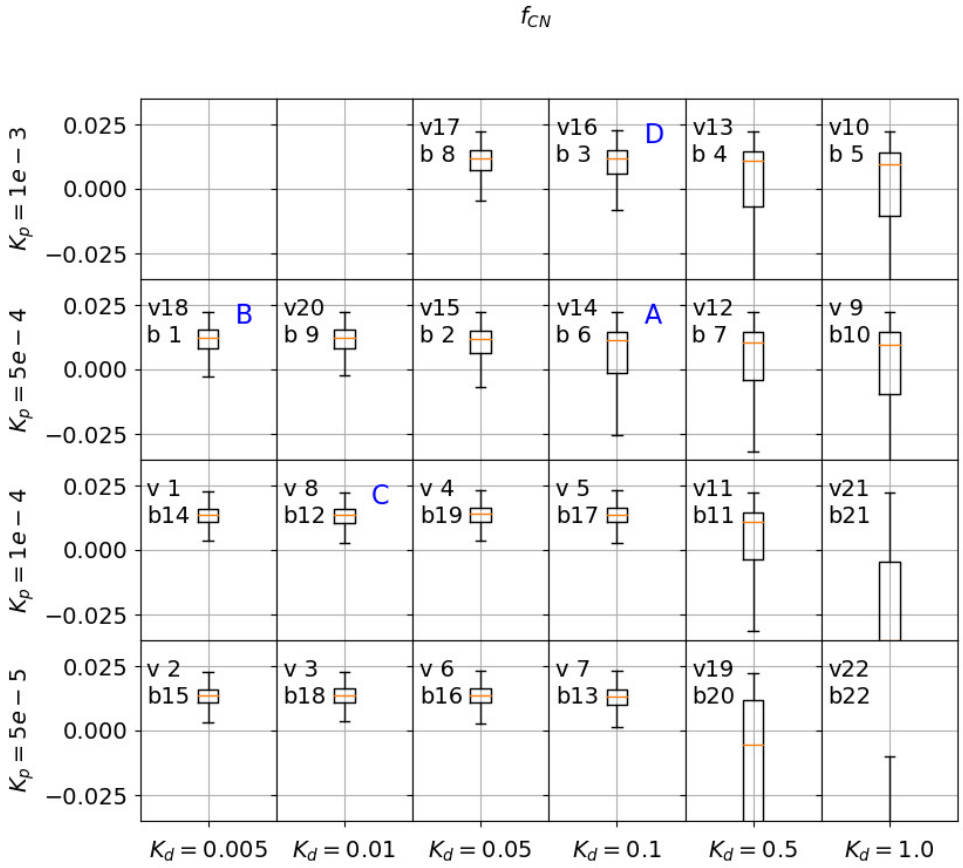

Figure F5. Time series model response to the two different total ecosystem nitrogen fixation hypotheses in ELM, fixation proportional to NPP (npp-fix) and fixation proportional to evapotranspiration (et-fix).

The two methods generate qualitatively different results, particularly in reference to the total nitrogen fixation flux into the system. Both methods could be calibrated by adjusting scaling parameters, but we chose to use the default scaling coefficients in the ELM model, as the differences between the two options provide good end-points to study the system. Note that while the NPP method introduces more nitrogen as a whole, it also continues to increase indefinitely with CO2 increases, while the evapotranspiration method saturates and even decreases late in the 21st century. However, availability of nitrogen limits the models (as indicated by the plant unit N uptake, the nitrogen uptake per gram of fine-root, and the depleting mineralized (aqueous) N pool) in both scenarios. The differences are mostly manifested in increased growth and biomass in the vegetation canopy with access to increased nitrogen, particularly late in the 21st century. The carbon usage efficiency is higher with more nitrogen availability, presumably because the vegetation can use the carbon it acquires to build tissues, instead of respiring it.

Soil nitrogen responses are also provided in the supplement, see Figure F6. Note that in each fixation hypothesis, there are similar pattern responses to the fraction of mineralized nitrogen that can be immobilized for decomposition, as well as leaching, nitrification and denitrification response.

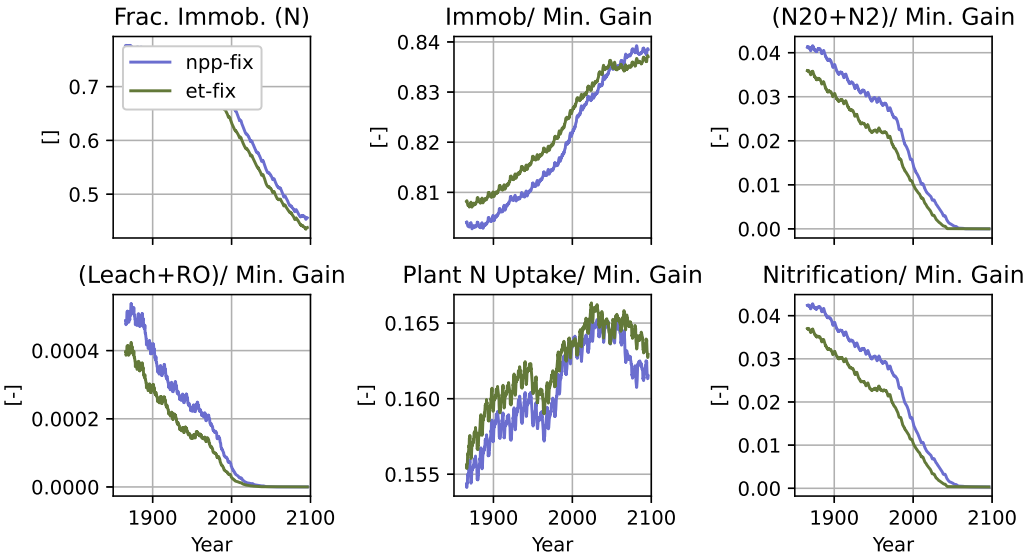

Figure F6. Differential responses of soil nitrogen flux to the two free-living fixation hypotheses (NPP based and evapotranspiration based).

Appendix G Open Research

The data and software code used to reproduce the model simulations and analysis in this manuscript have been made publicly available.

G1 Data Availability

The "Next Generation Ecosystem Experiment - Tropics" project provides model driver data at the Barro Colorado Island Site, including soils and meteorological data (Knox et al., 2019). The data can be found here: `https://ngt-data.lbl.gov/dois/NGT0086/`

G2 Software Availability

Both the FATES and E3SM models use Git (`https://git-scm.com/`) version control to manage their software, and Github (`https://github.com/`) to host their software. The model software of both projects and their dependencies are publicly available. Readers who wish to either reproduce or do similar work in this manuscript are encouraged to install git and use it to clone the E3SM model, also Zenodo DOIs are provided. FATES will be imported as a submodule of E3SM. To initialize submodules following a clone, and assuming the user has "checked out" the correct tag or branch, they should run the command "git submodule update –init –recursive".

The specific E3SM tag used in this research is DOI 10.5281/zenodo.7684977, `https://doi.org/10.5281/zenodo.7684977`; or the github tag can be found here: `https://github.com/rgknox/E3SM/releases/tag/elm-fates-cnp-ms` (?, ?).

The specific FATES tag used in this research is DOI 10.5281/zenodo.7685350, `https://doi.org/10.5281/zenodo.7685350`; or the github tag can be found here: `https://github.com/rgknox/fates/releases/tag/fates-cnp-ms-anlsys` (?, ?).

The python analysis scripts (contained in (?, ?)) used to generate the figures in this manuscript are provided in the directory: "./ms-analysis/".

This file (contained in (?, ?)) will patch the default FATES parameter file to generate parameterizations specifically for one tropical evergreen plant functional type at Barro Colorado Island Panama: `https://github.com/rgknox/fates/blob/fates-cnp-ms/parameter_files/patch_default_bciopt224.xml`

A nix-type "shell" script (contained in (?, ?)) is provided, that was used to build and setup the simulations. This script should be executed from the directory: "./cime/scripts". This file also assumes that the driver data package listed above is unpacked in the same directory as well. The user will need to modify many of the paths in the script to accommodate their file structure. This script should facilitate other users running simulations at BCI, but this file is provided as-is, and absolutely no support will be provided for making this script work. `https://github.com/rgknox/fates/blob/fates-cnp-ms/parameter_files/create_bci_fatescnp_mscopy.sh`

Acknowledgments

This research was supported as part of the Next Generation Ecosystem Experiments-Tropics, funded by the U.S. Department of Energy, Office of Science, Office of Biological and Environmental Research. RF acknowledges funding by the European Union's Horizon 2020 (H2020) research and innovation program under Grant Agreement No. 101003536 (ESM2025 – Earth System Models for the Future) and 821003 (4C, Climate-Carbon Interactions in the Coming Century). Steve Paton of the Smithsonian Tropical Research Institute was involved in providing the original measurements of meteorological data used to drive these simulations. The Smithsonian Tropical Research Institute was the provider of the original unprocessed meteorological data, as well as the provider of the census data as referenced in (Condit et al., 2017), see `http://biogeodb.stri.si.edu/physical_monitoring/research/barrocolorado`. Helene Muller-Landau provided consultation on the interpretation of raw census data that was used in the calibration of the carbon-only model.

References

Ahrens, B., Hansson, K., Solly, E. F., & Schrumpf, M. (2014). Reconcilable differences: a joint calibration of fine-root turnover times with radiocarbon and minirhizotrons. *New Phytologist*, *204*(4), 932-942. doi: https://doi.org/10.1111/nph.12979

Arora, V. K., Katavouta, A., Williams, R. G., Jones, C. D., Brovkin, V., Friedlingstein, P., ... Ziehn, T. (2020). Carbon–concentration and carbon–climate feedbacks in cmip6 models and their comparison to cmip5 models. *Biogeosciences*, *17*(16), 4173–4222. Retrieved from `https://bg.copernicus.org/articles/17/4173/2020/` doi: 10.5194/bg-17-4173-2020

Batterman, S., Hedin, L., van Breugel, M., Ransijn, J., Craven, D., & JS, H. (2013). Key role of symbiotic dinitrogen fixation in tropical forest secondary succession. *Nature*, *502*, 224-229. doi: 10.1038/nature12525

Bloom, A. J., Chapin III, F. S., & Mooney, H. A. (1985). Resource limitation in plants-an economic analogy. *Annual review of Ecology and Systematics*, *16*(1), 363–392.

Bonan, G., Williams, M., Fisher, R., & Oleson, K. (2014). Modeling stomatal conductance in the earth system: linking leaf water-use efficiency and water transport along the soil–plant–atmosphere continuum. *Geoscientific Model Development*, *7*(5), 2193–2222.

Bonan, G. B., Oleson, K. W., Fisher, R. A., Lasslop, G., & Reichstein, M. (2012). Reconciling leaf physiological traits and canopy flux data: Use of the try and

fluxnet databases in the community land model version 4. *Journal of Geophysical Research: Biogeosciences (2005–2012)*, *117*(G2).

Botta, A., Viovy, N., Ciais, P., Friedlingstein, P., & Monfray, P. (2000). A global prognostic scheme of leaf onset using satellite data. *Global Change Biology*, *6*(7), 709–725.

Buotte, P. C., Koven, C. D., Xu, C., Shuman, J. K., Goulden, M. L., Levis, S., ... Kueppers, L. M. (2021). Capturing functional strategies and compositional dynamics in vegetation demographic models. *Biogeosciences*, *18*(14), 4473–4490. Retrieved from https://bg.copernicus.org/articles/18/4473/2021/ doi: 10.5194/bg-18-4473-2021

Burrows, S. M., Maltrud, M., Yang, X., Zhu, Q., Jeffery, N., Shi, X., ... Leung, L. R. (2020). The doe e3sm v1.1 biogeochemistry configuration: Description and simulated ecosystem-climate responses to historical changes in forcing. *Journal of Advances in Modeling Earth Systems*, *12*(9), e2019MS001766. Retrieved from https://agupubs.onlinelibrary.wiley.com/doi/abs/10.1029/2019MS001766 (e2019MS001766 10.1029/2019MS001766) doi: 10.1029/2019MS001766

Bytnerowicz, T., Akana, P., Griffin, K., & Menge, D. (2022). Temperature sensitivity of woody nitrogen fixation across species and growing temperatures. *Nature Plants*, *8*, 209–216. doi: https://doi.org/10.1038/s41477-021-01090-x

Caldwell, P. M., Mametjanov, A., Tang, Q., Van Roekel, L. P., Golaz, J.-C., Lin, W., ... Zhou, T. (2019). The doe e3sm coupled model version 1: Description and results at high resolution. *Journal of Advances in Modeling Earth Systems*, *11*(12), 4095-4146. Retrieved from https://agupubs.onlinelibrary.wiley.com/doi/abs/10.1029/2019MS001870 doi: https://doi.org/10.1029/2019MS001870

Christoffersen, B. O., Restrepo-Coupe, N., Arain, M. A., Baker, I. T., Cestaro, B. P., Ciais, P., ... others (2014). Mechanisms of water supply and vegetation demand govern the seasonality and magnitude of evapotranspiration in amazonia and cerrado. *Agricultural and Forest Meteorology*, *191*, 33–50.

Cleveland, C., Townsend, A., Schimel, D., Fisher, H., Howarth, R., Hedin, L., ... Wasson, M. (1999). Global patterns of terrestrial biological nitrogen (n2) fixation in natural ecosystems. *Global Biogeochemical Cycles*, *13*(2), 623–645. doi: doi:10.1029/1999GB900014

Collatz, G., Ball, J., Grivet, C., & Berry, J. A. (1991). Physiological and environmental regulation of stomatal conductance, photosynthesis and transpiration: a model that includes a laminar boundary layer. *Agricultural and Forest Meteorology*, *54*(2), 107-136. Retrieved from https://www.sciencedirect.com/science/article/pii/0168192391900028 doi: https://doi.org/10.1016/0168-1923(91)90002-8

Condit, R., Pérez, R., Lao, S., Aguilar, S., & SP, H. (2017). Demographic trends and climate over 35 years in the barro colorado 50 ha plot. *Forest Ecosystems*, *4*(17). doi: https://doi.org/10.1186/s40663-017-0103-1

Cushman, K. C., Bunyavejchewin, S., Cárdenas, D., Condit, R., Davies, S. J., Duque, A., ... Muller-Landau, H. C. (2021). Variation in trunk taper of buttressed trees within and among five lowland tropical forests. *Biotropica*, *53*(5), 1442-1453. Retrieved from https://onlinelibrary.wiley.com/doi/abs/10.1111/btp.12994 doi: https://doi.org/10.1111/btp.12994

de Kauwe, M. G., Medlyn, B. E., Zaehle, S., Walker, A. P., Dietze, M. C., Wang, Y.-P., ... others (2014). Where does the carbon go? a model–data intercomparison of vegetation carbon allocation and turnover processes at two temperate forest free-air co2 enrichment sites. *New Phytologist*, *203*(3), 883–899.

Ely, K., Rogers, A., Serbin, S., Wu, J., Dickman, T., Collins, A., ... Michaletz, S. (2019). *Leaf mass area, feb2016-may2016, pa-slz, pa-pnm, pa-bci: Panama. 1.0. ngee tropics data collection. (dataset).* http://dx.doi.org/10.15486/

ngt/1411973. doi: 10.15486/ngt/1411973

Fang, Y., Leung, L. R., Knox, R., Koven, C., & Bond-Lamberty, B. (2022). Impact of the numerical solution approach of a plant hydrodynamic model (v0.1) on vegetation dynamics. *Geoscientific Model Development*, *15*(16), 6385–6398. Retrieved from https://gmd.copernicus.org/articles/15/6385/2022/ doi: 10.5194/gmd-15-6385-2022

Farquhar, G., von Caemmerer, S., & Berry, J. (1980). A biochemical model of photosynthetic co2 assimilation in leaves of c3 species. *Planta*, *149*, 78–90. doi: https://doi.org/10.1007/BF00386231

Farrior, C. E., Tilman, D., Dybzinski, R., Reich, P. B., Levin, S. A., & Pacala, S. W. (2013). Resource limitation in a competitive context determines complex plant responses to experimental resource additions. *Ecology*, *94*(11), 2505–2517.

FATES-Development-Team. (2019, October). *Technical note for the functionally assembled terrestrial ecosystem simulator (fates).* Zenodo. Retrieved from https://doi.org/10.5281/zenodo.3517272 doi: 10.5281/zenodo.3517272

Faybishenko, B., Paton, S., Powell, T., Knox, R., Pastorello, G., Varadharajan, C., ... Agarwal, D. (2018). *Qa/qc-ed bci meteorological drivers. ngee tropics data collection* (dataset No. NGT0062-v1.0). doi: http://dx.doi.org/10.15486/ngt/1423307

Fisher, J., Sitch, S., Malhi, Y., Fisher, R., Huntingford, C., & Tan, S. (2010). A mechanistic, globally applicable model of plant nitrogen uptake, retranslocation, and fixation. *Global Biogeochemical Cycles*, *24*. doi: https://doi.org/10.1029/2009GB003621

Fisher, R. A., Muszala, S., Verteinstein, M., Lawrence, P., Xu, C., McDowell, N. G., ... Bonan, G. (2015). Taking off the training wheels: the properties of a dynamic vegetation model without climate envelopes. *Geoscientific Model Development Discussions*, *8*(4), 3293–3357. Retrieved from http://www.geosci-model-dev-discuss.net/8/3293/2015/ doi: 10.5194/gmdd-8-3293-2015

Forde, B., & Lorenzo, H. (2001). The nutritional control of root development. *Plant and Soil*, *232*, 51-68. doi: 10.1023/A:1010329902165

Freschet, G., Cornelissen, J., van Logstestijn, R., & Aerts, R. (2010). Substantial nutrient resorption from leaaves, stems and roots in subarctic flora: what is the link with other resource economics traits? *New Phytologist*, *186*(4). doi: 10.1111/j.1469-8137.2010.03228.x

Fyllas, N., Gloor, E., Mercado, L., Sitch, S., Quesada, C., Domingues, T., ... others (2014). Analysing amazonian forest productivity using a new individual and trait-based model (tfs v. 1). *Geoscientific Model Development*, *7*(4), 1251–1269.

Gaudinski, J. B., Torn, M. S., Riley, W. J., Dawson, T. E., Joslin, J. D., & Majdi, H. (2010). Measuring and modeling the spectrum of fine-root turnover times in three forests using isotopes, minirhizotrons, and the radix model. *Global Biogeochemical Cycles*, *24*(3). doi: https://doi.org/10.1029/2009GB003649

Hanbury-Brown, A. R., Ward, R. E., & Kueppers, L. M. (2022). Forest regeneration within earth system models: current process representations and ways forward. *New Phytologist*, *235*(1), 20-40.

Houlton, B., Wang, Y., Vitousek, P., & C.B., F. (2008). A unifying framework for dinitrogen fixation in the terrestrial biosphere. *Nature*, *454*, 327–330. doi: 10.1038/nature07028

Hungate, B., Dukes, J., Shaw, M., Luo, Y., & Field, C. (2003). Nitrogen and climate change. *Science*, *302*(5650), 1512-1513. doi: 10.1126/science.1091390

Iversen, C. M., McCormack, M. L., Powell, A. S., Blackwood, C. B., Freschet, G. T., Kattge, J., ... Violle, C. (2017). A global fine-root ecology database to address below-ground challenges in plant ecology. *New Phytologist*, *215*(1), 15-26.

doi: https://doi.org/10.1111/nph.14486

Knox, R., Faybishenko, B., Paton, S., Powell, T., Pastorello, G., Koven, C., ... Bisht, G. (2019). *Panama land model (clm/elm) site drivers* (dataset No. NGT0086-v1.0). doi: http://dx.doi.org/10.15486/ngt/1570244

Kou-Giesbrecht, S., Malyshev, S., Martínez Cano, I., Pacala, S., Shevliakova, E., Bytnerowicz, T., & Menge, D. (2021b). A novel representation of biological nitrogen fixation and competitive dynamics between nitrogen-fixing and non-fixing plants in a land model (gfdl lm4.1-bnf). *Biogeosciences*, *18*, 4143-4183. doi: https://doi.org/10.5194/bg-18-4143-2021

Kou-Giesbrecht, S., Malyshev, S., Martínez Cano, I., Pacala, S. W., Shevliakova, E., Bytnerowicz, T. A., & Menge, D. N. L. (2021a). A novel representation of biological nitrogen fixation and competitive dynamics between nitrogen-fixing and non-fixing plants in a land model (gfdl lm4.1-bnf). *Biogeosciences*, *18*(13), 4143–4183. Retrieved from `https://bg.copernicus.org/articles/18/4143/2021/` doi: 10.5194/bg-18-4143-2021

Koven, C., Riley, W., Subin, Z., Tang, J., Torn, M., Collins, W., ... Swenson, S. (2013). The effect of vertically resolved soil biogeochemistry and alternate soil c and n models on c dynamics of clm4. *Biogeosciences*, *10*, 7109–7131. doi: doi:10.5194/bg-10-7109-2013

Koven, C. D., Knox, R. G., Fisher, R. A., Chambers, J. Q., Christoffersen, B. O., Davies, S. J., ... Xu, C. (2020). Benchmarking and parameter sensitivity of physiological and vegetation dynamics using the functionally assembled terrestrial ecosystem simulator (fates) at barro colorado island, panama. *Biogeosciences*, *17*(11), 3017–3044. Retrieved from `https://bg.copernicus.org/articles/17/3017/2020/` doi: 10.5194/bg-17-3017-2020

Lawrence, D., Fisher, R., Koven, C., Oleson, K., Swenson, S., Vertenstein, M., ... Xu, C. (2020). Technical description of version 5.0 of the community land model (clm). *Geoscientific Model Development*. Retrieved from `https://www2.cesm.ucar.edu/models/cesm2/land/CLM50_Tech_Note.pdf`

Ma, W., Zhai, L., Pivovaroff, A., Shuman, J., Buotte, P., Ding, J., ... Xu, C. (2021). Assessing climate change impacts on live fuel moisture and wildfire risk using a hydrodynamic vegetation model. *Biogeosciences*, *18*(13), 4005–4020. Retrieved from `https://bg.copernicus.org/articles/18/4005/2021/` doi: 10.5194/bg-18-4005-2021

Martínez Cano, I., Muller-Landau, H. C., Wright, S. J., Bohlman, S. A., & Pacala, S. W. (2019). Tropical tree height and crown allometries for the barro colorado nature monument, panama: a comparison of alternative hierarchical models incorporating interspecific variation in relation to life history traits. *Biogeosciences*, *16*(4), 847–862. Retrieved from `https://bg.copernicus.org/articles/16/847/2019/` doi: 10.5194/bg-16-847-2019

McCormack, M. L., Dickie, I. A., Eissenstat, D. M., Fahey, T. J., Fernandez, C. W., Guo, D., ... Zadworny, M. (2015). Redefining fine roots improves understanding of below-ground contributions to terrestrial biosphere processes. *New Phytologist*, *207*(3), 505-518. Retrieved from `https://nph.onlinelibrary.wiley.com/doi/abs/10.1111/nph.13363` doi: https://doi.org/10.1111/nph.13363

McMurtrie, R. E., & Näsholm, T. (2018). Quantifying the contribution of mass flow to nitrogen acquisition by an individual plant root. *New Phytologist*, *218*(1), 119–130.

Medvigy, D., Wang, G., Zhu, Q., Riley, W. J., Trierweiler, A. M., Waring, B., ... Powers, J. S. (2019). Observed variation in soil properties can drive large variation in modelled forest functioning and composition during tropical forest secondary succession. *New Phytologist*, *223*(4), 1820-1833. Retrieved from `https://nph.onlinelibrary.wiley.com/doi/abs/10.1111/nph.15848` doi: https://doi.org/10.1111/nph.15848

Menge, D. N. L., Wolf, A. A., Funk, J. L., Perakis, S. S., Akana, P. R., Arkebauer, R., ... Ortiz, S. K. (n.d.). Tree symbioses sustain nitrogen fixation despite excess nitrogen supply. *Ecological Monographs*, *n/a*(n/a), e1562. Retrieved from `https://esajournals.onlinelibrary.wiley.com/doi/abs/10.1002/ecm.1562` doi: https://doi.org/10.1002/ecm.1562

Millard, P., & Grelet, G.-a. (2010, 06). Nitrogen storage and remobilization by trees: ecophysiological relevance in a changing world. *Tree Physiology*, *30*(9), 1083-1095. Retrieved from `https://doi.org/10.1093/treephys/tpq042` doi: 10.1093/treephys/tpq042

Mirabello, M. J., Yavitt, J. B., Garcia, M., Harms, K. E., Turner, B. L., & J., W. S. (2013). Soil phosphorus responses to chronic nutrient fertilisation and seasonal drought in a humid lowland forest, panama. *Soil Research*, *51*, 215-221. doi: 10.1071/SR12188

Moorcroft, P., Hurtt, G., & Pacala, S. W. (2001). A method for scaling vegetation dynamics: the ecosystem demography model ed. *Ecological monographs*, *71*(4), 557–586.

Nambiar, E. (1987). Do nutrients restranslocate from fine roots? *Canadian Journal of Forest Research*, *17*(8). doi: 10.1139/x87-143

Needham, J. F., Arellano, G., Davies, S. J., Fisher, R. A., Hammer, V., Knox, R. G., ... Koven, C. D. (2022). Tree crown damage and its effects on forest carbon cycling in a tropical forest. *Global Change Biology*, *28*(18), 5560–5574.

Needham, J. F., Chambers, J., Fisher, R., Knox, R., & Koven, C. D. (2020). Forest responses to simulated elevated co2 under alternate hypotheses of size- and age-dependent mortality. *Global Change Biology*, *26*(10), 5734-5753. Retrieved from `https://onlinelibrary.wiley.com/doi/abs/10.1111/gcb.15254` doi: https://doi.org/10.1111/gcb.15254

Norman, J. (1979). Modeling the complete crop canopy. modification of the aerial environment of crops. *American Society Agricultural Engineers*, 249-280.

Oleson, K., Lawrence, D., Bonan, G., M, D., Huang, C., Koven, C., ... et al., Y. Z. (2013). Technical description of version 4.5 of the community land model (clm). *Geoscientific Model Development*.

Parton, W., Stewart, J., & Cole, C. (1988). Dynamics of c, n, p and s in grassland soils – a model. *Biogeochemistry*, *5*, 109–131.

Patton, S. (2019a). *Barro colorado island, lutz tower 48m air temperature. smithsonian tropical research institute. dataset.* doi: 10.25573/data.10042442.v24

Patton, S. (2019b). *Barro colorado island, lutz tower 48m relative humidity. smithsonian tropical research institute. dataset.* doi: 10.25573/data.10042418.v23

Patton, S. (2019c). *Barro colorado island, lutz tower 48m solar radiation, pyranometer. smithsonian tropical research institute. dataset.* doi: 10.25573/data.10042406.v20

Patton, S. (2019d). *Barro colorado island, lutz tower 48m wind speed. smithsonian tropical research institute. dataset.* doi: 10.25573/data.10042427.v20

Powers, J., Treseder, K., & Lerdau, M. (2005). Fine roots, arbuscular mycorrhizal hyphae and soil nutrients in four neotropical rain forests: patterns across large geographic distances. *New Phytologist*, *165*, 913-921. doi: https://doi.org/10.1111/j.1469-8137.2004.01279.x

Prentice, I., Liang, X., Medlyn, B., & Wang, Y.-P. (2015). Reliable, robust and realistic: the three r's of next-generation land-surface modelling. *Atmospheric Chemistry and Physics*, *15*(10), 5987–6005. Retrieved from `https://acp.copernicus.org/articles/15/5987/2015/` doi: 10.5194/acp-15-5987-2015

Purves, D., & Pacala, S. (2008). Predictive models of forest dynamics. *Science*, *320*(5882), 1452–1453.

Purves, D. W., Lichstein, J. W., Strigul, N., & Pacala, S. W. (2008). Predicting and understanding forest dynamics using a simple tractable model. *Proceedings of*

the National Academy of Sciences, *105*(44), 17018–17022.

Ryan, M. G. (1991). A simple method for estimating gross carbon budgets for vegetation in forest ecosystems. *Tree physiology*, *9*(1-2), 255–266.

Stanton, D., Batterman, S., Von Fischer, J., & Hedin, L. (2019). Rapid nitrogen fixation by canopy microbiome in tropical forest determined by both phosphorus and molybdenum. *Ecology*, *100*(9), 1-8.

Steudle, E., & Peterson, C. A. (1998). How does water get through roots? *Journal of experimental Botany*, *49*(322), 775–788.

Sulman, B., Shevliakova, E., Brzostek, E., Kivlin, S., Malyshev, S., Menge, D., & Zhang, X. (2019). Diverse mycorrhizal associations enhance terrestrial c storage in a global model. *Global Biogeochemical Cycles*, *33*(4), 501-523. Retrieved from `https://agupubs.onlinelibrary.wiley.com/doi/abs/10.1029/2018GB005973` doi: https://doi.org/10.1029/2018GB005973

Tang, J., & Riley, W. (2013). A total quasi-steady-state formulation of substrate uptake kinetics in complex networks and an example application to microbial litter decomposition. *Biogeosciences*, *10*(12), 8329–8351. doi: 10.5194/bg1083292013

Taylor, B. N., Strand, A. E., Cooper, E. R., Beidler, K. V., Schönholz, M., & Pritchard, S. G. (2014). Root length, biomass, tissue chemistry and mycorrhizal colonization following 14 years of co2 enrichment and 6 years of n fertilization in a warm temperate forest. *Tree Physiology*, *34*(9), 955–965.

Thonicke, K., Spessa, A., Prentice, I., Harrison, S., Dong, L., & Carmona-Moreno, C. (2010). The influence of vegetation, fire spread and fire behaviour on biomass burning and trace gas emissions: results from a process-based model. *Biogeosciences*, *7*(6), 1991–2011.

Thornley, J. (1995). Shoot:root allocation with respect to c, n and p: an investigation and comparison of resistance and teleonomic models. *Annals of Botany*, *75*.

Thornton, P., Lamarque, J.-F., Rosenbloom, N., & Mahowald, N. (2007). Influence of carbon-nitrogen cycle coupling on land model response to co2 fertilization and climate variability. *Global Biogeochemical Cycles*, *21*(GB4018). doi: 10.1029/2006gb002868

Thornton, P. E., & Rosenbloom, N. A. (2005). Ecosystem model spin-up: Estimating steady state conditions in a coupled terrestrial carbon and nitrogen cycle model. *Ecological Modelling*, *189*(1-2), 25–48.

Thum, T., Caldararu, S., Engel, J., Kern, M., Pallandt, M., Schnur, R., ... Zaehle, S. (2019). A new model of the coupled carbon, nitrogen, and phosphorus cycles in the terrestrial biosphere (quincy v1.0; revision 1996). *Geoscientific Model Development*, *12*(11), 4781–4802. Retrieved from `https://gmd.copernicus.org/articles/12/4781/2019/` doi: 10.5194/gmd-12-4781-2019

Wang, Y. P., Law, R. M., & Pak, B. (2010). A global model of carbon, nitrogen and phosphorus cycles for the terrestrial biosphere. *Biogeosciences*, *7*(7), 2261–2282. Retrieved from `https://bg.copernicus.org/articles/7/2261/2010/` doi: 10.5194/bg-7-2261-2010

Wang, Y.-P., Zhang, Q., Pitman, A., & Dai, Y. (2015). Nitrogen and phosphorous limitation reduces the effects of land use change on land carbon uptake or emission. *Environmental Research Letters*, *10*(1). doi: 10.1088/1748-9326/10/1/014001

Wieder, R. K., & Wright, S. J. (1995). Tropical forest litter dynamics and dry season irrigation on barro colorado island, panama. *Ecology*, *76*(6), 1971–1979.

Wright, S. J., Kitajima, K., Kraft, N. J. B., Reich, P. B., Wright, I. J., Bunker, D. E., ... Zanne, A. E. (2010). Functional traits and the growth–mortality trade-off in tropical trees. *Ecology*, *91*(12), 3664-3674. Retrieved from `https://esajournals.onlinelibrary.wiley.com/doi/abs/10.1890/`

09-2335.1 doi: https://doi.org/10.1890/09-2335.1

Wright, S. J., Yavitt, J. B., Wurzburger, N., Turner, B. L., Tanner, E. V., Sayer, E. J., ... others (2011). Potassium, phosphorus, or nitrogen limit root allocation, tree growth, or litter production in a lowland tropical forest. *Ecology*, *92*(8), 1616–1625.

Yang, S.-Y., Huang, T.-K., Kuo, H.-F., & Chiou, T.-J. (2017, 01). Role of vacuoles in phosphorus storage and remobilization. *Journal of Experimental Botany*, *68*(12), 3045-3055. Retrieved from https://doi.org/10.1093/jxb/erw481 doi: 10.1093/jxb/erw481

Yang, X., Ricciuto, D., Thornton, P., Shi, X., Xu, M., Hoffman, F., & Norby, R. (2019). The effects of phosphorus cycle dynamics on carbon sources and sinks in the amazon region: a modeling study using elm v1. *Journal of Geophysical Research: Biogeosciences*, *124*, 3686– 3698. doi: 10.1029/2019JG005082

Yang, X., Thornton, P., Ricciuto, D., & Post, W. (2014). The role of phosphorus dynamics in tropical forests- a modeling study using cnp. *Biogeosciences*, *11*, 1667-1681. doi: doi.org/10.5194/bg-11-1667-2014

Yavitt, J., Harms, K., Garcia, M., Mirabello, M., & Wright, S. (2011). Soil fertility and fine root dynamics in response to 4 years of nutrient (n,p,k) fertilization in a lowland tropical moist forest, panama. *Austral Ecology*, *36*, 433-445. doi: https://doi.org/10.1111/j.1442-9993.2010.02157.x

Yavitt, J., & Wright, S. (2001). Drought and irrigation effects on fine root dynamics in a tropical moist forest, panama. *Biotropica*, *33*, 421-434. doi: https://doi.org/10.1646/0006-3606(2001)033[0421:DAIEOF]2.0.CO;2

Zaehle, S., & Friend, A. (2010). Carbon and nitrogen cycle dynamics in the o-cn land surface model: 1. model description, site-scale evaluation, and sensitivity to parameter estimates. *Global Biogeochemical Cycles*, *24*(1).

Zhu, Q., Riley, W., Tang, J., Collier, N., Hoffman, F., Yang, X., & Bisht, G. (2019). Representing nitrogen, phosphorus, and carbon interactions in the e3sm land model: Development and global benchmarking. *Journal of Advances in Modeling Earth Systems*, *11*, 2238–2258. doi: 10.1029/2018MS001571

Zhu, Q., Riley, W., Tang, J., & Koven, C. (2016). Multiple soil nutrient competition between plants, microbes, and mineral surfaces: Model development, parameterization, and example applications in several tropical forests. *Biogeosciences*, *12*(5), 4057–4106. doi: 10.5194/bgd1240572015

Figure 1.

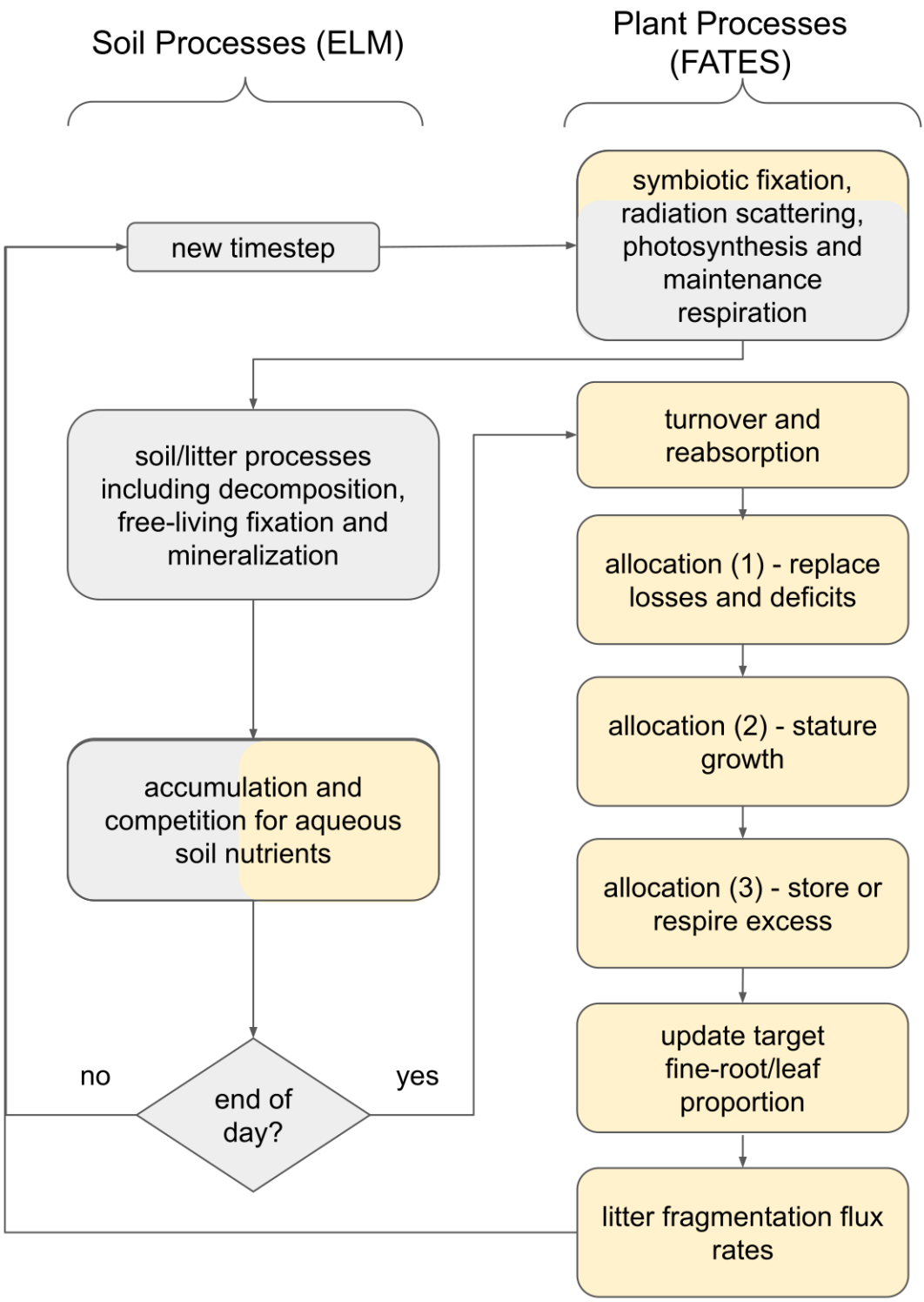
Soil Processes (ELM)
Plant Processes (FATES)
new timestep
symbiotic fixation, radiation scattering, photosynthesis and maintenance respiration
soil/litter processes including decomposition, free-living fixation and mineralization
turnover and reabsorption
allocation (1) - replace losses and deficits
allocation (2) - stature growth
allocation (3) - store or respire excess
update target fine-root/leaf proportion
litter fragmentation flux rates
accumulation and competition for aqueous soil nutrients
end of day?
no
yes

Figure 2.

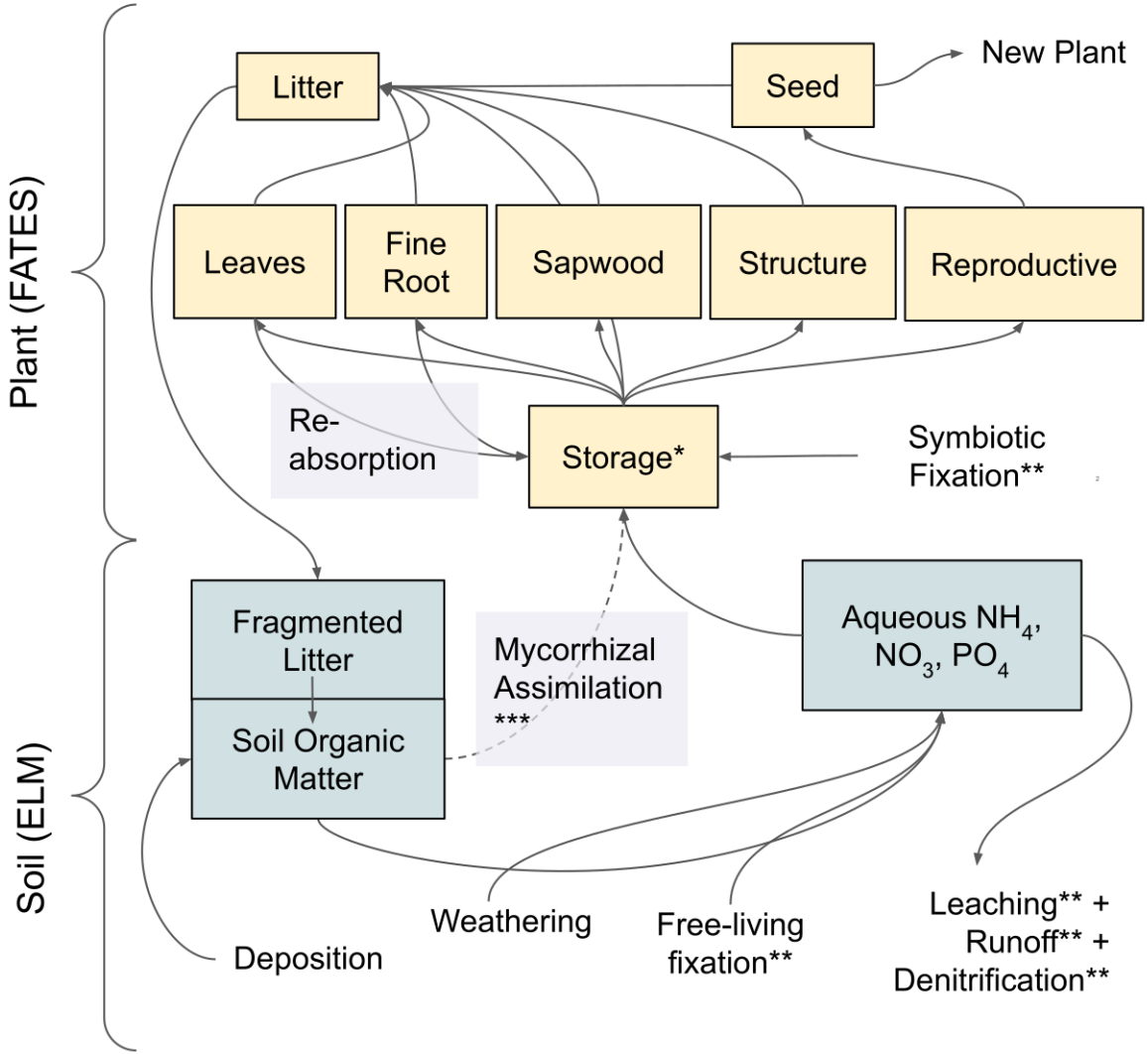
Plant (FATES)
Soil (ELM)
Litter
Seed
New Plant
Leaves
Fine Root
Sapwood
Structure
Reproductive
Re-absorption
Storage*
Symbiotic Fixation**
Fragmented Litter
Soil Organic Matter
Mycorrhizal Assimilation ***
Aqueous NH_4, NO_3, PO_4
Deposition
Weathering
Free-living fixation**
Leaching** + Runoff** + Denitrification**

Figure 3.

C < N

Optimize fine-root biomass to balance Carbon and Nutrient storage

C > N

More fine-root (large λ) =
Higher Nutrient Uptake
Higher Respiration

Less fine-root (small λ) =
Lower Nutrient Uptake
Lower Respiration

EESA23-007

Figure 4.

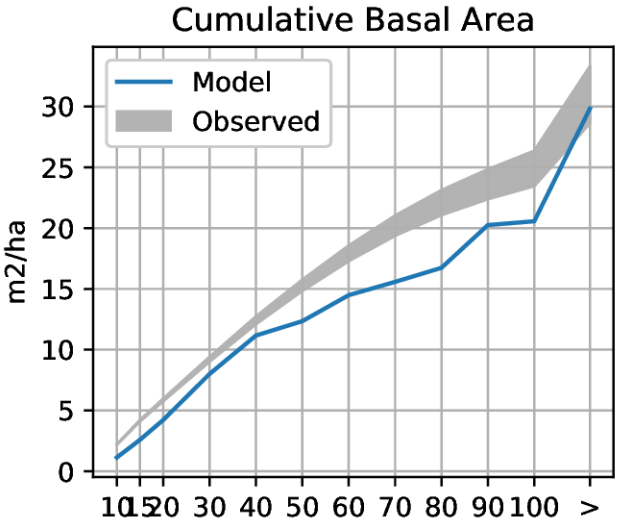

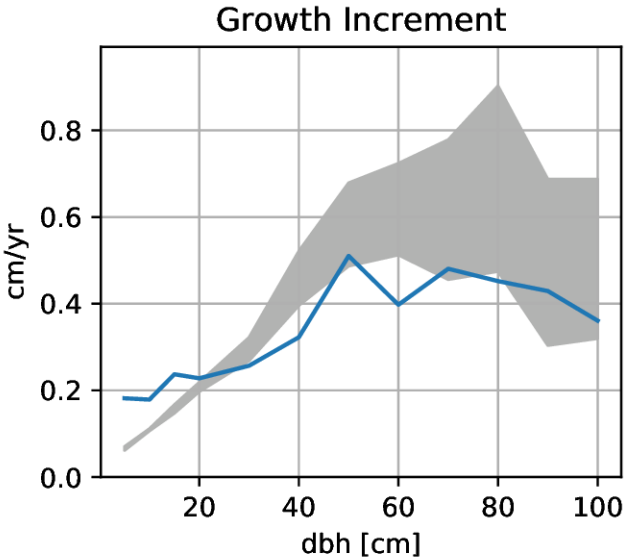

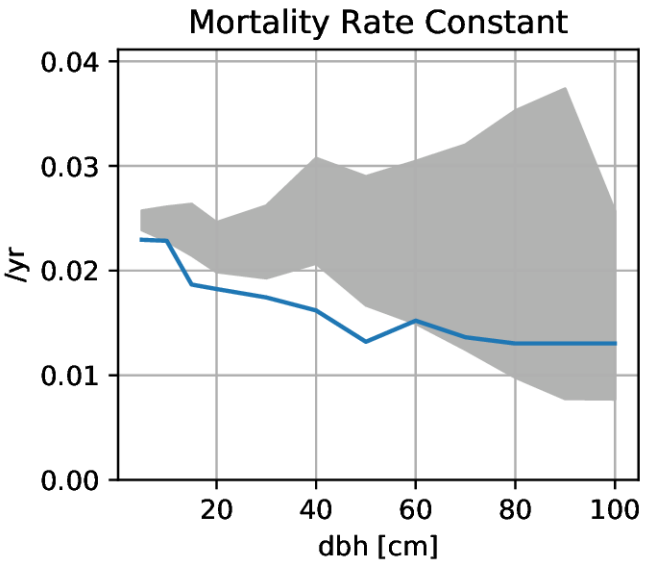

	Model	Observed
LAI	5.39	5.93 [m2/m2]
GPP	2.18	2.72 [kgC/m2/yr]

Figure 5.

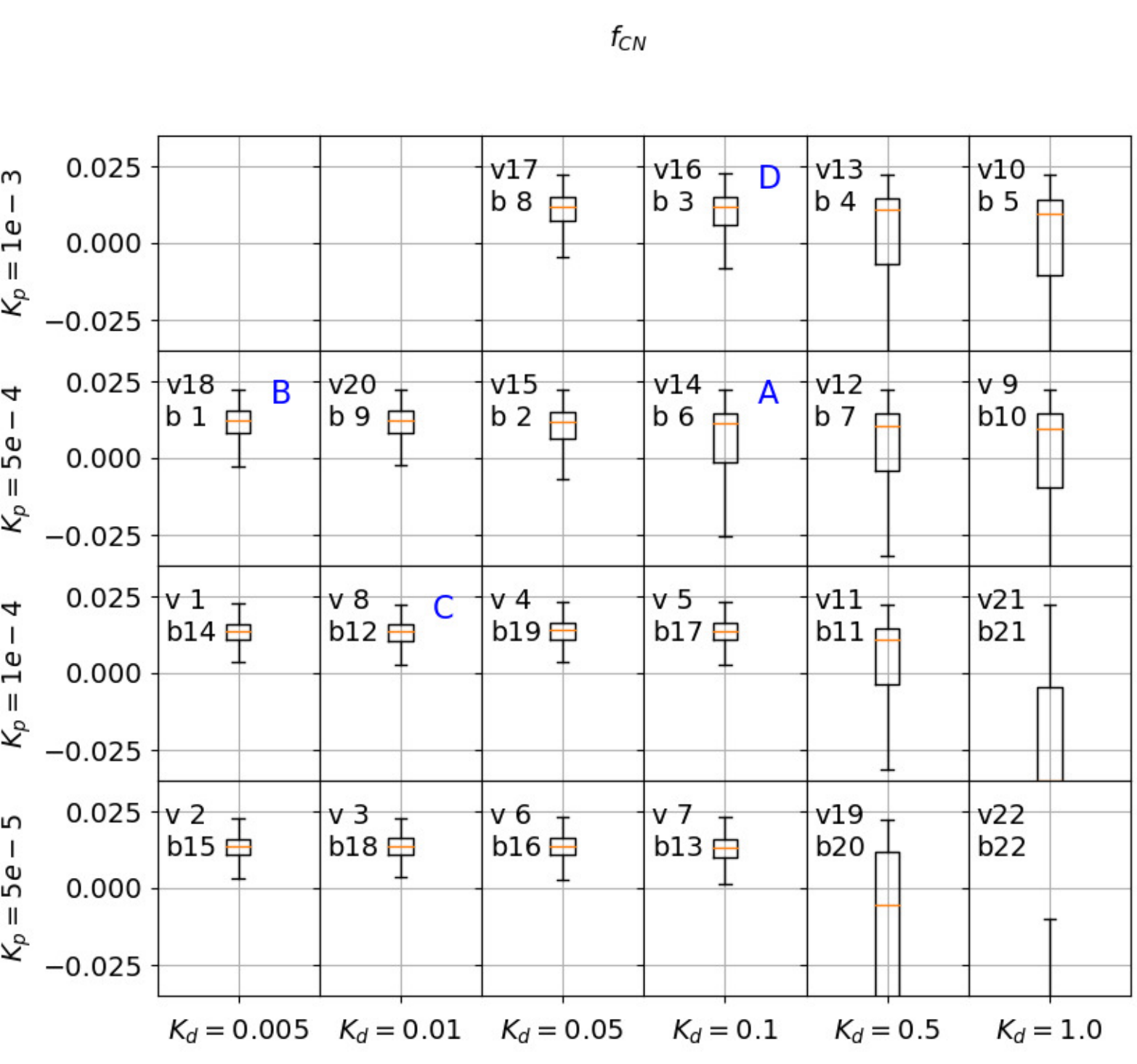
f_{CN}
$K_p = 1e-3$
$K_p = 5e-4$
$K_p = 1e-4$
$K_p = 5e-5$
0.025
0.000
−0.025
v17 b 8
v16 b 3
D
v13 b 4
v10 b 5
v18 b 1
B
v20 b 9
v15 b 2
v14 b 6
A
v12 b 7
v 9 b10
v 1 b14
v 8 b12
C
v 4 b19
v 5 b17
v11 b11
v21 b21
v 2 b15
v 3 b18
v 6 b16
v 7 b13
v19 b20
v22 b22
$K_d = 0.005$
$K_d = 0.01$
$K_d = 0.05$
$K_d = 0.1$
$K_d = 0.5$
$K_d = 1.0$

Figure 6.

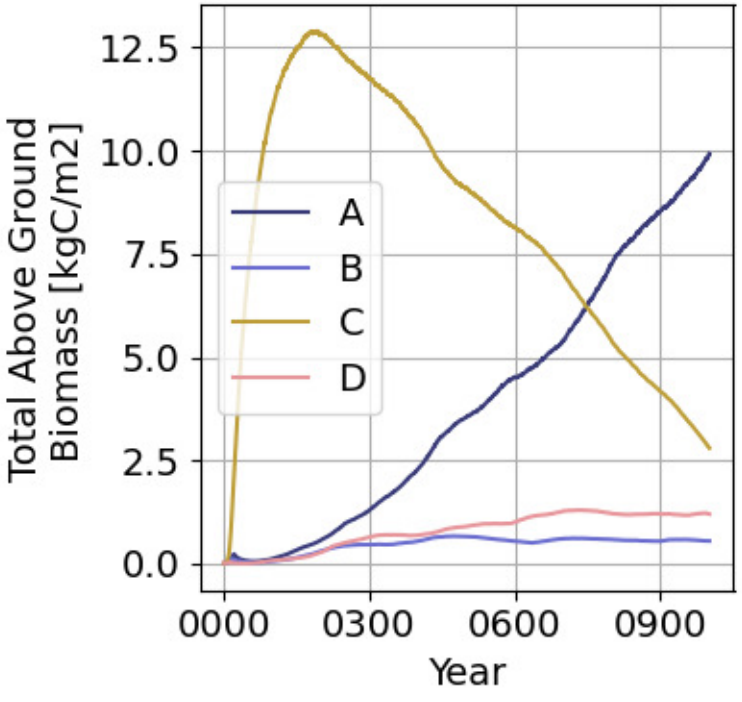
Total Above Ground Biomass [kgC/m2]
12.5
10.0
7.5
5.0
2.5
0.0
A
B
C
D
0000
0300
0600
0900
Year

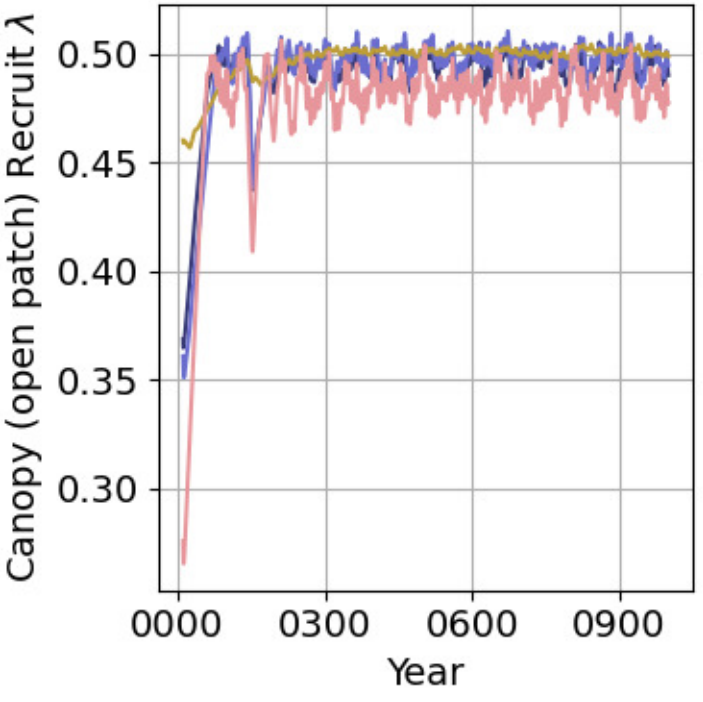
Canopy (open patch) Recruit λ
0.50
0.45
0.40
0.35
0.30
0000
0300
0600
0900
Year

Figure 7.

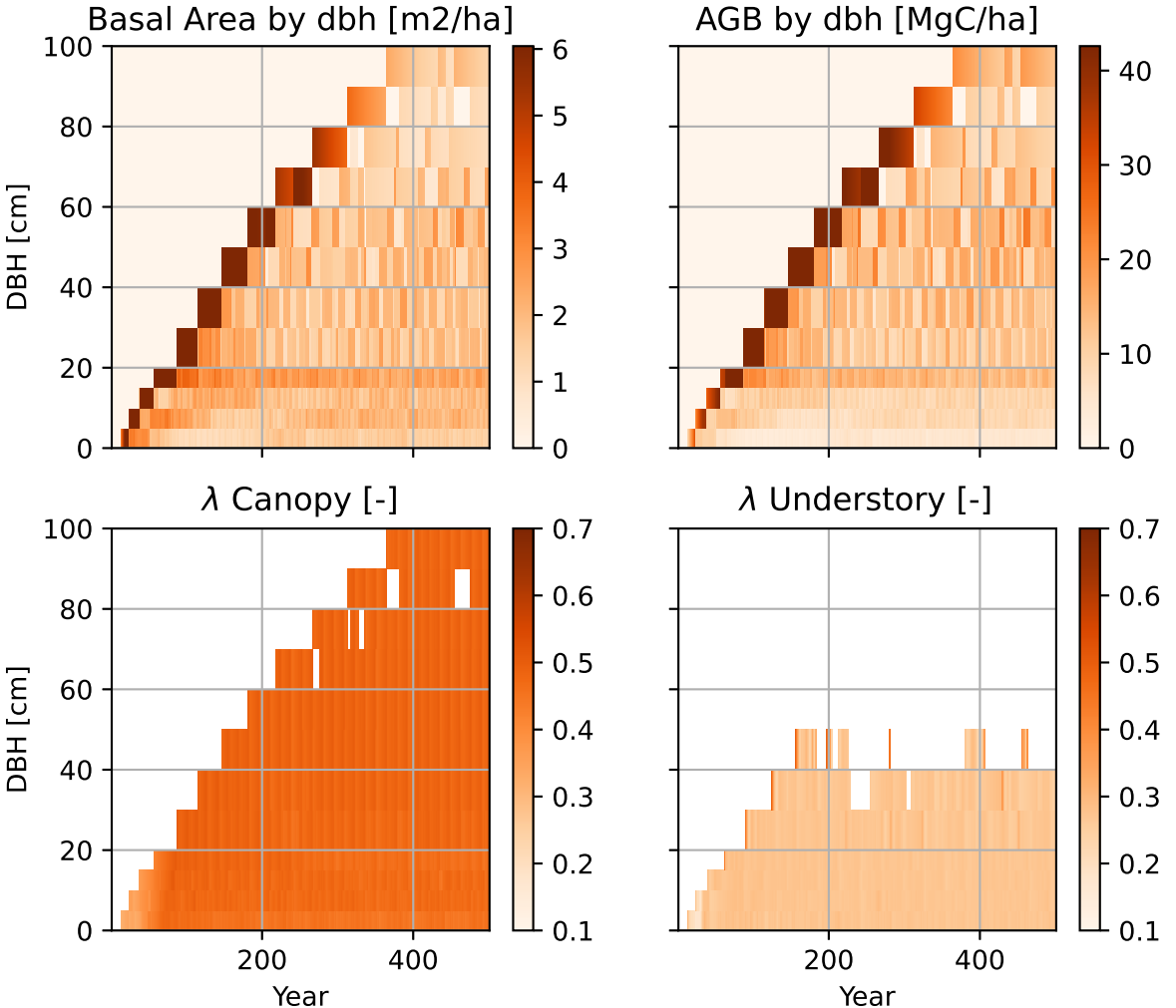
Basal Area by dbh [m2/ha]
AGB by dbh [MgC/ha]
λ Canopy [-]
λ Understory [-]
DBH [cm]
Year
0
20
40
60
80
100
200
400
0
1
2
3
4
5
6
10
30
0.1
0.2
0.3
0.4
0.5
0.6
0.7

Figure 8.

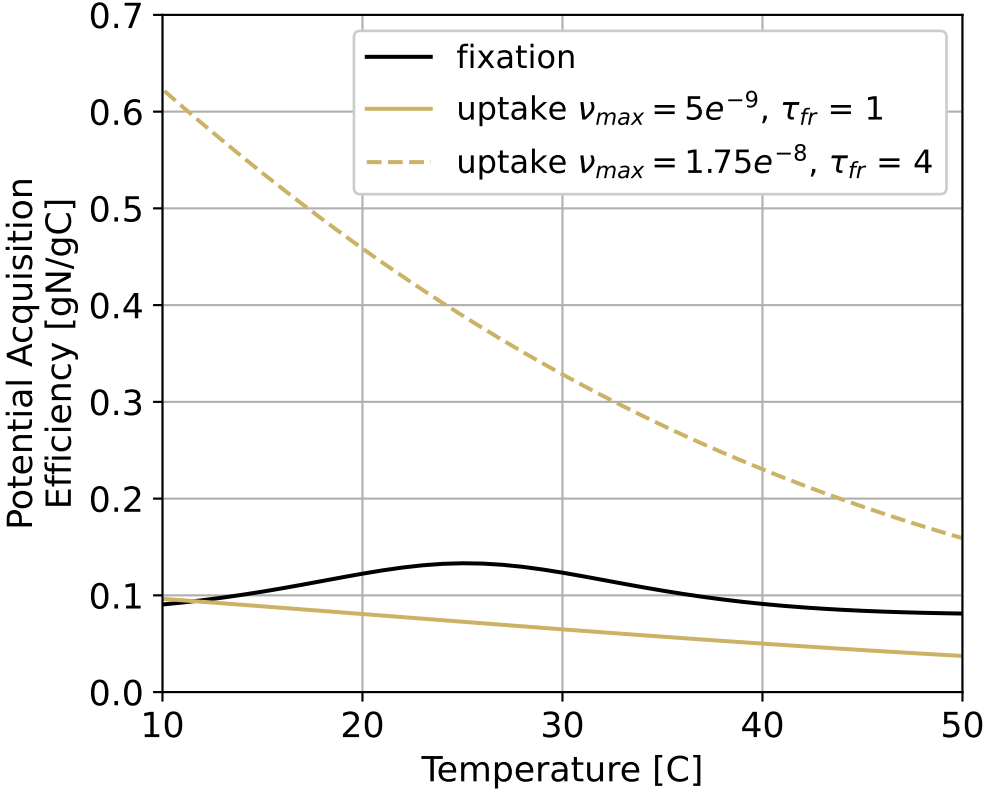
0.7
0.6
0.5
0.4
0.3
0.2
0.1
0.0
Potential Acquisition Efficiency [gN/gC]
10
20
30
40
50
Temperature [C]
fixation
uptake $\nu_{max} = 5e^{-9}$, $\tau_{fr} = 1$
uptake $\nu_{max} = 1.75e^{-8}$, $\tau_{fr} = 4$

Figure 9.

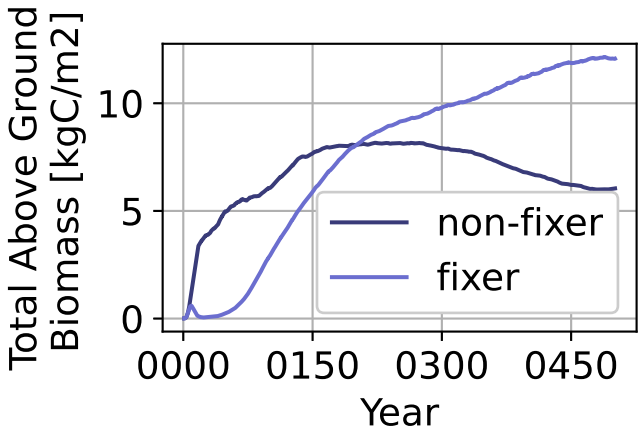
Total Above Ground Biomass [kgC/m2]
10
5
0
non-fixer
fixer
0000
0150
0300
0450
Year

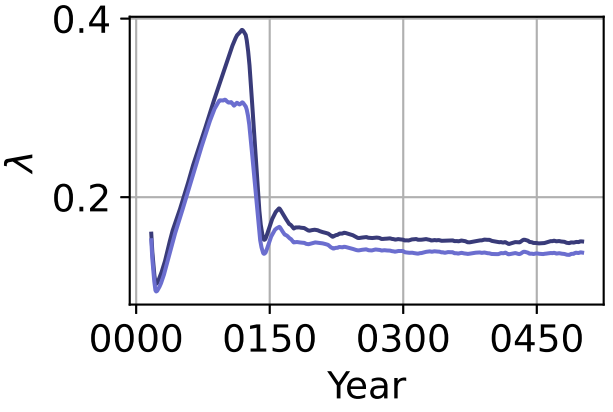
λ
0.4
0.2
0000
0150
0300
0450
Year

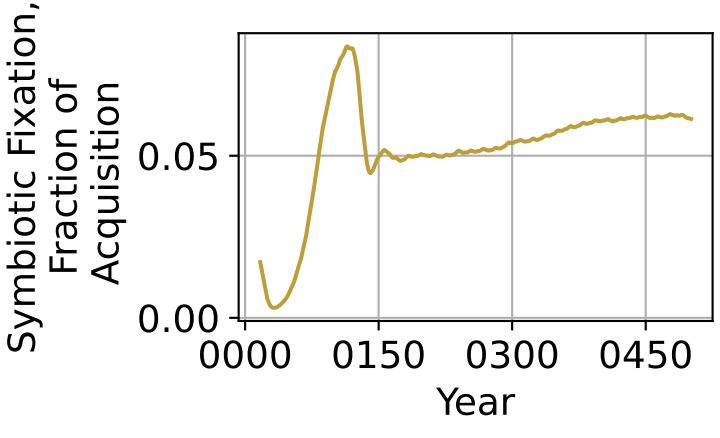
Symbiotic Fixation, Fraction of Acquisition
0.05
0.00
0000
0150
0300
0450
Year

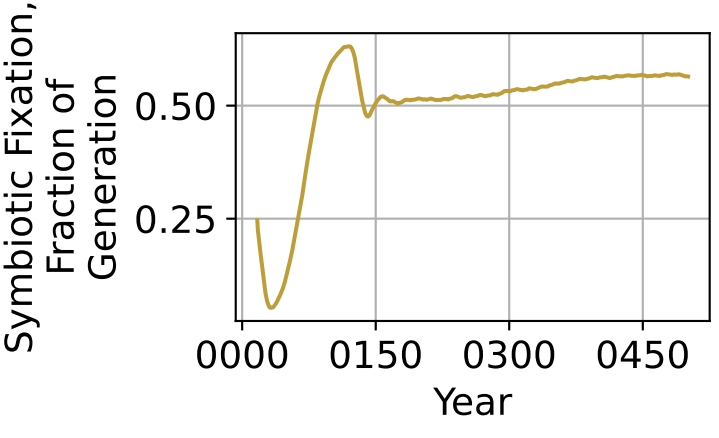
Symbiotic Fixation, Fraction of Generation
0.50
0.25
0000
0150
0300
0450
Year

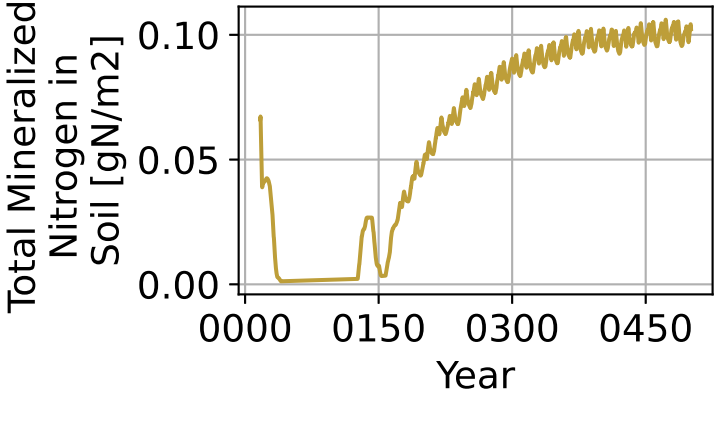
Total Mineralized Nitrogen in Soil [gN/m2]
0.10
0.05
0.00
0000
0150
0300
0450
Year

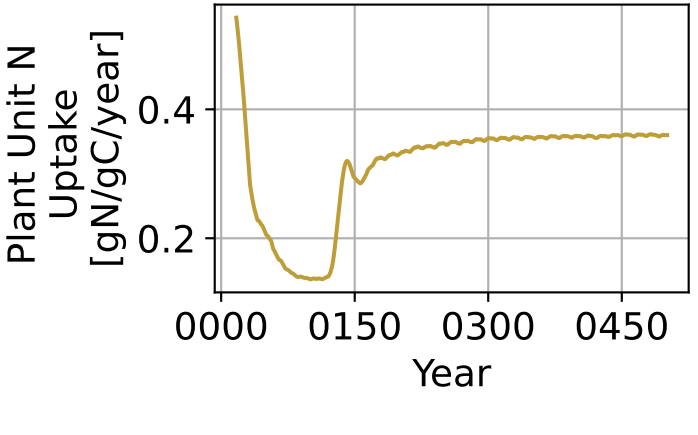
Plant Unit N Uptake [gN/gC/year]
0.4
0.2
0000
0150
0300
0450
Year

Figure 10.

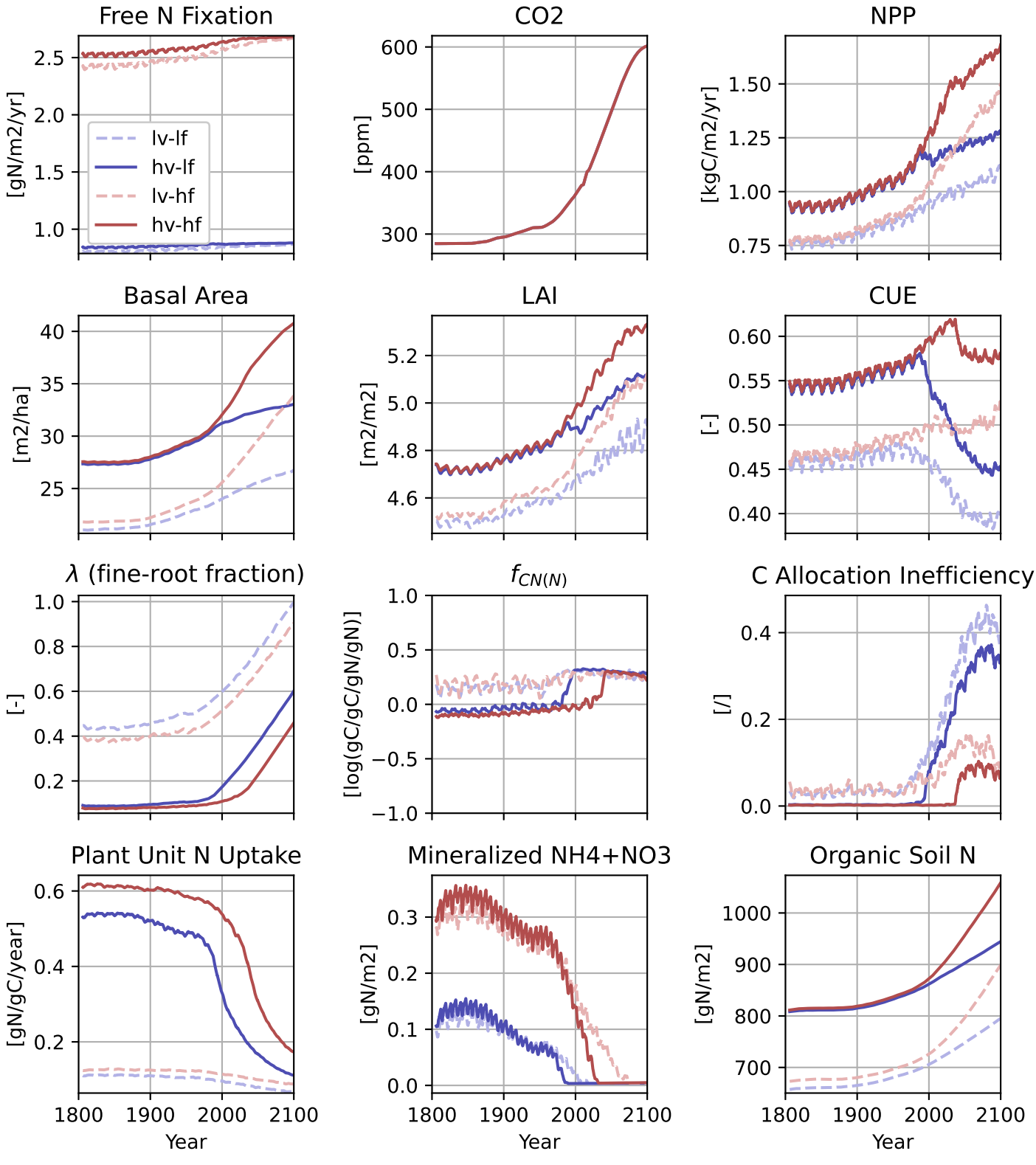
Free N Fixation
[gN/m2/yr]
lv-lf
hv-lf
lv-hf
hv-hf
CO2
[ppm]
NPP
[kgC/m2/yr]
Basal Area
[m2/ha]
LAI
[m2/m2]
CUE
[-]
λ (fine-root fraction)
[-]
$f_{CN(N)}$
[log(gC/gC/gN/gN)]
C Allocation Inefficiency
[/]
Plant Unit N Uptake
[gN/gC/year]
Mineralized NH4+NO3
[gN/m2]
Organic Soil N
[gN/m2]
Year
Year
Year

Figure 11.

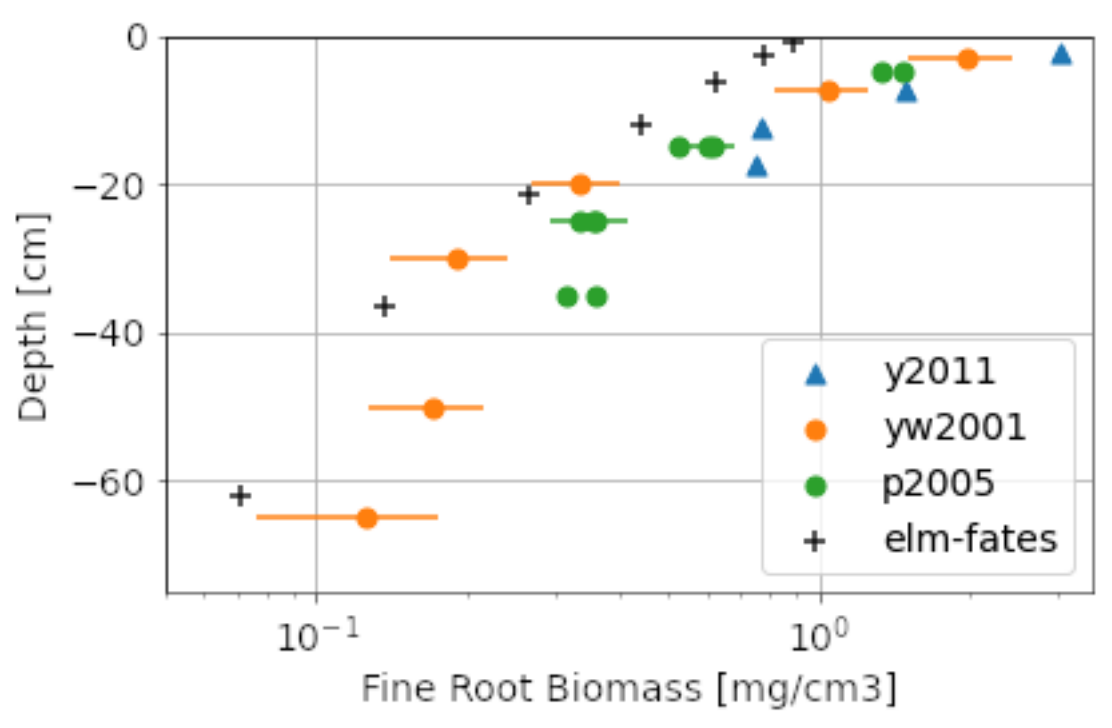
0
−20
−40
−60
Depth [cm]
10^{-1}
10^{0}
Fine Root Biomass [mg/cm3]
y2011
yw2001
p2005
elm-fates

Figure E1.

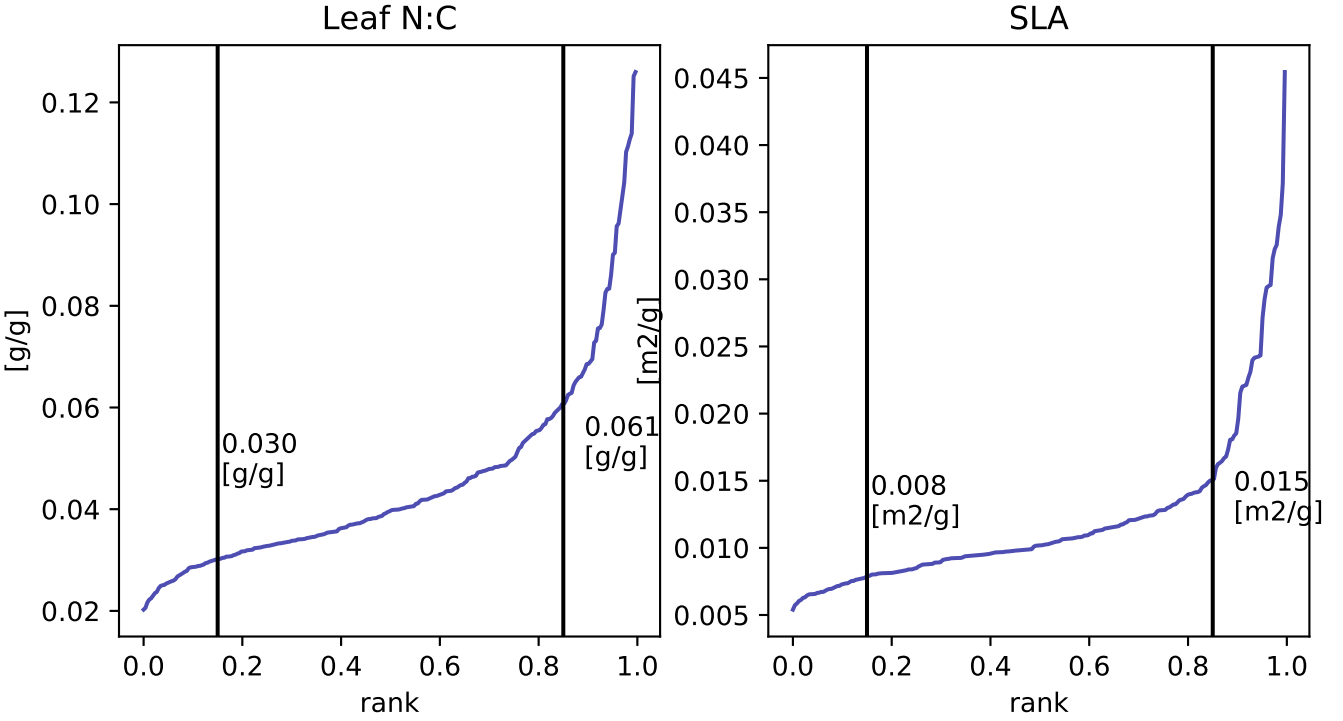
Leaf N:C
[g/g]
0.12
0.10
0.08
0.06
0.04
0.02
0.030
[g/g]
0.061
[g/g]
0.0
0.2
0.4
0.6
0.8
1.0
rank
SLA
[m2/g]
0.045
0.040
0.035
0.030
0.025
0.020
0.015
0.010
0.005
0.008
[m2/g]
0.015
[m2/g]
0.0
0.2
0.4
0.6
0.8
1.0
rank

Figure E2.

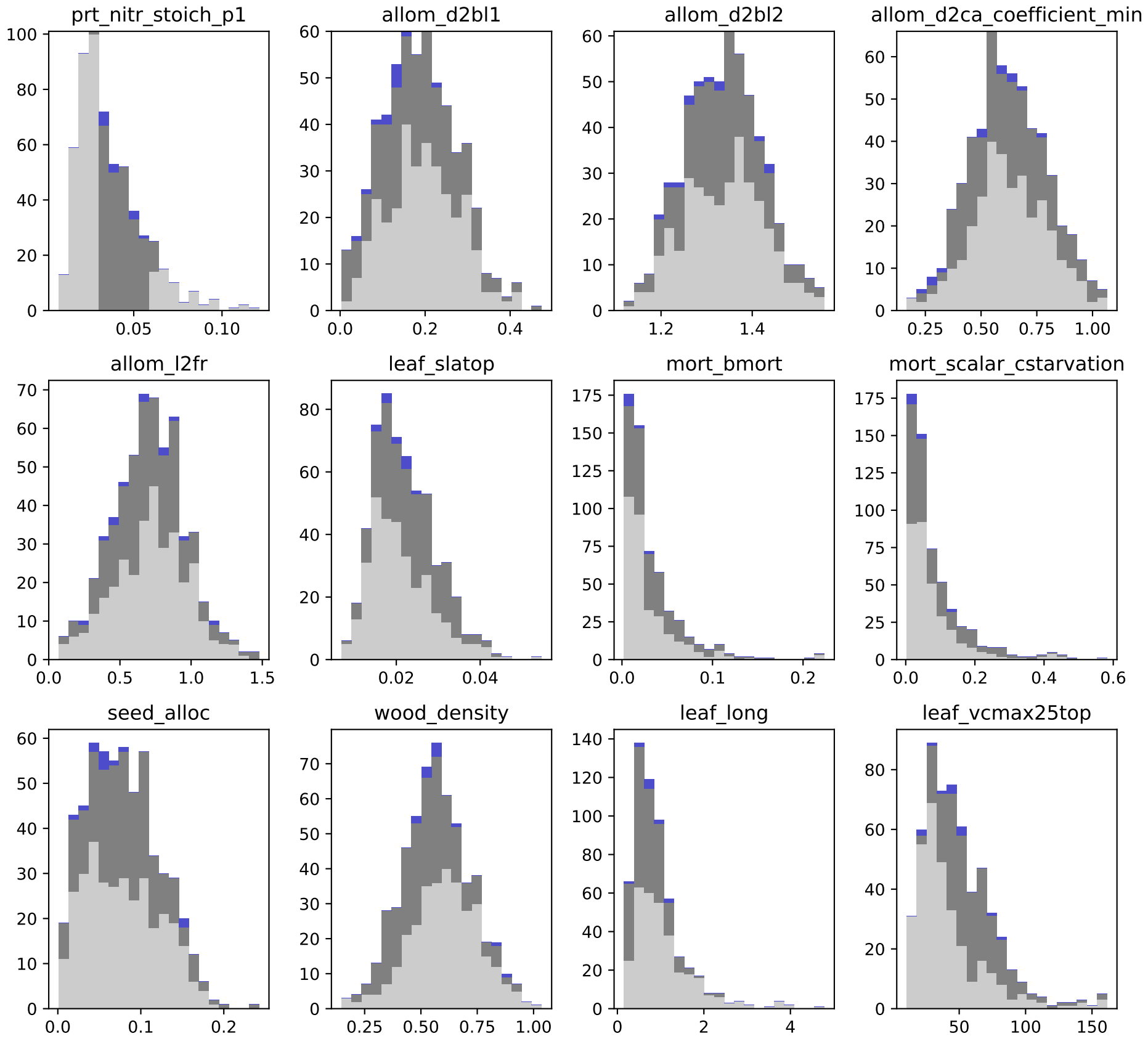
prt_nitr_stoich_p1
allom_d2bl1
allom_d2bl2
allom_d2ca_coefficient_min
allom_l2fr
leaf_slatop
mort_bmort
mort_scalar_cstarvation
seed_alloc
wood_density
leaf_long
leaf_vcmax25top

Figure F1.

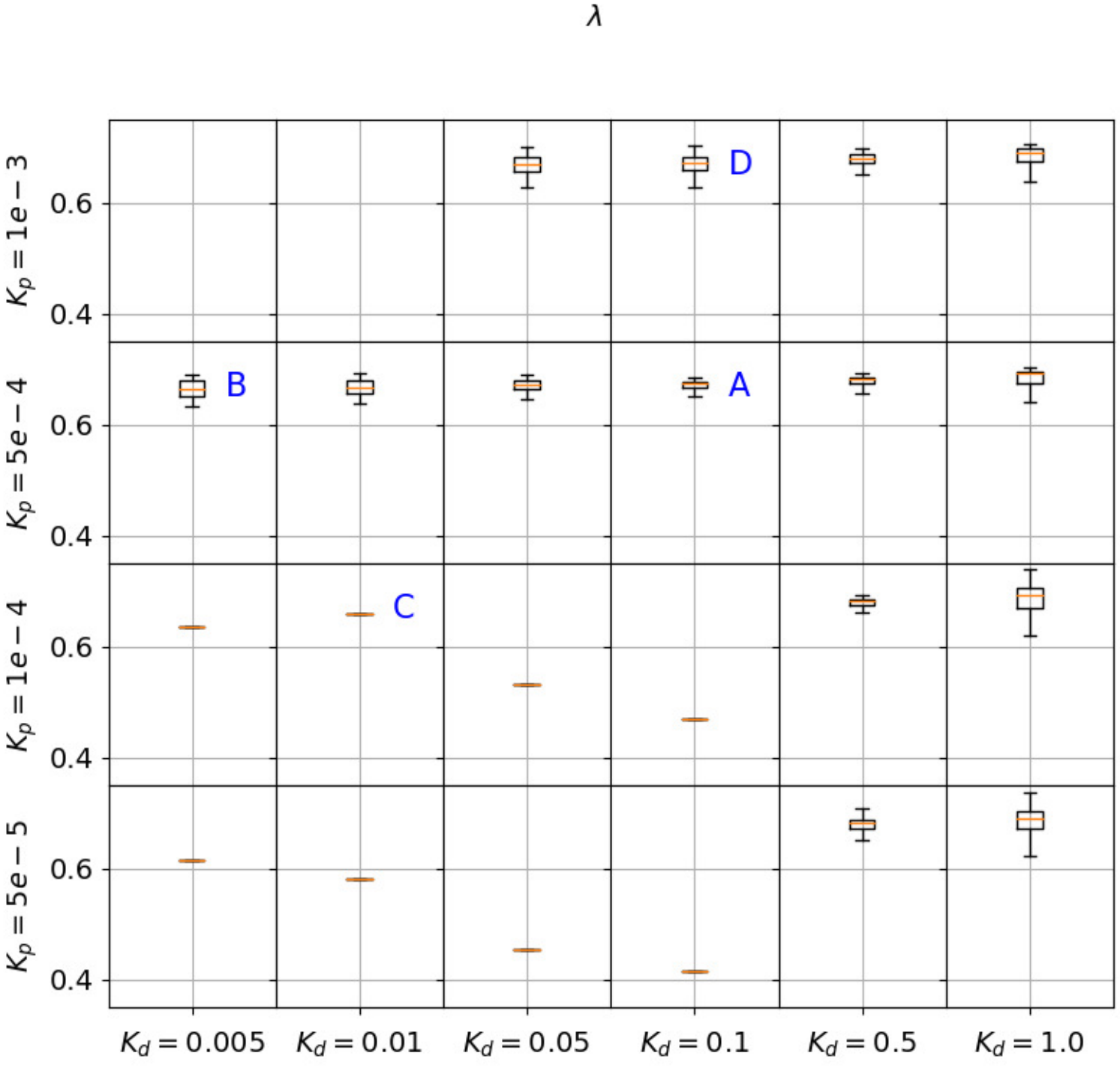
λ
$K_p = 1e-3$
$K_p = 5e-4$
$K_p = 1e-4$
$K_p = 5e-5$
0.6
0.4
A
B
C
D
$K_d = 0.005$
$K_d = 0.01$
$K_d = 0.05$
$K_d = 0.1$
$K_d = 0.5$
$K_d = 1.0$

Figure F2.

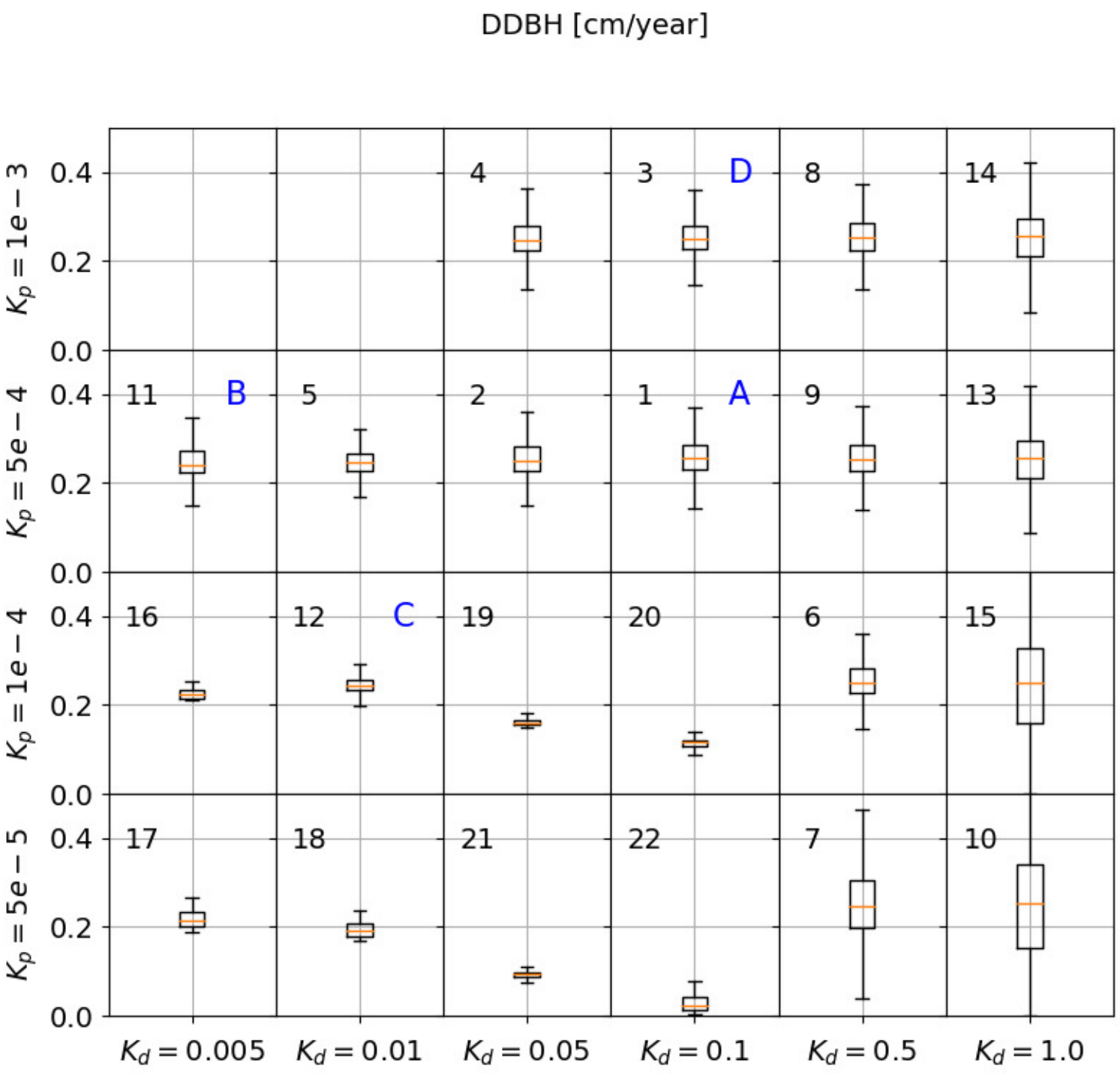
DDBH [cm/year]
$K_p = 1e-3$
$K_p = 5e-4$
$K_p = 1e-4$
$K_p = 5e-5$
0.0
0.2
0.4
4
3
D
8
14
11
B
5
2
1
A
9
13
16
12
C
19
20
6
15
17
18
21
22
7
10
$K_d = 0.005$
$K_d = 0.01$
$K_d = 0.05$
$K_d = 0.1$
$K_d = 0.5$
$K_d = 1.0$

Figure F3.

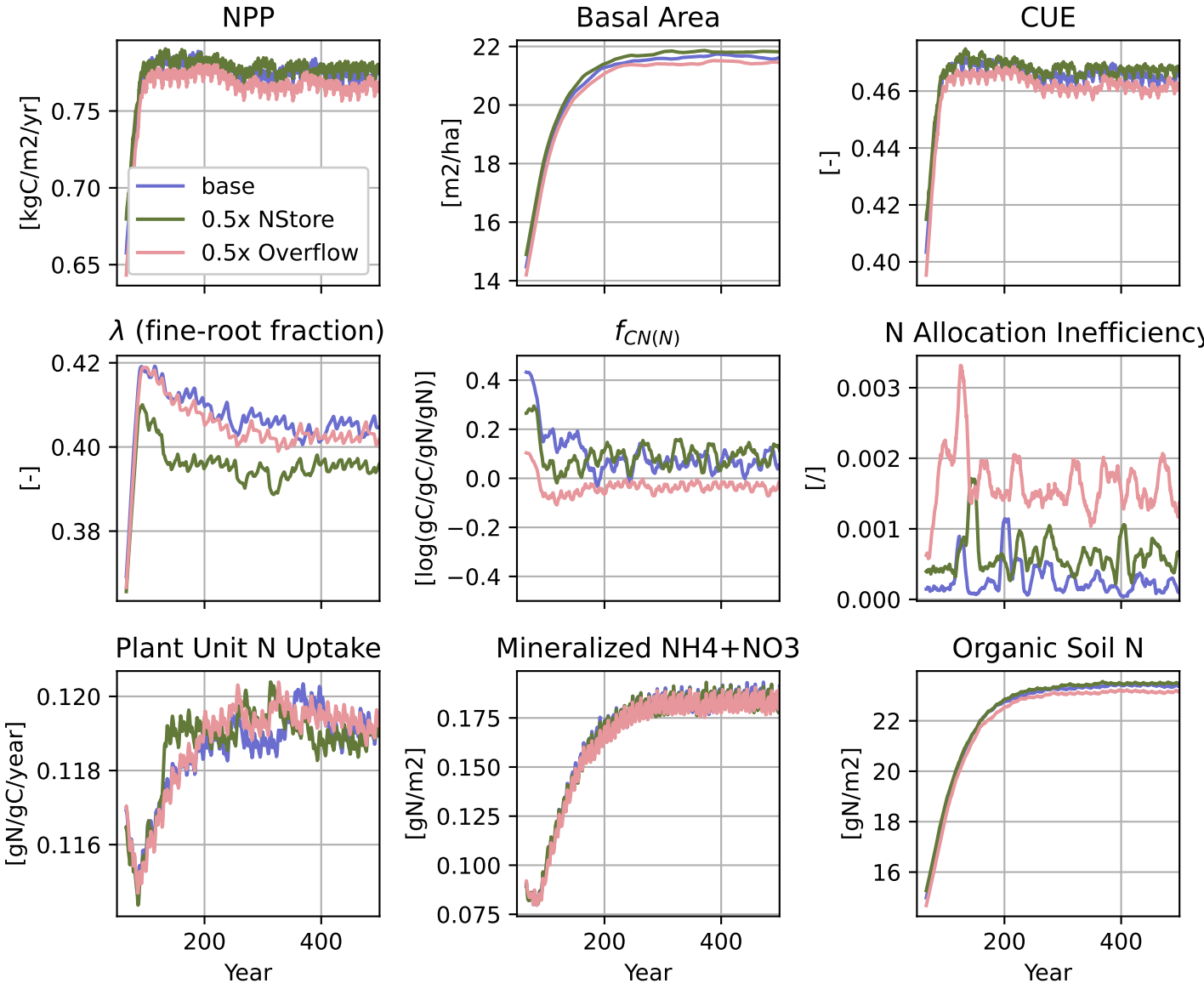
NPP
[kgC/m2/yr]
0.75
0.70
0.65
base
0.5x NStore
0.5x Overflow
Basal Area
[m2/ha]
22
20
18
16
14
CUE
[-]
0.46
0.44
0.42
0.40
λ (fine-root fraction)
[-]
0.42
0.40
0.38
$f_{CN(N)}$
[log(gC/gC/gN/gN)]
0.4
0.2
0.0
−0.2
−0.4
N Allocation Inefficiency
[/]
0.003
0.002
0.001
0.000
Plant Unit N Uptake
[gN/gC/year]
0.120
0.118
0.116
Mineralized NH4+NO3
[gN/m2]
0.175
0.150
0.125
0.100
0.075
Organic Soil N
[gN/m2]
22
20
18
16
200
400
Year

Figure F4.

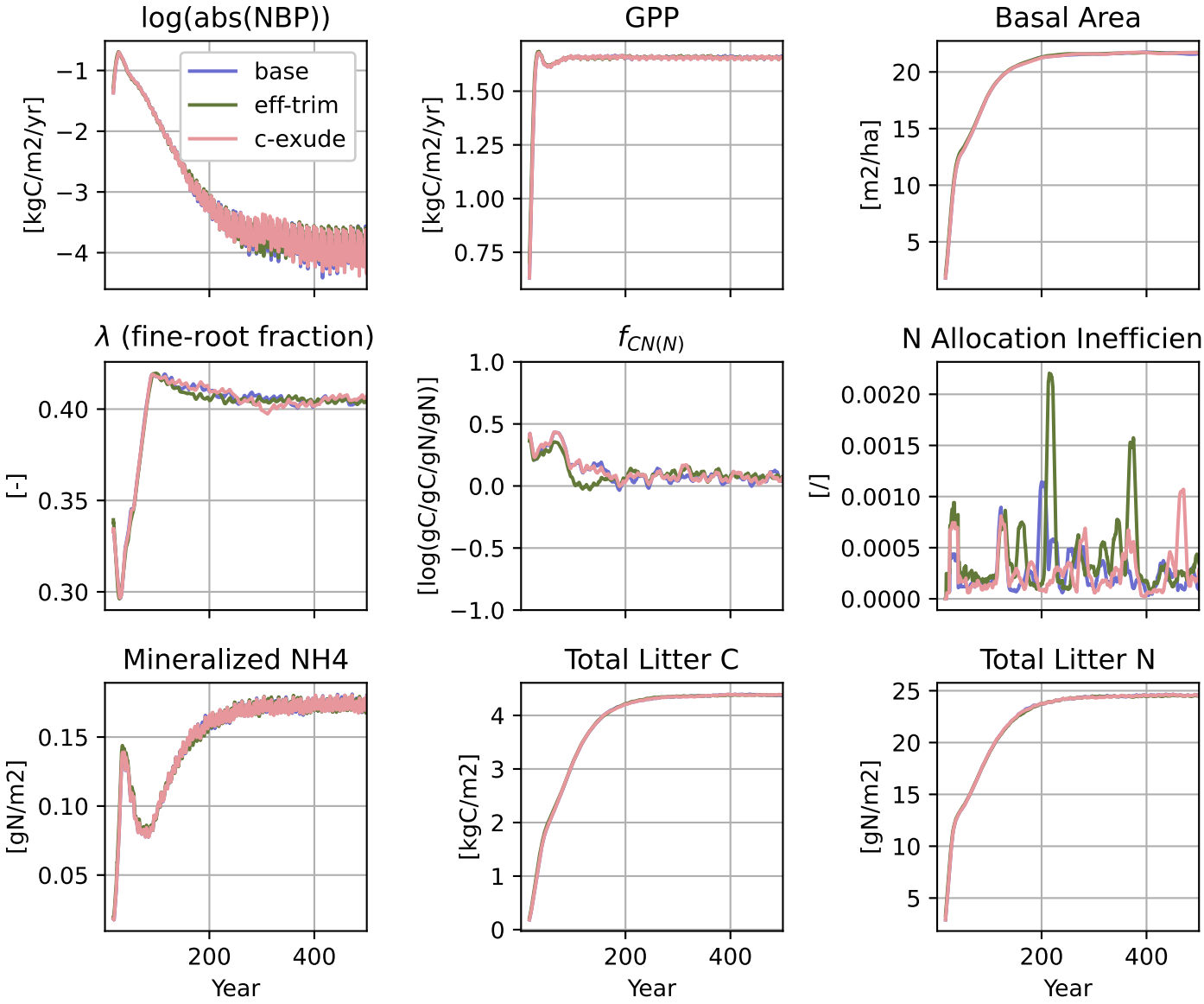
log(abs(NBP))
[kgC/m2/yr]
base
eff-trim
c-exude
GPP
[kgC/m2/yr]
Basal Area
[m2/ha]
λ (fine-root fraction)
[-]
$f_{CN(N)}$
[log(gC/gC/gN/gN)]
N Allocation Inefficiency
[/]
Mineralized NH4
[gN/m2]
Total Litter C
[kgC/m2]
Total Litter N
[gN/m2]
Year
Year
Year

Figure F5.

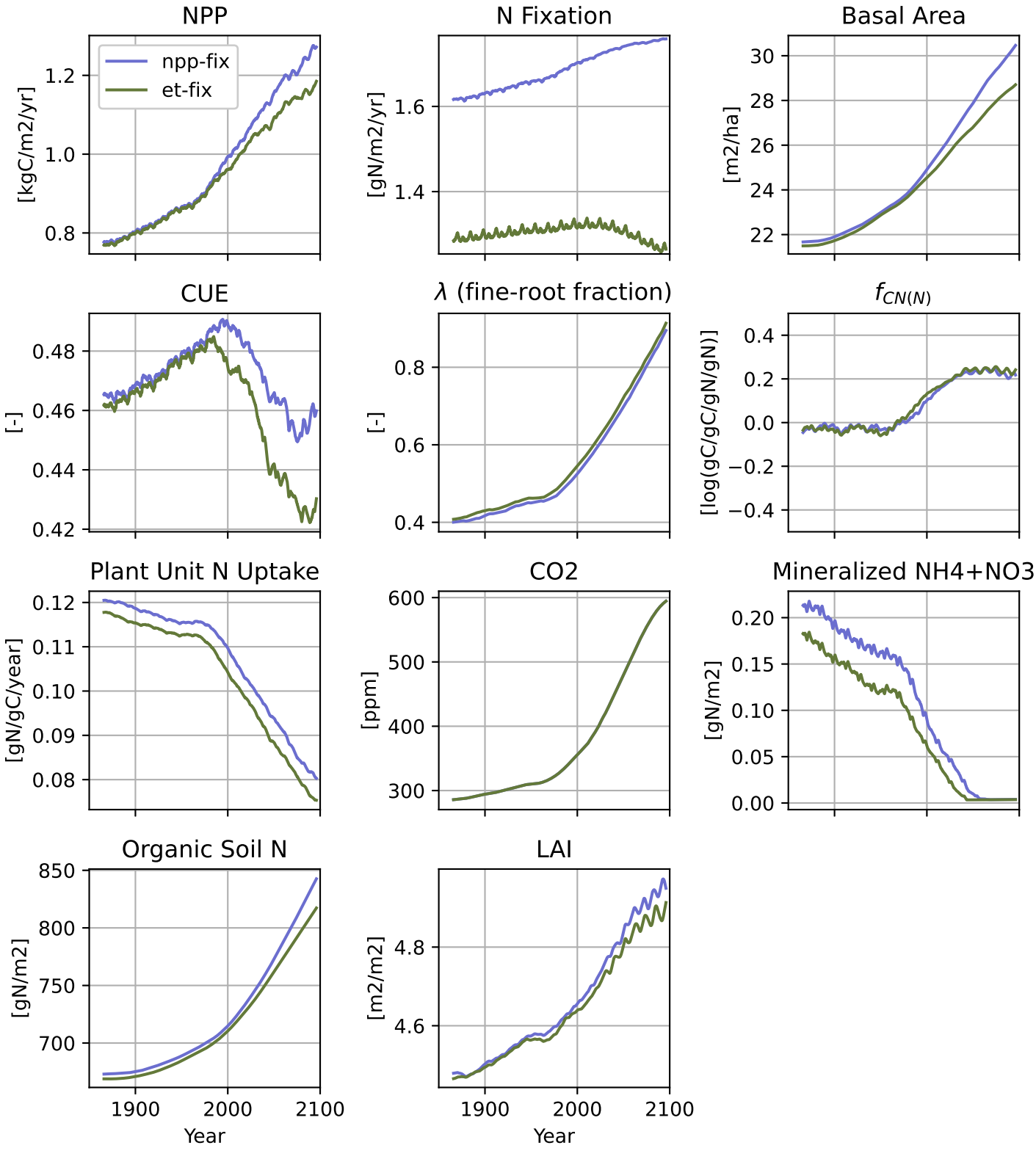
NPP
[kgC/m2/yr]
npp-fix
et-fix
N Fixation
[gN/m2/yr]
Basal Area
[m2/ha]
CUE
[-]
λ (fine-root fraction)
[-]
$f_{CN(N)}$
[log(gC/gC/gN/gN)]
Plant Unit N Uptake
[gN/gC/year]
CO2
[ppm]
Mineralized NH4+NO3
[gN/m2]
Organic Soil N
[gN/m2]
LAI
[m2/m2]
1900
2000
2100
Year

Figure F6.

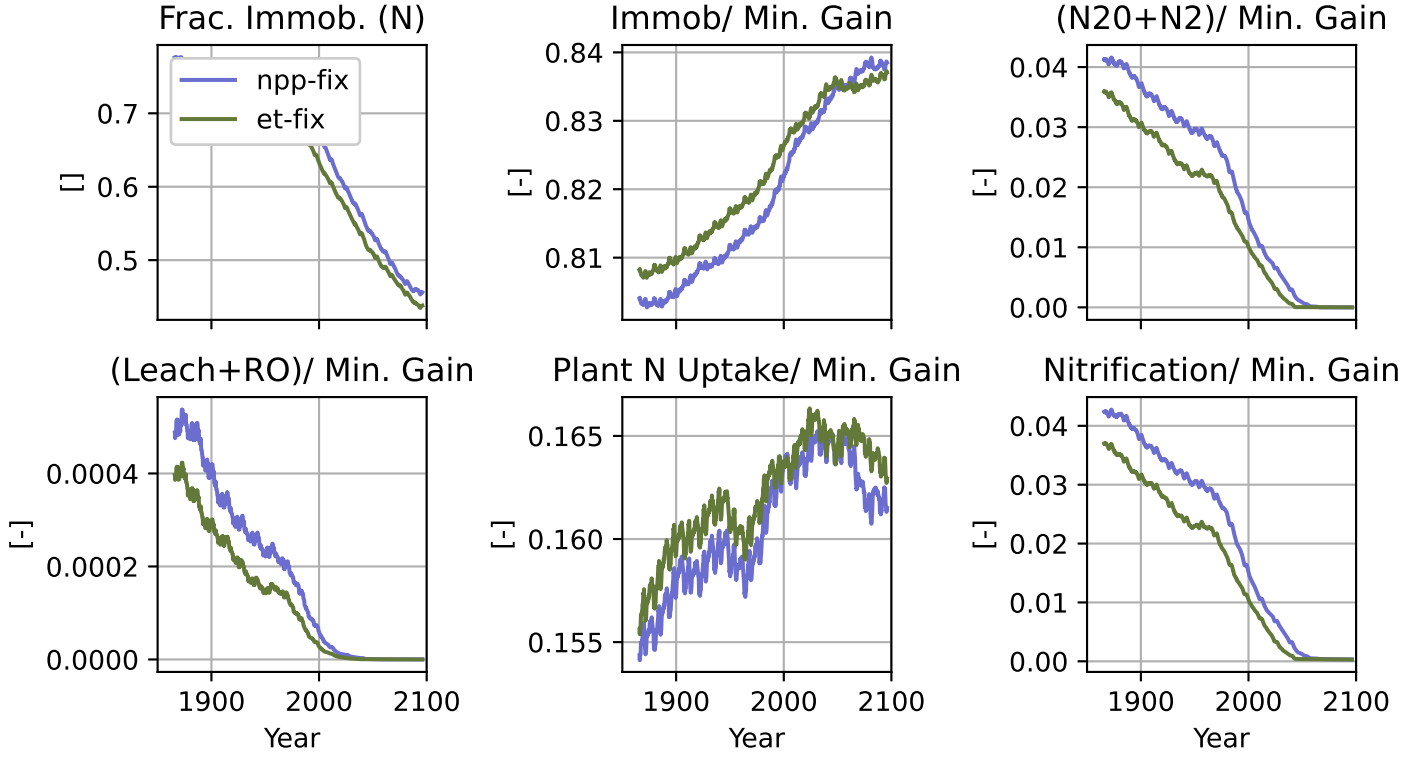
Frac. Immob. (N)
npp-fix
et-fix
[]
0.7
0.6
0.5
Immob/ Min. Gain
[-]
0.84
0.83
0.82
0.81
(N20+N2)/ Min. Gain
[-]
0.04
0.03
0.02
0.01
0.00
(Leach+RO)/ Min. Gain
[-]
0.0004
0.0002
0.0000
Plant N Uptake/ Min. Gain
[-]
0.165
0.160
0.155
Nitrification/ Min. Gain
[-]
0.04
0.03
0.02
0.01
0.00
1900
2000
2100
Year